R-05-02

# Äspö Pillar Stability Experiment

## Final experiment design, monitoring results and observations

Christer Andersson
Svensk Kärnbränslehantering AB

Anders Eng, Acuo Engineering AB

December 2005

**Svensk Kärnbränslehantering AB**
Swedish Nuclear Fuel
and Waste Management Co
Box 5864
SE-102 40 Stockholm Sweden
Tel 08-459 84 00
+46 8 459 84 00
Fax 08-661 57 19
+46 8 661 57 19

SKB

ISSN 1402-3091
SKB Rapport R-05-02

# Äspö Pillar Stability Experiment

## Final experiment design, monitoring results and observations

Christer Andersson
Svensk Kärnbränslehantering AB

Anders Eng, Acuo Engineering AB

December 2005

*Keywords:* Spalling, Spalling strength, Failure, Heating, Confinement, Displacements, Acoustic emission, Temperature, LVDT, Thermocouple.

# Summary

The field part of the Äspö Pillar Stability Experiment at the Äspö Hard Rock Laboratory (HRL) was finished in 2004. The experiment was designed to induce and monitor the process of brittle failure, spalling, in a fractured rock mass under controlled conditions. The field part was successfully conducted and a large data set was obtained.

This report presents the final design of the experiment, the results of the monitoring, and the observations made during the spalling process and when the spalled rock was removed.

When heating of the rock was initiated the rock responded quickly. After only a few days the spalling process was activated in the notch, as indicated by the acoustic emission system, and shortly thereafter displacement readings were recorded. Contraction (radial expansion) of the rock was recorded by several instruments before the notch reached the instrument levels. This contraction is probably the result of a 3D re-distribution of the stresses.

The temperature increase in the system was both slower and reached a steady state much earlier than predicted by the numerical models. The propagation of the notch was therefore halted after approximately one month of heating. The power to the electrical heaters was therefore doubled. Spalling then started up again, and in one month's time it had propagated to a depth of approximately five metres in the hole. A second steady state was now reached, but this time the heater power was kept constant for a while to let the rock settle before the confinement pressure was reduced from 700 kPa to 0 in decrements of 50 kPa. The rock mass response to the pressure drop was very limited until the pressure was lowered to approximately 200 kPa (the atmospheric pressure is not included in the given pressure values). Large displacements and a high acoustic emission hit frequency were then measured in the open hole.

After the de-pressurization of the confined hole, the heaters were left on for approximately one week before they were turned off. When the rock mass had cooled down the slabs created by the spalling process were carefully removed and the spalled area was laser-scanned to get its full 3D geometry.

When the spalled chips are removed the edges are thin, less than a millimetre. This indicates that normal displacement and not shearing has occurred in the notch. Shearing would most likely have damaged the thin edges and broken them off. In the deepest part of the notch a white powder was present. It indicates that crushing of the rock had taken place there.

The monitoring equipment consisting of thermocouples, deformation transducers and an acoustic system has worked well. The data sets can be combined which enables an integrated analysis of the rock mass behaviour during the experiment.

# Sammanfattning

Vid Äspö Hard Rock laboratory har fältdelen av Äspö Pillar Stability Experiment färdigställts under år 2004. Syftet med experimentet var att under kontrollerade former inducera och övervaka processen för sprött brott, spjälkning, i en sprucken bergmassa.

Denna rapport presenterar experimentets slutliga design samt resultaten från moneteringen både under tiden berget spjälkades och då det spjälkade berget plockades bort.

När värmningen av berget startade reagerade berget i pelaren snabbt. Efter bara några dagar initierades spjälkningsprocessen vilket observerades av det akusitksa systemet. Ytterligare en kort tid efter detta började deformationer att uppmätas. Ett flertal instrument visade att berget drog ihop sig (radien ökade) innan det synligt spjälkade området propagerat ned till instrumenten på de olika nivåerna. Kontraktionen beror troligen på en omfördelning av det tre-dimensionella spänningsfältet när spetsen på det spjälkade området närmar sig.

Temperaturökningen till följd av värmningen skedde både långsammare och nådde jämvikt tidigare än vad de numeriska modellerna predikterat. Propagerandet av spjälkningsfronten stannade därför upp ungefär en månad efter att värmningen startats. Effekten till de elektriska värmarna fördubblades därför varefter spjälkningen stratade upp igen. Under ytterligare en månads tid nådde spjälkfronten ett djup på ungefär fem meter. Ett nytt jämviktsläge nåddes då men denna gång hölls effekten till värmarna konstant under en tid för att jämvikten skulle nås i hela pelaren. När detta skett reducerades det mothållande trycket i det trycksatta hålet från 700 kPa övertryck till 0 i omgångar om 50 kPa. Väldigt lite hände i bergmassan innan övertrycket sänkts till 200 kPa. Relativt stora deformationer och många akustiska händelser registrerades då i det öppna hålet.

Efter trycksänkningen lämnades värmarna på med oförändrad effekt under cirka en veckas tid varefter de slogs av. När bergmassan hade svalnat plockades de bildade spjälkbitarna försiktigt ned varefter ytan laserskannades för att det spjälkade områdets fullständiga 3D-geometri skulle erhållas.

När de spjälkade bergbitarna togs bort noterades att de flesta kanter var tunnare än en millimeter. Detta indikerar att normalförskjutningar och inte skjuvning har bildat sprickorna i det själkade området. Skjuvning hade sannolikt skadat de tunna kanterna så att de brutits loss från bitarna under spjälkningens gång. Längst in i det spjälkade området fanns ett vitt pulver som tyder på att berget krossats där.

Moniteringen bestående av temperaturmätning, deformationsmätning och ett akustiskt system har fungerat väl. Data kan kombineras vilket möjliggör att en integrerad analys av skeendena under experimentet kan göras.

# Contents


**1 Introduction** 7
1.1 Rock behaviour 9

**2 Geotechnical setting** 11
2.1 Rock mass properties 11
2.2 Rock stress 11
2.3 Geology of pillar walls 12

**3 Experimental set-up** 15
3.1 Geometry 15
3.1.1 Drift and large boreholes 15
3.1.2 Cored boreholes 16
3.2 Heating equipment 18
3.2.1 Insulation 20
3.3 Confinement 21
3.4 Water inflows 23
3.5 Temperature and displacement monitoring 24
3.5.1 Pillar monitoring 25
3.5.2 Displacement measurement 26
3.5.3 Temperature sensors 30
3.5.4 Sources of error 31
3.6 Acoustic monitoring 31
3.7 Logging of work at the experimental site 33

**4 Heating** 35

**5 Monitoring** 37
5.1 Temperature 37
5.1.1 DQ0066G01 37
5.1.2 DQ0063G01 39
5.1.3 KQ0064G06, between the heaters on the left side 41
5.1.4 KQ0064G07, between the heaters on the right side 41
5.1.5 KQ0064G08, the inclined hole on the left side 42
5.2 Displacement 43
5.3 Confinement 54
5.3.1 Release of confinement 54
5.4 Spalling 56
5.4.1 General spalling observations 56
5.4.2 April 26, 2004 58
5.4.3 March 5, 2004 58
5.4.4 May 12, 2004 58
5.4.5 May 14, 2004 58
5.4.6 May 18, 2004 59
5.4.7 May 25, 2004 61
5.4.8 May 27–28, 2004 62
5.4.9 June 2, 2004 62
5.4.10 June 8, 2004 62
5.4.11 June 16, 2004 66
5.4.12 June 23, 2004 66

5.4.13 June 29 2004 69
5.4.14 July 6, 2004 69
5.4.15 July 12, 2004 69
5.5 Removal of spalled slabs 73
5.5.1 Depth 4.9 to 4.3 m 74
5.5.2 Depth 4.3 to 3.7 m 76
5.5.3 Depth 3.7 to 3.3 m 77
5.5.4 Depth 3.3 to 2.7 m 79
5.5.5 Depth 2.7 to 2.1 m 81
5.5.6 Depth 2.1 to 1.6 m 82
5.5.7 Depth 1.6 to 1.1 m 82
5.5.8 Depth 1.1 to 0 m 84
5.6 Extent of spalled and drummy area 84

**6 General summary** 89
6.1 Acoustic emissions and displacements 89
6.2 Confinement 92
6.3 Spalling strength 92

**7 Planned work** 93

**8 Äspö Pillar Stability Experiment reports** 95

**9 References** 97

**Appendix 1** 99

**Appendix 2** 101

**Appendix 3** 109

# 1 Introduction

The full-scale Äspö Pillar Stability Experiment has been carried out at the Äspö Hard Rock Laboratory. In the experiment, stress-induced brittle failure, spalling, was induced and monitored in a pillar between two large boreholes. The monitoring programme included displacements, temperature and acoustic emission.

The objectives of the experiment were to:

- Demonstrate our understanding of brittle failure, spalling, in a fractured rock mass.
- Demonstrate the effect of a confinement pressure (backfill) on the brittle failure process.
- Compare 2D and 3D mechanical and thermal predicting capabilities.

This report presents the final design of the experiment and the results of the displacement and temperature measurements. The report also includes observations of rock behaviour during the spalling phase and removal of the spalled rock. The monitoring programme for the experiment also included an acoustic emission system. Those results are reported separately by /Haycox et al. 2005/.

A new drift had to be excavated /Olsson et al. 2004/ for the experiment for two reasons. Firstly, the experiment had to be carried out in a rock mass where the in situ stresses not are distorted by anything but the experimental drift itself. Secondly, the stresses had to be carefully concentrated by the drift geometry. The new experimental drift was excavated at a depth of 450 m and oriented perpendicular to σ1 to permit maximum effect of the in situ stresses. The new drift is shown in relation to the deeper parts of Äspö HRL in Figure 1-1.

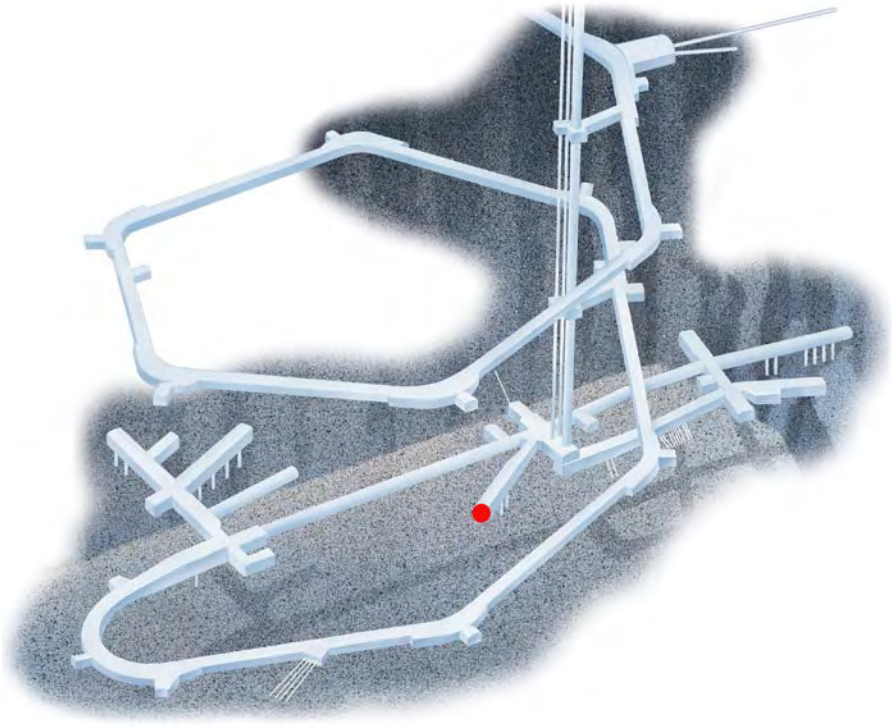

***Figure 1-1.*** *Illustration of the experimental drift in relation to the deeper parts of the Äspö HRL.*

The floor of the drift was arched to get the highest stress concentration in the centre. After excavation the stress level in the drift floor was approximately 80 MPa (2.7 times the maximum principal stress). The pillar was now created by boring two large holes with a diameter of approximately 1.75 m. The holes were spaced so that a 1 m wide rock pillar was created between them, Figure 1-2. The stress level in the upper part of the hole was now increased to 180 MPa (6 times σ1). This was enough to initiate spalling in the upper part of the holes, especially the second-bored one. More details on the design and predictive modelling are found in /Andersson 2003a, Andersson and Martin 2003, Andersson et al. 2004/.

Heating of the rock around the pillar volume induced the stresses needed to propagate the spalling notch further down the hole. The temperature and displacement monitoring instruments were installed before the electrical heaters were turned on. In addition to these instruments, an acoustic emission system was used. This system was installed before excavation of the large holes and was continuously monitored from the time of installation until the experiment was terminated.

LVDT transducers were used for displacement monitoring /Eng and Andersson 2005/. The instruments have very high resolution and accuracy. The displacements caused by spalling were measured at four different levels in the open hole.

Thermocouples placed in the large holes and cored boreholes around the pillar volume monitored the temperature.

Confinement was achieved by imposing water pressure on the first-bored large hole. This was done before the second hole was bored. The effect of confinement soon became clear as boring of the second hole began. There were acoustic responses in the upper part of the second hole but not in the first confined hole.

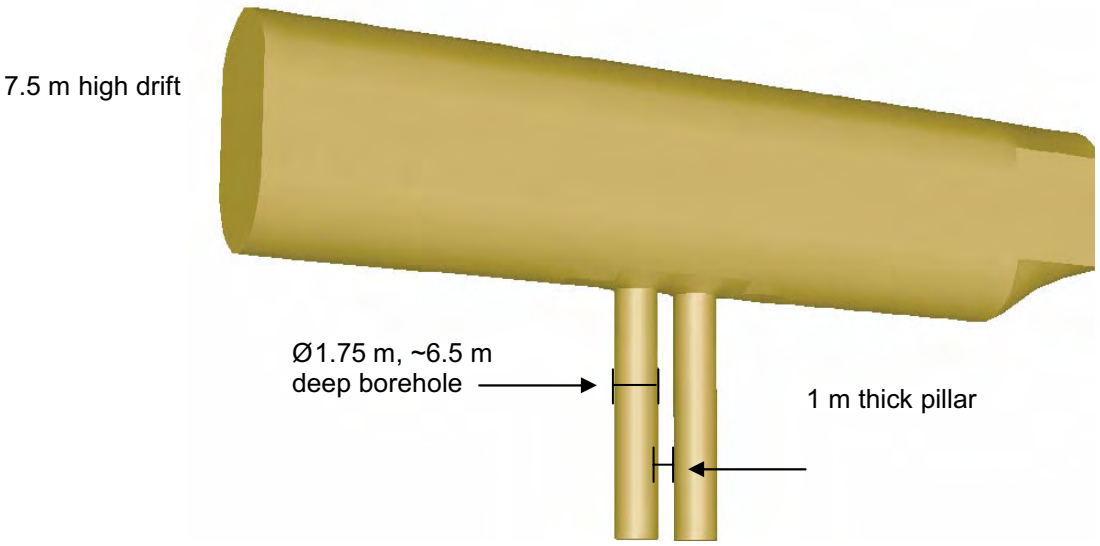


***Figure 1-2.*** *Geometry of the experiment drift.*

## 1.1 Rock behaviour

As an introduction to the presentation of the monitoring results, an overview of the response in the pillar to the heating is presented. Figure 1-3 shows the accumulated acoustic activity and the temperature at a depth of 3.5 m in the borehole between the heaters on the right side. As can be seen in the graph, the acoustic events occur in clusters with many events followed by reasonably quiet periods. When the deformations are presented later in this report, it will be clear that the deformations follow the same pattern.

To show how the notch propagates downwards with temperature and time, the locations of the acoustic emission hits during the most of the heating phase are presented in Figure 1-4. There are approximately 16 days of accumulated AEs in each figure. Only the AEs recorded during the period for each figure are included. The effect of confinement can be seen clearly in the figure on the lack of events in the confined hole.

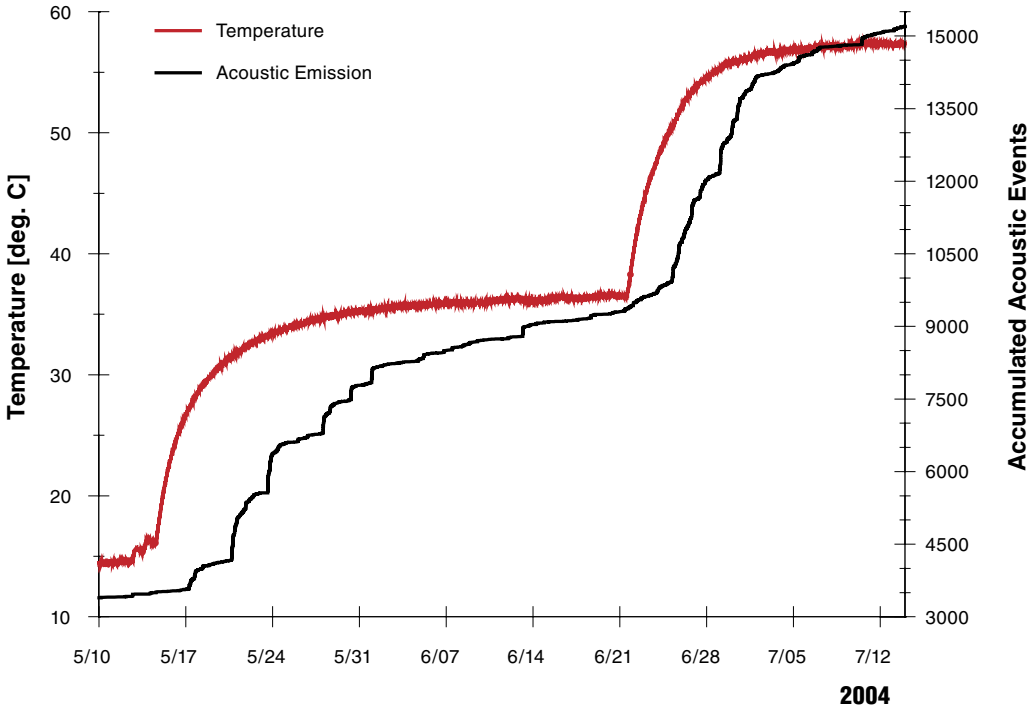


***Figure 1-3.*** *Temperature measured at a depth of 3.5 m in the cored borehole between the heaters on the right side of the pillar (ID KQ0064G06) and the total accumulated acoustic emission. Note how the acoustic emission increases in increments.*

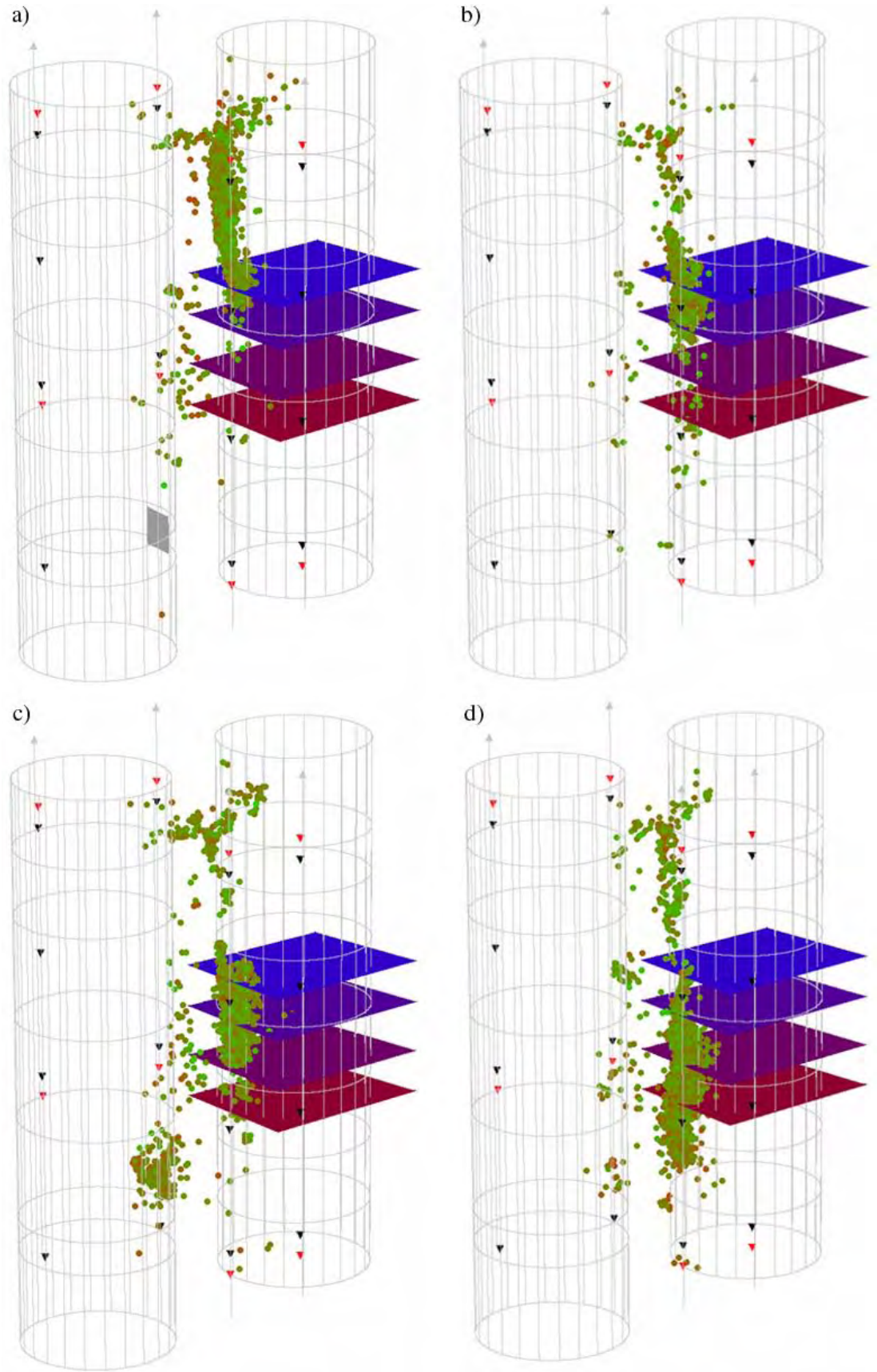


***Figure 1-4.*** *Accumulated acoustic emission divided into the four periods of the experiment. The instrument levels are indicated by four horizontal planes. The left hole is the confined one, and only a fraction of the AEs are located there, indicating the effect of confinement. The periods are in chronological order a) 040510–040525, b) 040526–040610, c) 040611–040626, d) 040627–040713.*

# 2 Geotechnical setting

The experimental drift and the large holes have been excavated in Äspö diorite, which is the typical rock type at the HRL. The diorite at the experimental site is, however, not as fresh as in the rest of the HRL. There are volumes with oxidized rock and a minor shear zone close to the experimental volume. The fractures in the mylonite shear zone are healed, but they nevertheless comprise tentative planes of weakness. The oxidized rock also appears to have a somewhat lower strength than the fresh diorite. The geology and mechanical properties of the rock in the experimental drift are thoroughly described in /Staub et al. 2004, Magnor 2004/.

## 2.1 Rock mass properties

Fourteen 7.5 m deep cored boreholes were drilled to permit determination of the rock mass properties and assessment of the suitability of the target area. The boreholes were logged/filmed by the BIPS system and the cores were geologically mapped. Extensive laboratory testing of thermal and mechanical properties was performed on pieces from those cores. The results of the laboratory testing are presented in /Staub et al. 2004/ and are summarized in Table 2-1. The onset of dilation (Crack Initiation Stress) was interpreted using strain gauges and acoustic emission monitoring.

The deformation properties of the rock volume can be summarized as: Young's modulus 55 GPa and Poisson's ratio 0.26 (derived from convergence measurements).

**Table 2-1. Summary of the uniaxial compressive strength and deformation properties of Äspö Diorite.**

| UCS [MPa] | Tensile strength [MPa] | CIS [MPa] (compressive tests) | CIS [MPa] (AE measurements) |
|---|---|---|---|
| 211 | 15 | 96 | 121 |

## 2.2 Rock stress

Extensive rock stress measurements using different techniques have been performed for other projects in very close proximity to the experimental drift /Janson and Stigsson 2002/. To confirm these results and get a good assessment of the deformation properties of the rock mass close to the pillar volume, convergence measurements where preformed during access drift excavation. The round lengths were reduced to 2 m, where convergence measurements were obtained. The results were back-calculated using the boundary element code Examine3D to derive the best fit for elastic modulus and stress tensor /Staub et al. 2004, Andersson et al. 2003/. The results obtained from the model is presented in Table 2-2.

**Table 2-2. Recommended stress magnitudes and orientations derived from backanalysis of the convergence measurements.**

| | Magnitude (MPa) | Trend (deg) | Plunge from horizontal (deg) |
|---|---|---|---|
| $\sigma_1$ | 30 | 310 | 00 |
| $\sigma_2$ | 15 | – | 90 |
| $\sigma_3$ | 10 | 220 | 00 |

## 2.3 Geology of pillar walls

The geological mapping of the large holes and the five pillar blocks is documented in /Hardenby 2005/. The mapping of the parts of the large holes that created the pillar sides is presented in general terms in this section.

The geology of the pillar walls is quite varying, consisting of Äspö diorite altered in different ways. The upper part of the pillar is dominated by the ductile shear zone. The rock in the shear zone is completely oxidized and generally brecciated and healed with epidote. There are also partially mylonitized areas. As the distance to the shear zone increases the alteration of the rock decreases. At some locations, outside the volume affected by the shear zone, there are a few brecciated zones with mylonite bands.

Excerpts from the geological mapping covering the pillar sides are presented together with their legend in Figure 2-1 to Figure 2-3.

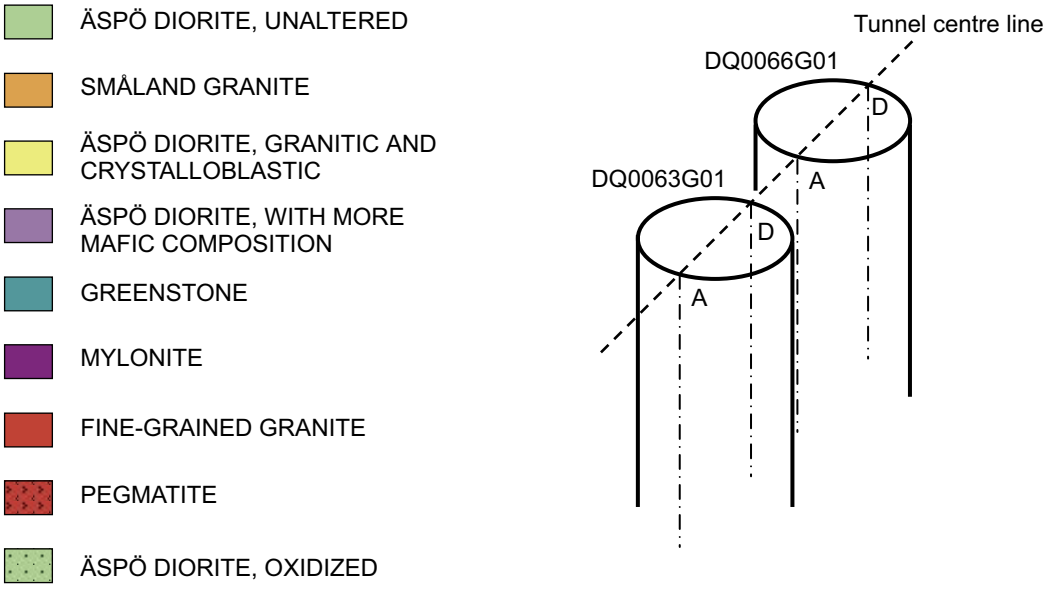


***Figure 2-1.*** *Legend for the geological mapping of the parts of the large holes that form the pillar walls. The sketch illustrates the vertical lines "A" and "D" in the Figure 2-2 and 2-3 in relation to the pillar geometry.*

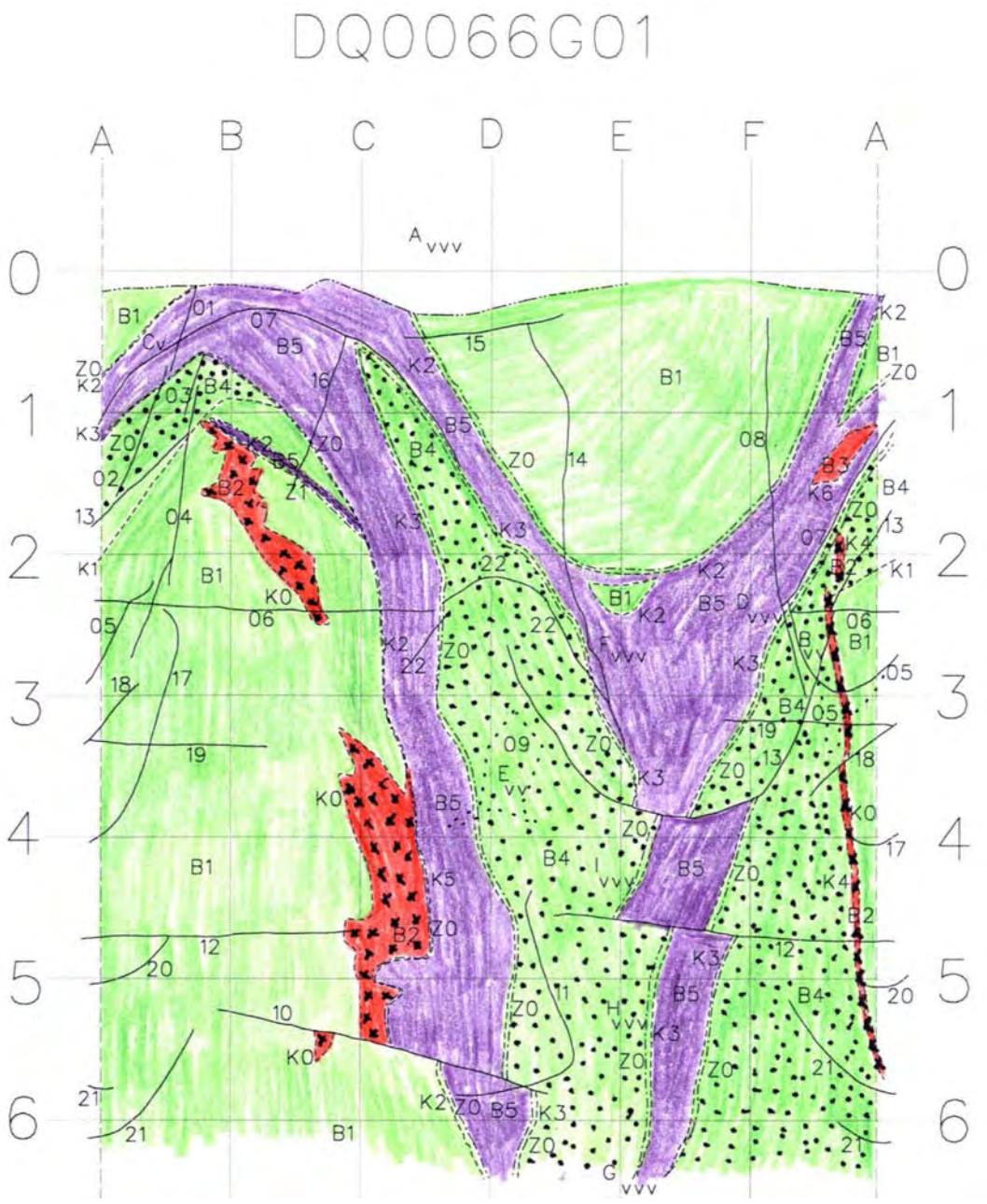


***Figure 2-2.*** *Geological mapping of the pillar side of DQ0066G01, the confined large hole. The vertical line "A" corresponds to the centre of the pillar (Figure 2-1).*

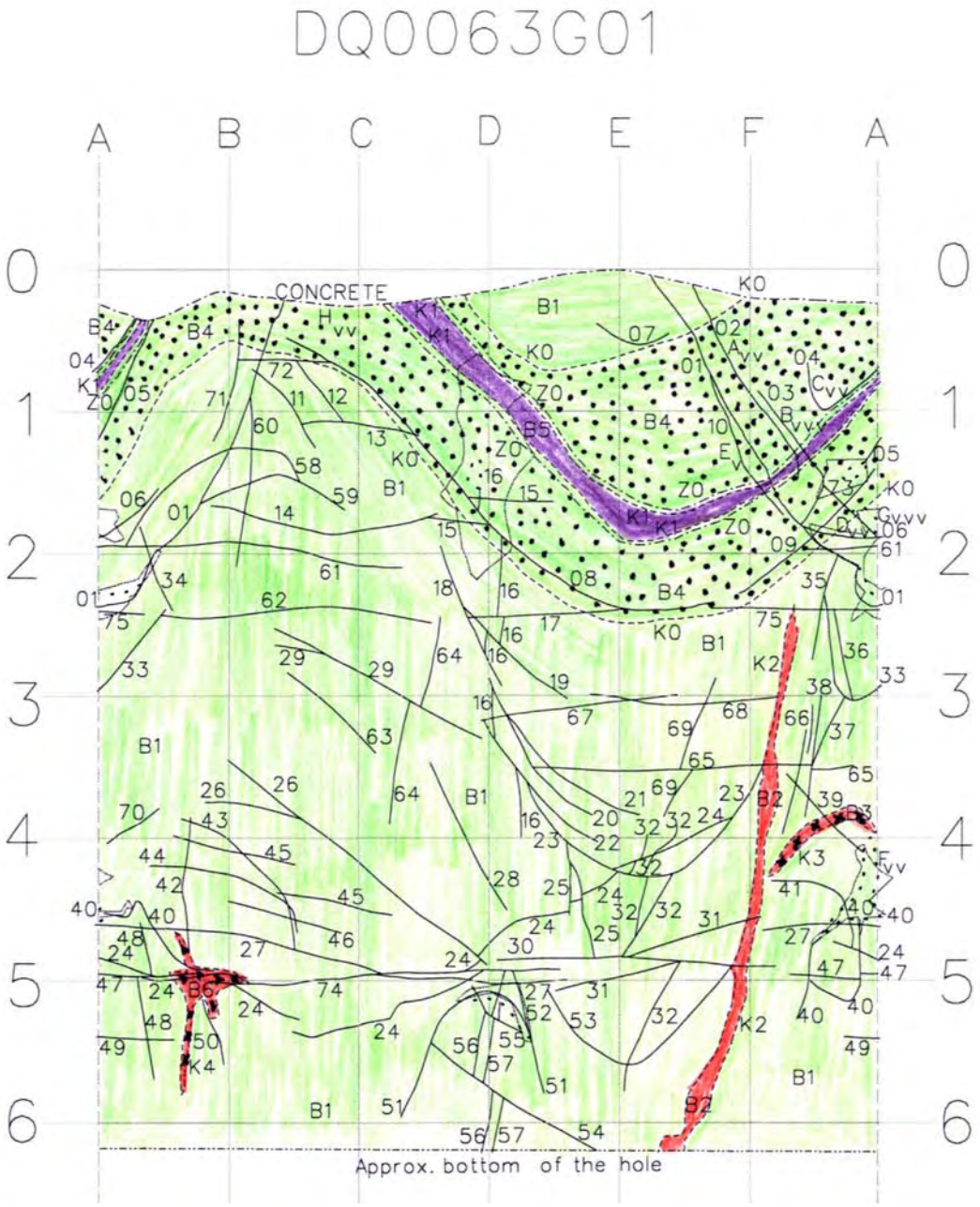


***Figure 2-3.*** *Geological mapping of the pillar side of DQ0063G01, the open large hole. The vertical line "D" corresponds to the centre of the pillar (Figure 2-1).*

# 3 Experimental set-up

The general design of the experiment has been described in /Andersson 2003a, 2003b/. Temperature and displacement monitoring equipment and installations are described in /Eng and Andersson 2005/, and the acoustic monitoring system design in /Haycox 2005/. This section will therefore not examine the design aspects of the experiment in detail but present an overview of it.

## 3.1 Geometry

The design chosen for the drift should ensure to elevate the stresses beneath the centre of the tunnel floor. The two large holes bored close to each other further increased the stress in the pillar created between them. After boring of the large holes the stresses should be elevated to a level close to initiation of spalling. The closer to the spalling limit the stress level caused by the geometry gets, the less thermal power needs to be applied to the rock to propagate the spalling. To maximize the geometry-induced stresses, the drift was oriented perpendicular to the major principal stress direction. The floor was arched to get the maximum stress concentration in the centre of the floor where the pillar should be located. The floor was excavated smoothly by a separate bench /Olson et al. 2004/. The choice of pillar width was not trivial. A thin pillar would be more stressed but also more sensitive to small-scale variations in geology. The finally width chosen was a compromise between these two variables.

The cored boreholes drilled for heater and instrument purposes were placed in order to get the best possible coverage with the acoustic system. The acoustic holes are therefore placed closest to the pillar to ensure that the waveforms originating from the pillar are not distorted by other boreholes and that those boreholes do not generate noise that would disturb the monitoring of AE events in the pillar.

### 3.1.1 Drift and large boreholes

A section of the experimental drift was surveyed every five meters along the tunnel. Chainage TASQ0065 which is almost directly over the centre of the pillar is presented in Figure 3-1, the total height is approximately 7.5 m and the width 5.5 m.

The depths of the large boreholes are not exactly equal. The inner hole, DQ0066G01, which was confined, was bored to a depth of 6.5 m. The outer open, instrumented hole, DQ0063G01, was bored to 6.2 m. The reason for this was that the boring machine did not work very well at the end of the boring due to technical problems and the penetration rate was therefore very low. An elastic 3D model of the stress distribution between the two holes indicated that the effect of a 30 cm difference in hole lengths was small and only present in the bottom of the pillar. To save time it was therefore decided to stop the boring at 6.2 m. The mean diameter of the large holes is approximately 1.75 m. The centre-to-centre distance between the two holes approximately 0.5 m below the tunnel floor is 2.78 m, which gives an actual pillar width of 1.03 m. The pillar width was surveyed at certain depths, and the results is presented in Table 3-1.

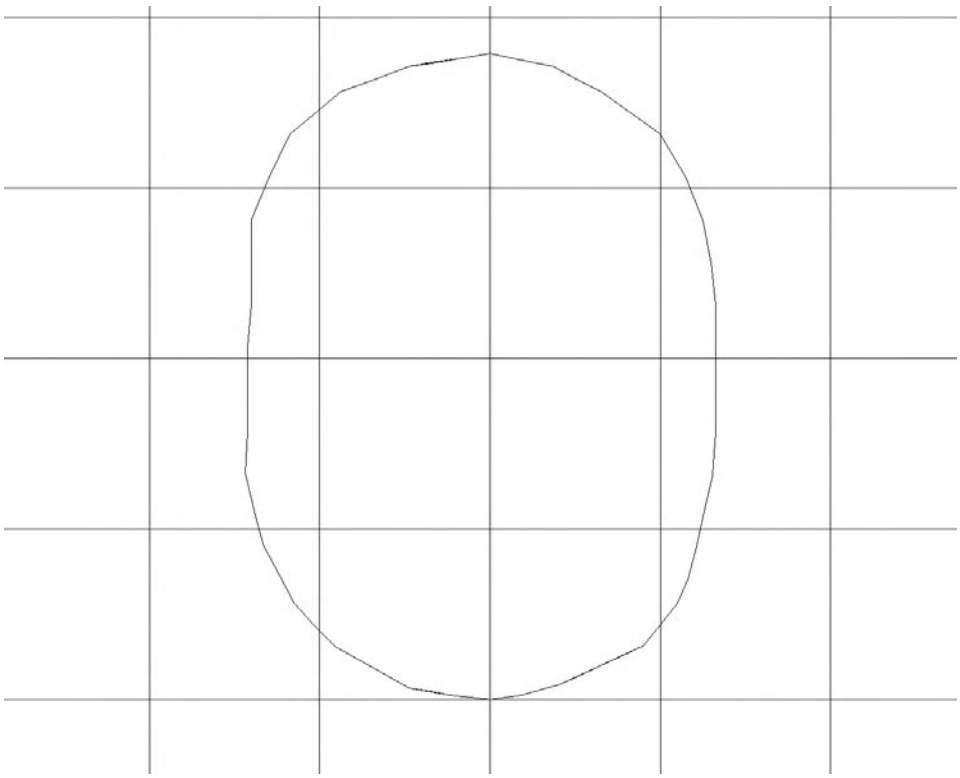

***Figure 3-1.*** *Section of the experiment drift fallen from section TASQ0065, which is almost directly above the centre of the pillar. Note the arched floor. The grid spacing is 2 m.*

**Table 3-1. Measured pillar width. Numbers are missing between the depths –0.62 and –2.22 m where spalling took place during boring. The excavation equipment produces slightly undulating walls why the pillar width varies some.**

| Depth (m) | Hole depth (m) | Pillar width (m) |
|---|---|---|
| –446.29 | –0.22 | 1.011 |
| –446.69 | –0.62 | 1.047 |
| –448.29 | –2.22 | 1.054 |
| –448.69 | –2.62 | 1.061 |
| –449.09 | –3.02 | 1.054 |
| –449.49 | –3.42 | 1.060 |
| –449.89 | –3.82 | 1.061 |
| –450.29 | –4.22 | 1.063 |
| –450.69 | –4.62 | 1.079 |
| –451.09 | –5.02 | 1.063 |
| –451.49 | –5.42 | 1.068 |
| –451.89 | –5.82 | 1.055 |

### 3.1.2 Cored boreholes

Twelve cored boreholes were drilled close to the pillar for heating and instrumentation purposes. All holes except KQ0064G08 are drilled vertically. KQ0064G08 is drilled with a plunge of 60 degrees to the northwest. In Table 3-2 the location of the boreholes, including the large confined hole, is presented in relation to the centre point of the large hole DQ0063G01, the open instrumented hole. A plan view of the boreholes is given in Figure 3-2.

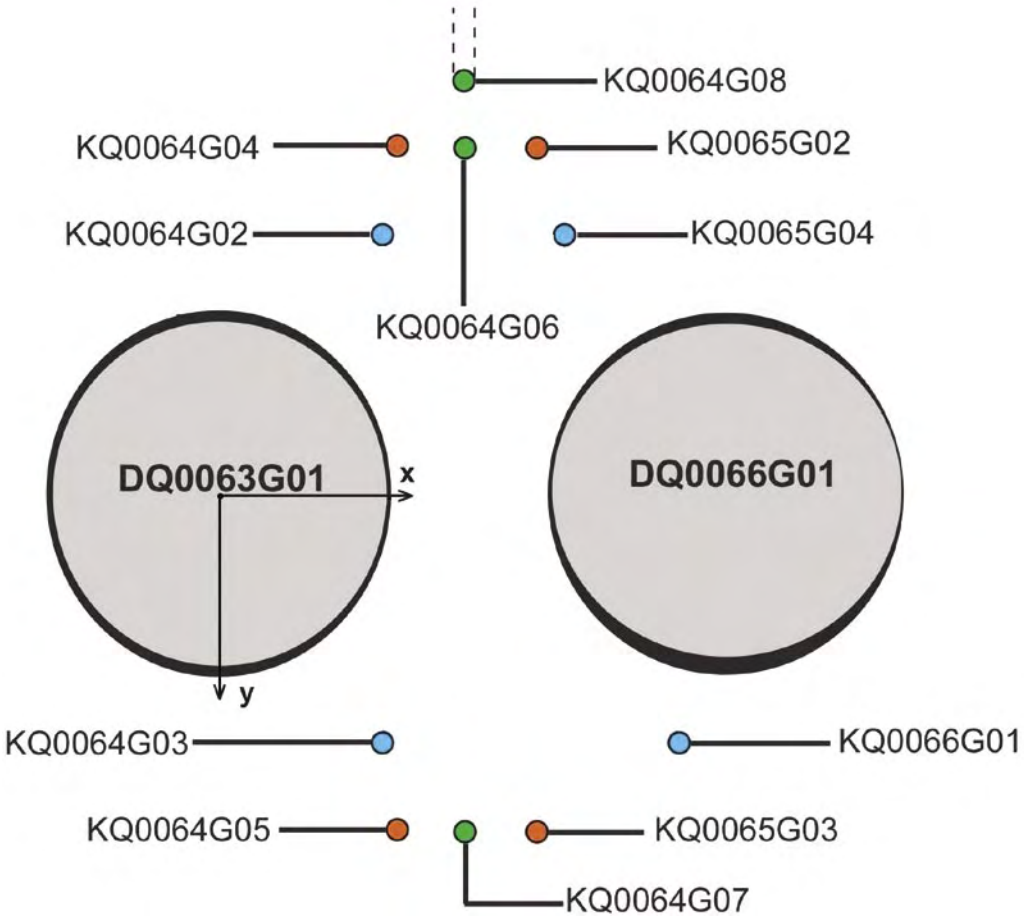


***Figure 3-2**. Plan view of the cored boreholes drilled for heating and instrumentation purposes close to the large boreholes. The boreholes were drilled for temperature monitoring – green, heaters – red, AE-system – blue.*

**Table 3-2. The location of the cored boreholes and the confined large hole in relation to the centre of DQ0063G01.**

| Borehole ID code | Distance along tunnel axis (m) (x) | Distance perpendicular to tunnel axis (m) (y) | Purpose of hole |
|---|---|---|---|
| DQ0066G01 | 2.783 | 0.030 | Displacement and temperature monitoring |
| KQ0064G02 | 0.917 | –1.377 | AE |
| KQ0064G03 | 0.924 | 1.460 | AE |
| KQ0064G04 | 1.024 | –1.859 | Heater |
| KQ0064G05 | 1.024 | 1.903 | Heater |
| KQ0064G06 | 1.413 | –1.849 | Temperature monitoring |
| KQ0064G07 | 1.415 | 1.929 | Temperature monitoring |
| KQ0064G08 | 1.401 | –2.090 | Temperature monitoring |
| KQ0065G02 | 1.801 | –1.857 | Heater |
| KQ0065G03 | 1.823 | 1.929 | Heater |
| KQ0065G04 | 1.928 | –1.373 | AE |
| KQ0065G05 | 1.915 | 1.426 | Not used |
| KQ0066G01 | 2.624 | 1.447 | AE |

## 3.2 Heating equipment

Electrical heaters were used for heating the pillar. The heaters had a length of 7 m. The upper 0.5 m part of the heaters was used for the electrical connections and was therefore not heated. The heaters are rated at 3000 W. In order to avoid large currents they are powered by AC 400V rather than AC 230V. The diameter of the heater is 14 mm, the diameter of the connection is 16 mm. The material used is steel, SS 2348 (AISL 316L). The maximum power output of the heaters corresponds to approximately 460 W/m.

Since the environment is extremely corrosive, the heater casings were protected as an extra precaution. The heaters were placed in copper tubes which were sealed at the bottom, ensuring that the heaters themselves not were in contact with the saline water. For added redundancy in the system, two separate electrical heaters were put into each of the four boreholes. The extra heaters were never needed.

The outer diameter of the copper tubes was 25 mm, and the cored boreholes into which they were placed had a diameter of 76 mm. To improve the connection between the heaters and the rock, the holes were filled with sand after the heaters were installed. To avoid cooling by air convection between the copper pipe and the heater, a rubber plug was inserted at the top. A photograph of parts of the installation coming up from the hole is shown in Figure 3-3.

***Figure 3-3***. *Photograph of the packer pipe and the heaters coming up from KQ0065G03 (Figure 3-4). The left photograph is the typical installation of heaters in the other three holes.*

Thyristor units were used to control the power input to the heaters. The model used was a "TYA-110/3, 025, 400, TR" thyristor. The output of the thyristors is adjustable with a maximum capacity 10,000 W each.

Water was leaking into one of the heaters holes (the others were dry). The rate of water inflow in KQ0065G03 was 5.36 l/min. The water came from a steeply dipping waterbearing fracture intersecting the borehole at a depth of approximately 6.1 m. The water had to be managed somehow, since if it were allowed to flow up the hole along the heaters the cooling effect might have been too great. First it was discussed whether the borehole should be grouted and then re-drilled. If that had been done, it was possible that the water would have taken another path and turned up in another of the heater or instrument boreholes. Injecting grout under high pressure in the hole could also affect the pillar if grout penetrated through interconnected fractures. Another solution was therefore chosen. A packer was placed above the fracture and the water was led through the packer pipe out of the hole. Approximately 0.5 m of grout was placed on top of the packer to insulate the packer rubber from some of the heat from the heater. The heaters were then placed in the hole next to the packer pipe. A sketch of the arrangement is shown in Figure 3-4 and a photograph of the heaters and the packer pipe coming up from the hole in Figure 3-3. The end depths of the electrical heaters in the different boreholes are given in Table 3-3.

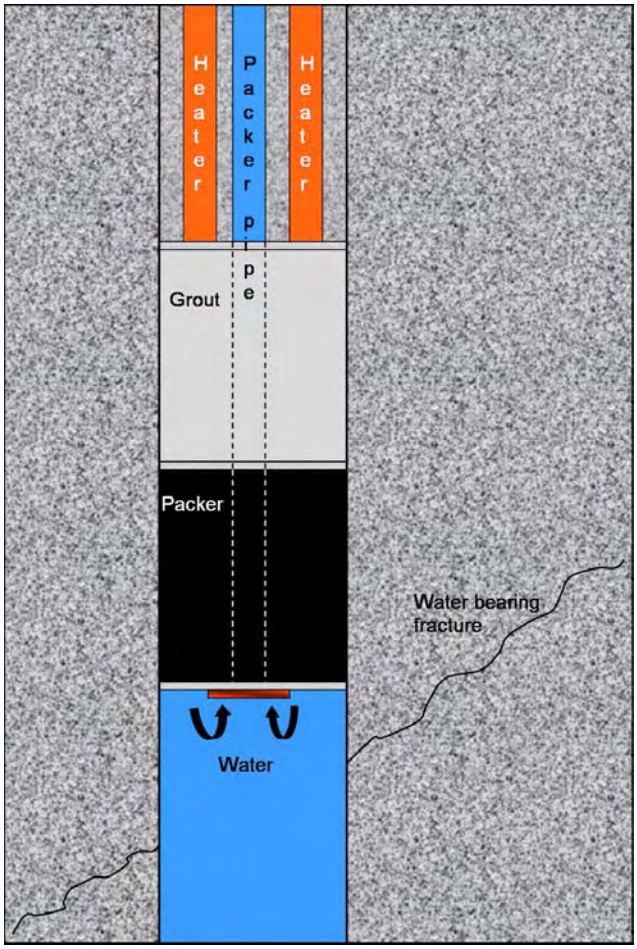


***Figure 3-4.*** *Sketch of the arrangement to evacuate water from KQ0065G03.*

**Table 3-3. End depth of the electrical heaters. The reference depth for the top of the pillar is –446.07 m.**

| Borehole ID | KQ0064G04 | KQ0065G02 | KQ0064G05 | KQ0065G03 |
|---|---|---|---|---|
| Heater end depth (m) | –452.40 | –452.46 | –452.35 | –450.85 |
| Effective heater length (m) | 6.5 | 6.5 | 6.5 | 5.0 |

### 3.2.1 Insulation

The numerical modelling assumed that the floor of the tunnel was perfectly insulated. To make reality as close to this as possible, the arched part of the tunnel floor was insulated with rock wool. An insulated plywood construction was built on top of the open hole to prevent air convection. In addition, a hut with insulated walls and roof was constructed on top of everything. Figure 3-5 is a photograph of the insulation of the rock floor and the plywood construction on top of DQ0063G01.

***Figure 3-5****. Photograph of rock floor insulation and the insulated plywood construction placed on top of the open hole (DQ0063G01) to prevent air convection.*

## 3.3 Confinement

An important part of the experiment was to study how the confinement pressure affects the strength of the rock mass. Water was chosen to apply the confinement pressure in one of the holes. Since the pressure in the confinement equipment should be 0.7 MPa (0.8 MPa including atmospheric pressure), it was necessary to have a membrane between the water and the rock wall to prevent water from leaking through existing fractures. The membrane needed to be rather flexible to avoid point loads on the hole wall and thus provide a uniform pressure. It was also necessary to design a structure to keep the pressurized water in the hole. This structure was not trivial, since the cross-sectional area of the hole is approximately 2.5 $m^2$, and a 0.7 MPa pressure acting on that area gives a force of 1,750 kN. A self-bearing structure that didn't need to be anchored to the rock in any way was chosen. The general idea of the structure was to use a rubber bladder as a membrane. The bladder was confined by steel lids at the top and bottom connected by load-bearing textile straps. The structure is visualized in Figure 3-6 to Figure 3-9. The length of the total package was approximately 6 m. It was very important that the rubber bladder should be totally confined by the steel lids and the textile straps. If there were a tiny opening somewhere in the structure the rubber would expand through it and burst due to the high pressure.

A pressure vessel filled with water connected to a nitrogen gas cylinder via a pressure reducing valve was connected to the steel lid and the rubber bladder by a flexible hose, Figure 3-9. The pressure reducing valve was set to the appropriate pressure, 0.7 MPa in this case, and the same pressure was transferred to the bladder. When the pillar was heated the water expanded, and to maintain the pressure in the bladder water had to be released to protect the integrity of the structure as well as to provide a uniform confining pressure in the hole. This was mainly done by hand, but as a precaution a safety valve was put on the lid. A pressure transducer was placed on top of the steel lid. The transducer was connected to the data acquisition system, permitting constant monitoring of the pressure in the hole.

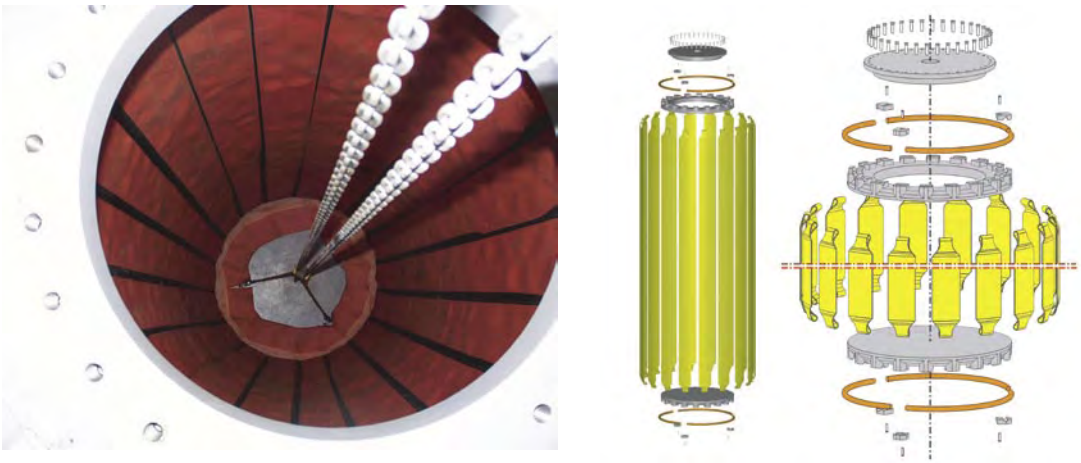

***Figure 3-6.*** *Left: the confinement equipment that held the rubber bladder membrane; right: Microstation drawing of the equipment. The load-bearing textile straps are orange/red in the construction and yellow in the drawing.*

***Figure 3-7.*** *Photographs of the steel lids.*


***Figure 3-8.*** *Photograph of the top steel lid with man-hatch after installation. Note the location of the pressure transducer, the safety valve and the connection point for the tubing from the pressure vessel.*

***Figure 3-9.*** *Photograph of the pressure vessel connected to a gas cylinder. The flexible Tecalan tube in the photograph is connected to the bladder via the top steel lid and ensures the pressure in the bladder.*

## 3.4 Water inflows

There were water inflows in three of the cored boreholes, all located on the right side of the pillar. There were also inflows in both of the deposition holes. The inflows are listed in Table 3-4.

Before the experimental drift was excavated, an exploratory cored borehole was drilled parallel to the tunnel axis. Water flow and temperature measurements were conducted in that borehole. The water temperature at the approximate section of the pillar was between 14 and 14.5°C.

**Table 3-4. Measured water inflow in large and cored boreholes in the experimental volume.**

| Hole ID | KQ0065G03 | KQ0065G05 | KQ0066G01 | DQ0063G01 | DQ0066G01 |
|---|---|---|---|---|---|
| Inflow [l/min] | 5.36 | 6.21 | 2.0 | Estimated 10–13 | 30.5 |

## 3.5 Temperature and displacement monitoring

In the predictive numerical modelling done before the excavations started, the maximum depth for spalling after heating in the open large hole was assessed to approximately 2 m below the tunnel floor. It was therefore planned to start with two instrument levels, one at a depth of 0.5 m depth and the other at 1.5 m. When boring of the second large hole was finished, spalling had already occurred down to 1.95 m, Figure 5-67. This was excellent news since the instrument now could be placed close to the existing failure and increase the possibility of picking up deformations as the notch propagated downwards. The two first instrument levels were therefore positioned at depths of 2.5 m and 3 m.

The notch responded quickly to the heating of the rock and propagated downwards earlier than assessed in the predictive modelling. The instruments at the 2.5 m level started to record dilatation shortly after the heaters were turned on. The notch also propagated faster than was anticipated. To increase the chances of collecting a good data set, four spare short-range LVDTs were mounted at a depth of 3.5 m on day 20. As time progressed the deformations at the 2.5 m level stopped, but the notch was still propagating. Both long- and short-range LVDTs were therefore moved from this level on day 34. The long-range LVDTs were placed just above the transducers at the 3.5 m level, and four of the six short-range LVDTs were moved to a depth of 4.1 m in the hole. The two LVDTs at positions #2 and #5 were left at the uppermost level to measure a possible widening of the spalled zone. The locations of the different sensors are plotted in Figure 3-10.

The details of the monitoring system and instrument specifications are described in /Eng and Andersson 2005/. Small steel plates were glued to the rock wall at each instrument position at the upper two levels (depths of 2.5 and 3 m). The plates gave the instrument tips a smooth surface to measure on. Since the temperature increase in the hole was predicted to be significantly higher than what was actually measured, the steel pipes the LVDTs were mounted on were designed to allow vertical expansion. The alignment of the steel plates was measured before the heating started by moving the pipes vertically during monitoring of the LVDT displacements. During the heating phase, the vertical movement of the centre pipe was monitored to enable the alignment of the plates to be taken into

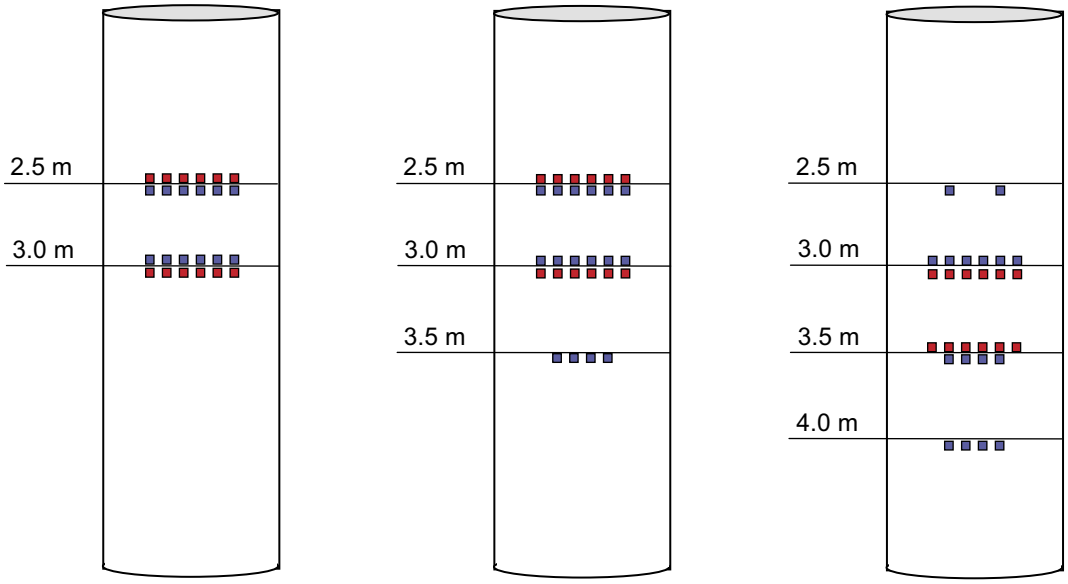


***Figure 3-10**. Complete measurement position layout, both short- and long-range LVDT sensors. Blue indicates a short-range sensor and red a long-range sensor. The left setup is the original; the middle one shows the setup after June 3rd and the right one the setup after June 17th /Eng and Andersson 2005/.*

consideration when calculating the real displacement. However, when the additional two levels of instruments were installed, steel plates were not used. There was one major reason for not using them. The reason was that it would not have been possible to make an alignment check of the plates. To do that the vertical steel pipes should have had to be moved up and down. Doing this would risk accidentally removing rock chips formed around the instrument positions at the first two levels. The measuring series would thereby be discontinuous and the quality of the data at those locations might then be less reliable. The decision not to use the plates was made easier by the fact that as above-mentioned the temperature increase was less than the modelled.

Concern was taken in selecting the exact rock spot for the instruments to measure on. The rough location of an instrument level was first chosen in an area where the hole surface was planar. The boring equipment made ridges in the rock wall at different places, and these were avoided since they can distort the nearby stress field. At suitable levels the geology of the rock was studied in greater detail. The tips of the instrument were not placed over fractures, large feldspar crystals, locally altered rock or close to any discontinuity in the rock.

### 3.5.1 Pillar monitoring

The previous sections explain the background to the sensor position strategy, the strategy for sensor placement and why sensors were moved during the experiment. In the following section, details concerning the sensors and the mounting structure are discussed.

Activity in the pillar is monitored using several different sensor types. The displacement and temperature sensors are presented in this section. In Figure 3-11 the experimental area is shown in plan view. The figure also shows the positions of the heaters and the AE system, which are discussed in other sections of the report.

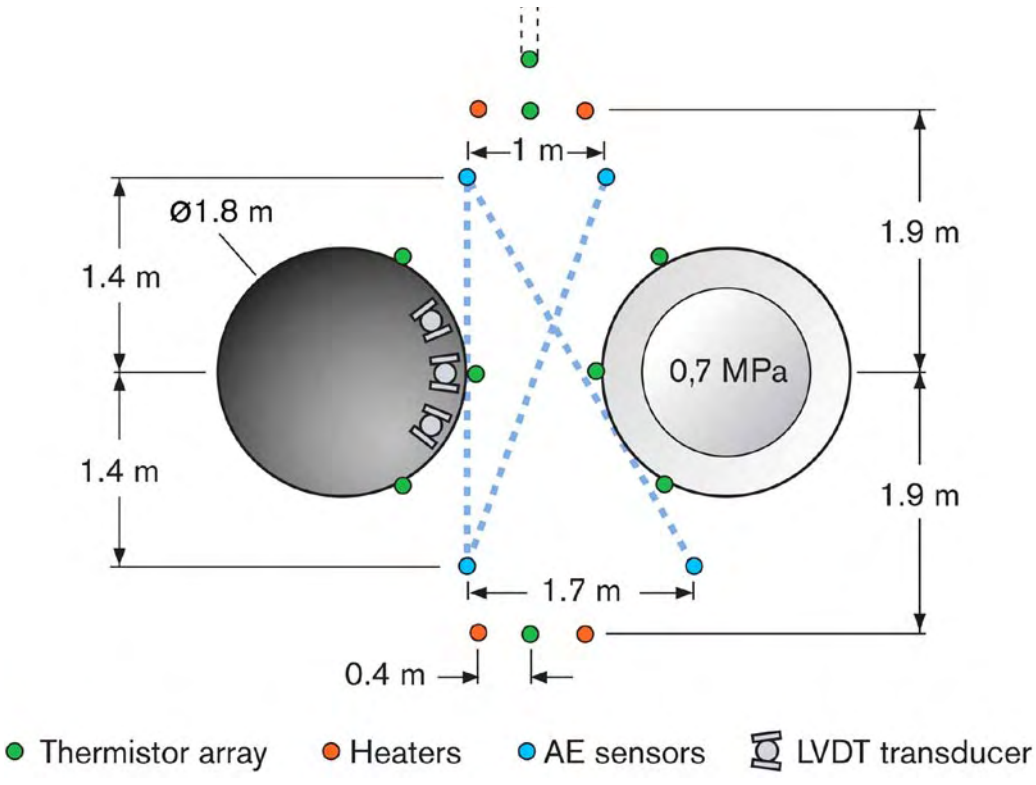


***Figure 3-11.*** *Plan view of the experimental area including the sensor positions.*

### 3.5.2 Displacement measurement

The system used to measure displacements was designed to meet high demands on reliability and accuracy. Besides the sensors, the system consists of a supporting structure that constitutes the foundation of the sensor mounting and a clamp on which the sensors are mounted. The different elements of the system are described below.

#### *LVDT sensors*

Pillar displacement was measured with Linear Variable Differential Transformer, LVDT, sensors. To be able to measure very small movements with extremely high accuracy, an LVDT type with an accuracy of 0.006 mm was used. The active range of that sensor was only 12 mm, however. A second type of LVDT with a longer measurement range, 40 mm, was therefore considered. The long-range LVDT has somewhat lower accuracy, however, about 0.025 mm. To maintain both high accuracy and a long measurement range, it was decided that both LVDT types should be used at the same time. More information about the sensors and their specifications is found in /Eng and Andersson 2005/.

#### *Supporting construction*

Several issues had to be considered during construction of the sensor supporting structure. The pillar must not be reinforced at any position, so the structure could not be attached to the pillar walls. The calculated temperature rise in the hole was also considered. The predicted temperature increase of 50°C made thermal expansion of the material an issue.

The final solution was to use three vertical pipes as the base of the structure. The pipes are secured at the hole bottom and above the hole. Pipe positioning in the experimental area is shown in Figure 3-12. The slimness of the pipes made them sensitive to both deflection as well as vibration. For that reason the pipes had to be stabilized. This was done by mounting two crossbars in the centre of the hole at depths of two and four meters. This placement does not reinforce the pillar. Sturdy steel plates were then used to connect the crossbars with the pipes. The crossbars and the plates are illustrated in Figure 3-13. More information can be found in /Eng and Andersson 2005/.

Thermal expansion of the material inside the large hole could not be prevented since the temperature increase was a part of the experiment. This left the option of calculating in advance the thermal expansion of all parts of the supporting structure and making sure that the effects would not jeopardize the measurements. A detailed description of the thermal effects as well as calculations are found in /Eng and Andersson 2005/.

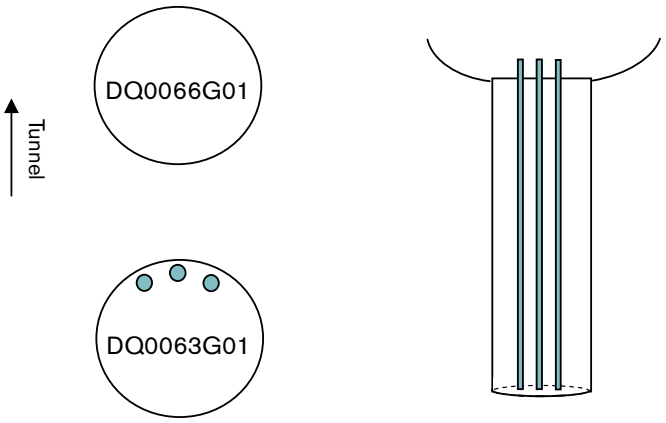


***Figure 3-12.*** *Overview of pipe positioning.*

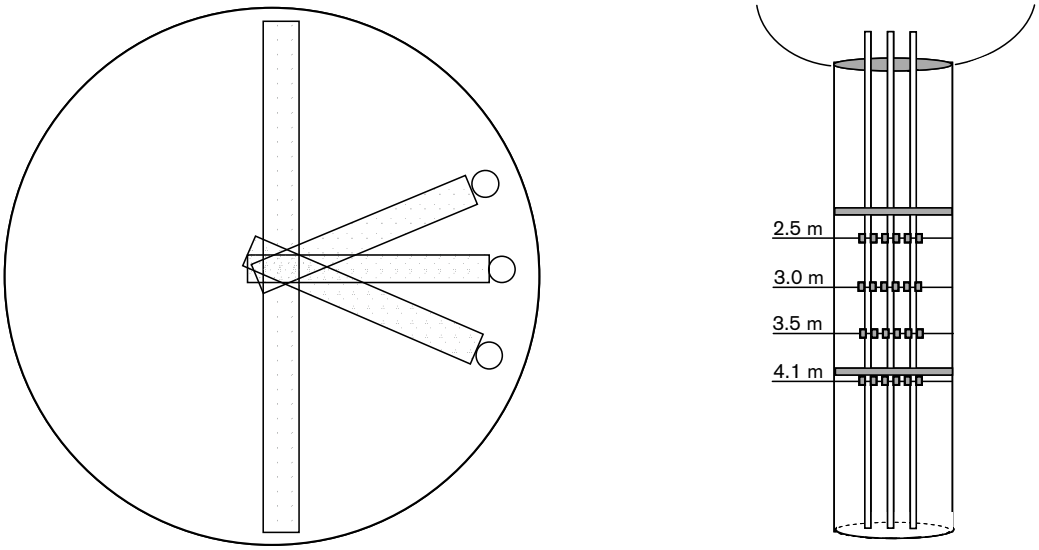


***Figure 3-13.*** *The stabilizing crossbars and the plates connecting them with the pipes inside the large hole. In the right image the vertical position of the crossbars is shown, the sensor positions are also marked in the figure.*

### *Mounting*

Besides the general supporting structure, a device that holds the sensor in place is also needed. The device had to meet the reliability requirement while allowing the sensors to be adjustable in height, angle and length. The solution was to use a clamp around the pipes and attach to that clamp a small plate to which the sensor is fastened. This solution meets the requirements and also makes mid-experiment changes possible. The clamp is shown in Figure 3-14.

During the experiment the stability of the device was questioned. The original setup was therefore modified when additional sensors were installed. The new solution uses the same parts that clamp around the pipes, but now standard aluminium hose clamps are used instead of the small plates. The new setup is shown in Figure 3-15. Only the short-range sensors were fitted with the new clamp solution. The measured data showed no changes in behaviour with the new clamp. The data collected with the original solution are therefore considered to be correct.

### *Positions*

A total of 24 positions were used for LVDT measurements in the normal direction to the hole wall. To make the measurements between the two LVDT types as comparable as possible, the sensors were mounted close together. Hence there are two sensors at each measurement position. The measurement depths in the large hole are approximately at 2.5, 3.0, 3.5 and 4.1 metres (relative to –446.07 m, which is the reference level of the floor). One additional LVDT was placed over the shear zone in the upper part of the hole. The sensor was mounted to measure eventual displacements along the zone. It was placed at approximately 0.30 m depth to the left of the pillar centre, Figure 3-16. The exact depths of the sensor levels are shown in Table 3-5. The positions are also shown in Table 3-5.

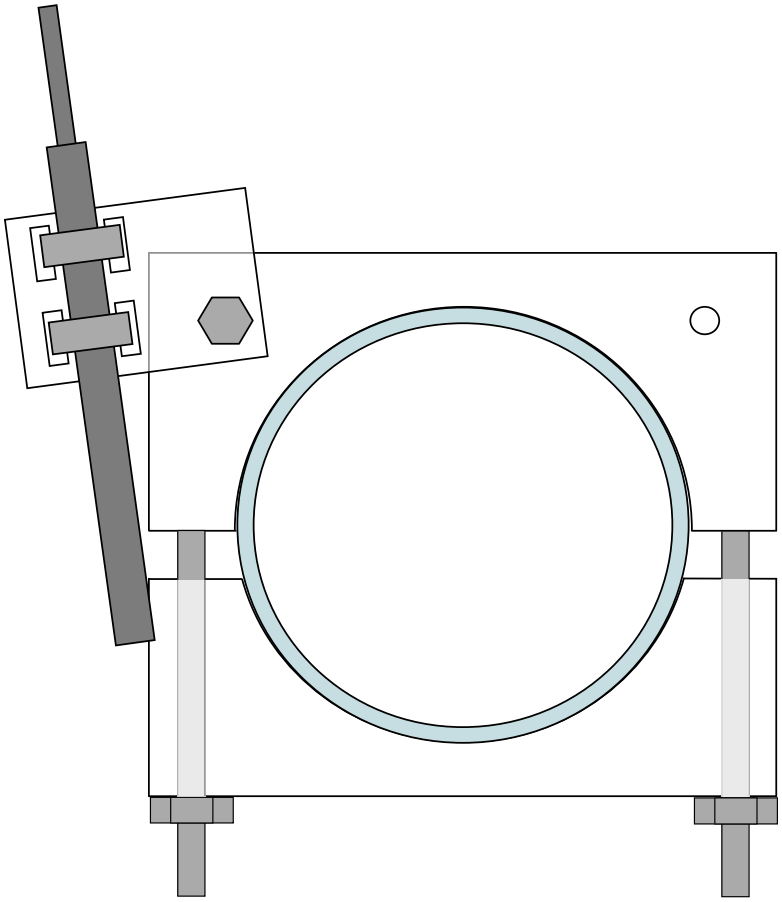

***Figure 3-14.*** *The sensor holding device equipped with one LVDT sensor. The device allows the sensors to be individually adjusted.*

***Figure 3-15.*** *The new clamp. The top sensor is the short-range LVDT and the lower ones are the long-range LVDT sensors. Only the short-range sensors were fitted with the new clamp system.*

***Figure 3-16.*** *Short range LVDT placed over the shear zone.*

**Table 3-5. Sensor row depths. Here a distinction is also made between the two sensor types.**

| Level | Position # (from left) | Sensor type | Depth [m] (below –446.07 m) |
|---|---|---|---|
| Shear zone | | Short range | 0.30 |
| 1 | 1–6 | Long range | 2.46 |
| 1 | 1–6 | Short range | 2.52 |
| 2 | 2–12 | Short range | 2.99 |
| 2 | 2–12 | Long range | 3.07 |
| 3 | 13–18 | Long range | 3.50 |
| 3 | 14–17 | Short range | 3.58 |
| 4 | 20–23 | Short range | 4.10 |
| 4 | – | Long range | Not installed |

The horizontal distance between the sensors is about 0.15 m, which makes the total width of the measured area 0.75 m, corresponding to an angle of about 48°. Figure 3-17 shows the sensor alignment both from above and as seen from the side. For detailed information on the sensor positions and the separation between the short- and long-range positions see /Eng and Andersson 2005/.

### *Calibrations*

Prior to installation, all sensors used were calibrated for accuracy. The short-range sensors were calibrated by AECL and the long-range sensors by the manufacturer. The complete calibration sheets can be found in /Eng and Andersson 2005/.

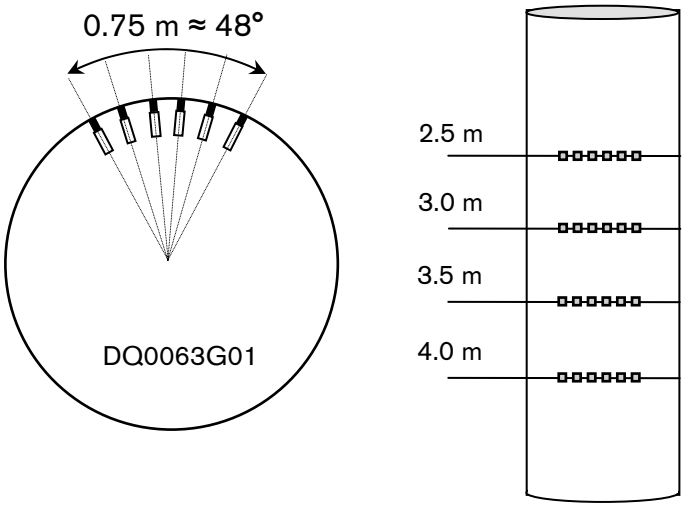


***Figure 3-17****. The LVDT sensor geometry in the large hole seen from above and from the side.*

### 3.5.3 Temperature sensors

Propagation of the temperature in the rock mass was monitored using 30 thermocouples, distributed spatially around the pillar. The large holes, both the open hole and the confined hole, were equipped with nine sensors each. These sensors measured the rock temperature at the pillar wall. In the open hole, two sensors were also used to monitor the air temperature during the experiment. The remaining ten sensors were placed in the cored boreholes. The vertical layout of the temperature sensors is shown in Figure 3-18, and the horizontal layout is shown in Figure 3-11. The temperature sensors are shown in green in both figures.

The temperature sensors were also calibrated by the manufacturer to ensure correct readings.

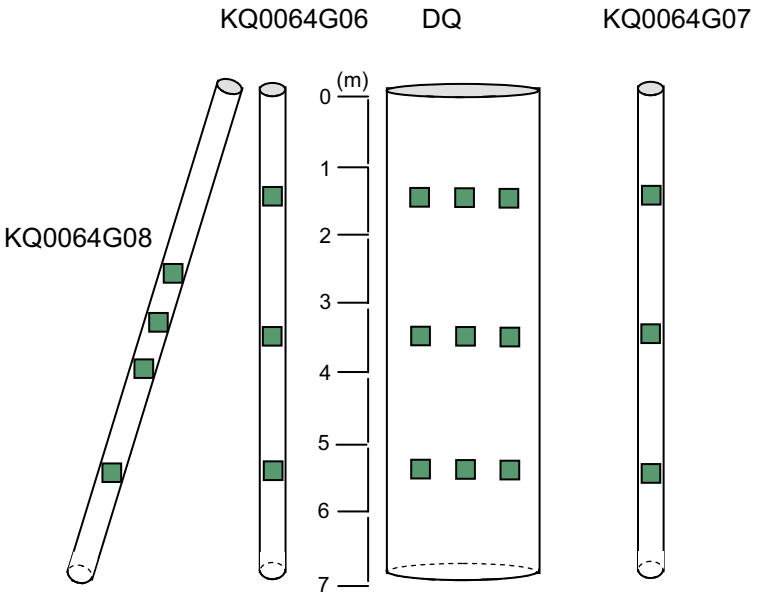


***Figure 3-18.*** *Thermocouple layout. The figure shows the vertical layout of the sensors. The layout of the sensors in the both large holes (DQ0063G01 and DQ0066G01) is identical, so only one large hole is shown.*

### 3.5.4 Sources of error

The sources of error for the displacement readings are mainly temperature-dependent. When the temperature increases the supporting structure is affected, and the pipes plates and crossbars are subject to thermal expansion. The sensors are subject to temperature-dependent drift. These factors must be addressed in the post-experiment analysis, and calculations have been made to adjust the values accordingly. Different aspects of this issue and calculations are found in /Eng and Andersson 2005/.

As an example, the thermal effect of a five degree temperature increase is calculated to be less than 0.1 mm for the interesting centre positions.

## 3.6 Acoustic monitoring

The ultrasonic array consists of twenty-four ultrasonic transducers mounted on four borehole frames, Figure 3-19, /Haycox et al. 2005/. Each frame contains two transmitters and four receivers. The frames are installed in vertical 76 mm diameter boreholes approximately 8 metres in length distributed to monitor the pillar between the two deposition holes efficiently (see Figure 3-21 for an illustration of the array geometry). The sensors are spring-loaded against the borehole wall for good coupling to the rock, Figure 3-20. The transducers respond to the frequency range 35–350 kHz and are connected to 60 dB pre-amplifiers enclosed in junction boxes at the side of the tunnel. The boxes are dustproof and protected against water infiltration by additional silicon sealant around the cables. Coaxial cables from the boxes are fed through protective tubing to the nearby instrumentation cabin and connected appropriately to the acquisition system.

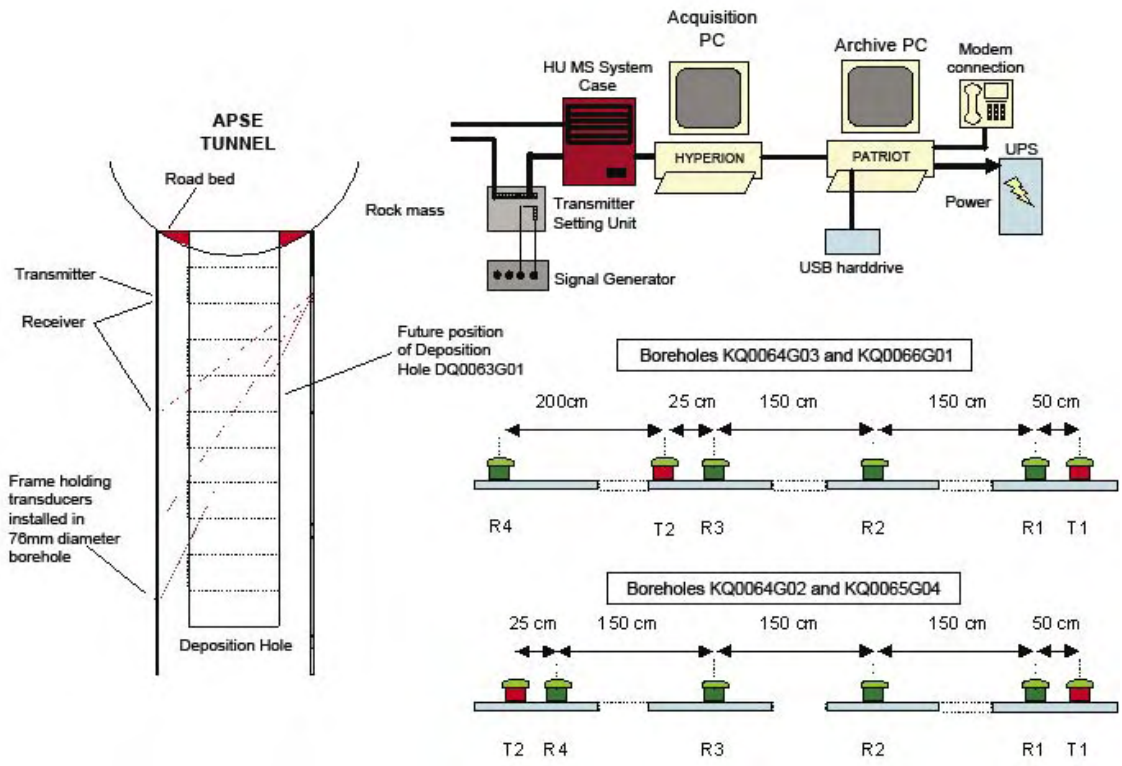


***Figure 3-19.*** *A schematic of the APSE, acquisition system and sensor configuration.*

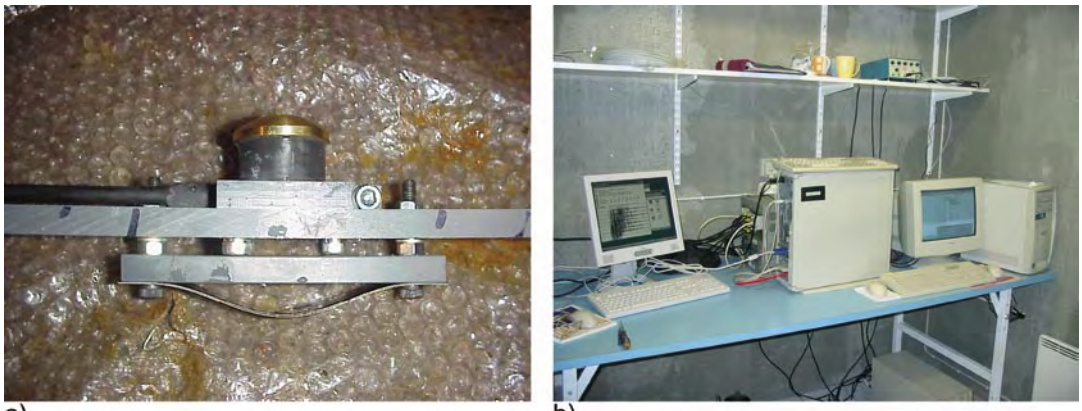


***Figure 3-20.*** *a) A transducer attached to an installation frame. The spring-loaded mechanism is adjustable to obtain the best possible coupling. b) Configuration of AE monitoring equipment in the Q-tunnel cabin.*

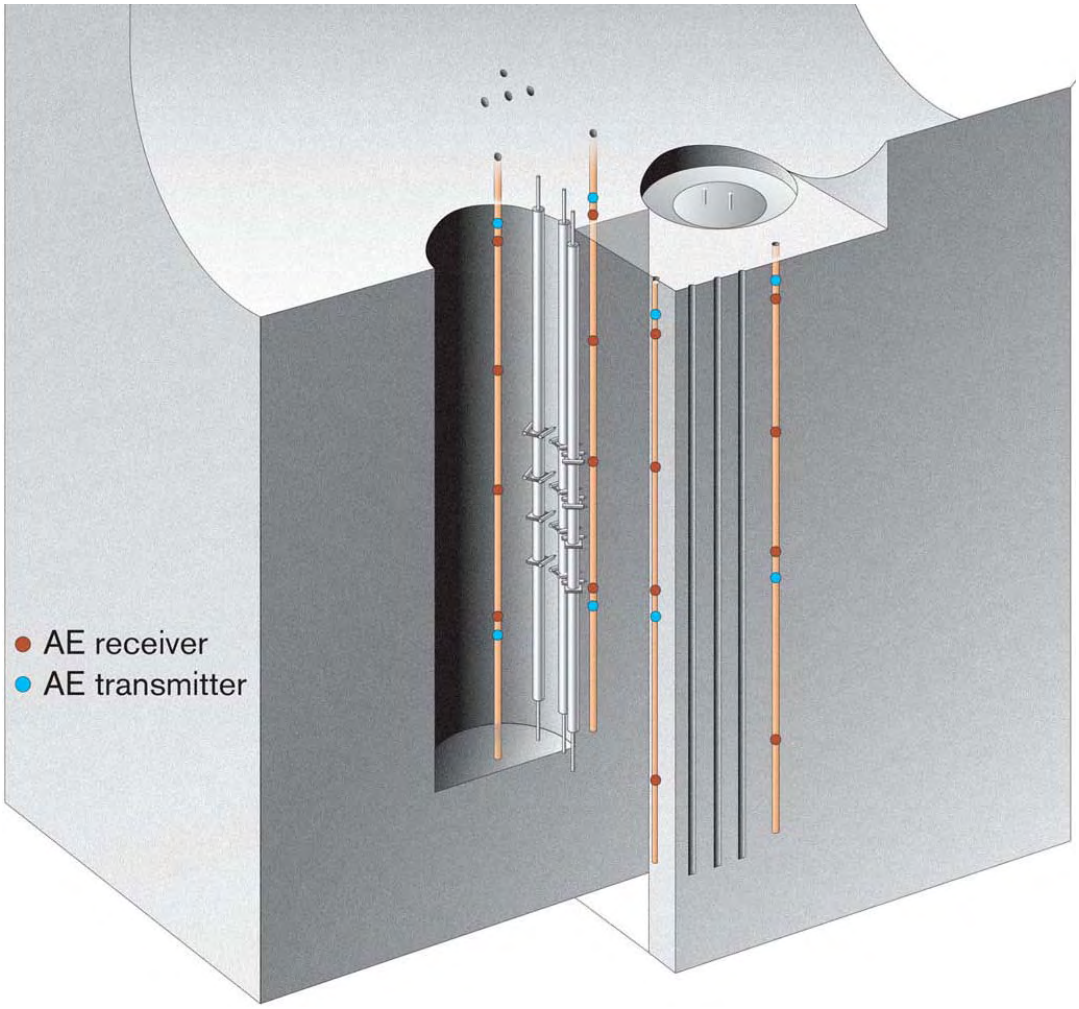


***Figure 3-21.*** *Illustration of the AE array geometry. The large open hole is the left one.*

The AE acquisition system, Figure 3-20, consists of an ESG Hyperion ultrasonic system, a switch-box, a Pa nametrics pulsing unit, an acquisition computer and an archiving computer (both of the PC Pentium type with Microsoft Windows). The acquisition computer is only used for data acquisition and, by using the switch-box, is capable of undertaking automated ultrasonic velocity surveys using each transmitter in turn. Full waveform information is acquired by the hardware and stored to the PC's hard drive. An archiving computer runs ASC's data management and processing software, InSite Seismic Processor. The InSite Leach software utility is used to capture data from the acquisition computer, archive it into a data base and process it 'on-line'. It was possible to remotely dial into the archiving computer to periodically check the data flow and quality. The use of the two computers means that data acquisition is never disturbed by processing and data examination activities occurring on the archiving computer.

The piezoelectric transducers operate by converting a transient elastic wave into an electric signal or vice versa. The monitoring system is then operated in one of two modes. The first was used to passively monitor AE activity preferentially within the array volume. AEs release elastic energy in the same way as 'earthquakes' but over a very small scale. At these frequencies AEs have a moment magnitude (Mw) of approximately –6. They occur either during the creation process of new fractures within the medium, or on pre-existing fractures due to small-scale movements. On the acquisition system an AE event is recorded when the amplitude of the signal on a specified number of channels (in this case 6 channels) exceeds a trigger threshold within a time window of 5 ms. The system then records the signals from all 16 transducers. In this case a trigger threshold of 500 mV on all channels was used. This gives the system sufficient sensitivity to record high-quality data without recording an abundance of activity that cannot be processed (due to a low signal-to–noise ratio on most of the channels). The captured signals are digitized with a sampling interval of 1μs and a total length of 4,096 data points. Background noise levels of approximately 10 mV were observed, giving a good signal-to-noise ratio.

The second operating mode actively acquires ultrasonic waveforms by scanning across the volume. This allows measurements of P- and S-wave velocities and signal amplitudes over a possible 128 different ray paths. By repeating these ultrasonic surveys at increments in time, a temporal analysis can be obtained for the variation in medium properties. A Panametrics signal generator is used to produce a high frequency electric spike, Figure 3-18. This is sent to each of the 8 transmitters in turn. The signal emitted from each transmitter is recorded over the 16 receivers in a similar fashion to that described above. An external trigger pulse from the signal generator is used to trigger the acquisition system and identifies the transmission start time to an accuracy of one sample point. In order to reduce random noise, the signal from each transmitter is stacked 100 times.

## 3.7 Logging of work at the experimental site

The acoustic emission system and the displacement monitoring instruments are very sensitive and hence easily disturbed. To help to ensure the quality of the sampled data, procedures were established for access and work at the experimental site. The experimental drift is 70 m long. A locked gate was set up ten metres into the drift to prevent unauthorized access. When passing the gate a log list was filled in. The list contains particulars on time of entry, kind of work performed and when the site was left again. When visits were made for various reasons in the open hole, the AE-system was switched off to keep the data set as free from noise as possible. These times were noted separately.

All the visits in the open hole affected displacement monitoring. To make it easier to follow the actual displacements over time, a copy of the measured data was filtered. In this case filtering means that man-made disturbances were removed from the data set, making the graphs much easier to read. For this purpose, the data sampled during the disturbed periods were removed. To make the data curves readable, the data after the disturbed period were adjusted, raised or lowered, to the level prior the disturbance. An example of this is shown in Figure 3-22. This makes the data continuous and shows only the total displacements from the start of the experiment. It is important to note that this kind of filtering was only done at times when the log lists stated that some kind of activity had taken place in the open hole. The filtered periods are shown in Appendix 1. The filtering process is described in greater detail in /Eng and Andersson 2005/.

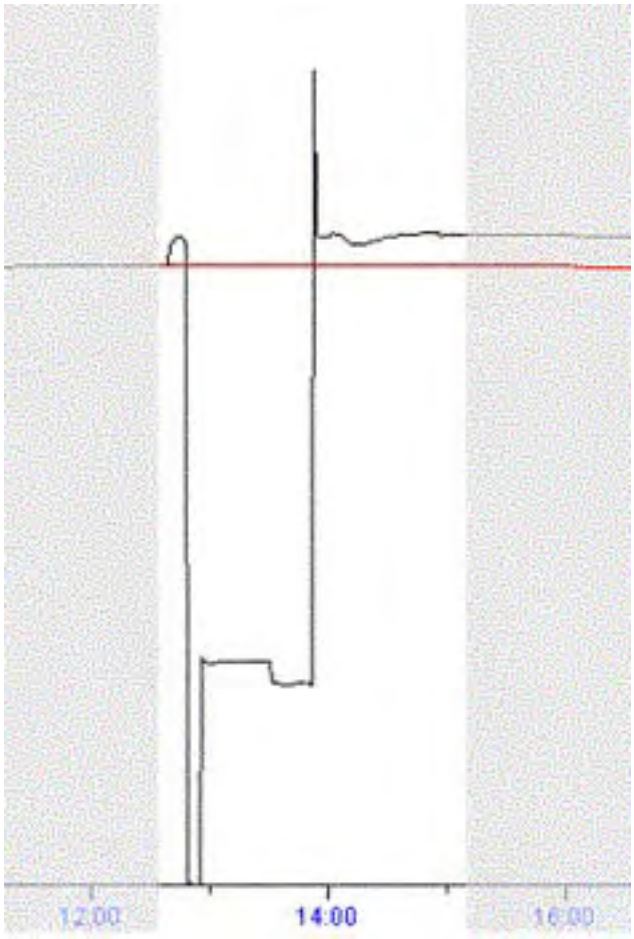


***Figure 3-22.*** *Example of the data filtering process. The white area is considered to be disturbed. The black line represents the measurement data from one sensor during the disturbed period. The red line represents the resulting data after filtering. As the figure shows, the filtering application removes the data from the disturbed time interval and the following data is adjusted so the displacements are the same imediately before and after the disturbed time. The result is a data set that shows only the effective displacements during the experiment.*

# 4 Heating

After two days of in itial tests with the heaters, the heating phase was started around noon on May 14, 2004. During the first couple of days two things became obvious. 1) the heat increase in the rock was much slower than what the models predicted. 2) the temperature between the heaters on the right side increased much slower than on the left side. The reasons are probably the water-bearing fracture in heater hole KQ0065G03 and the measures that were taken to reduce the cooling of heaters, Figure 3-4. This involved positioning the end of that heater at a depth of approximately 5.5 m instead of at 7 m as in the other holes. This is further described in Section 3.2 Heating.

When the temperature on one side is higher than on the other side the thermally induced stress will not be uniform. To make magnitude evaluation of the thermally induced stresses as easy as possible, the power input to the heaters can be adjusted to make the temperature on both sides more uniform. Since spalling started only a few days after the start of heating, we knew that high enough temperatures would be reached to ensure that the spalling would propagate down the hole. It was therefore decided to lower the power input on the warmer left side (without increasing the power input on the right side) to compensate for the temperature differences. An initial compensatory power reduction was done June 1st, after which the temperature on the left side between the heaters decreased about 5°C.

During the second and third weeks in June the temperature was almost constant. The acoustic activity during the third week was relatively low, indicating that a steady state had been reached. At this point in time the spalling had propagated from a depth of 2 to 3 m in the hole (spalling during drilling stopped at 2 m). To collect more data it was desirable to propagate the spalling another 2 m down to a depth of approximately 5 m. To achieve this, the power input to the heaters was almost doubled on June 21st (day 38).

After the power increase the temperature again rose faster on the left side of the pillar. Another adjustment of the power input was therefore necessary, and the input to the left side heaters was reduced one last time. The power input to the heaters during the experiment is shown in Table 4-1. A graph depicts the temperature at a depth of 3.5 m between the heaters on each side of the pillar and at the centre position of the open hole wall, DQ0063G01, at the same depth is given in Figure 4-1. The power reduction to the left side heaters is clearly visible in the temperature graph.

The power to the heaters was turned off on July 19 (day 66).

**Table 4-1. The power per metre of the heaters during the experiment. The heated length of each heater is 6.5 m.**

| Effect (W/m) | Left side heaters | | Right side heaters | |
|---|---|---|---|---|
| Date | KQ0064G04 | KQ0065G02 | KQ0064G05 | KQ0065G03 |
| 2004-05-14 | 200 | 200 | 200 | 200 |
| 2004-06-01 | 170 | 170 | 200 | 200 |
| 2004-06-21 | 354 | 354 | 400 | 400 |
| 2004-06-29 | 263 | 263 | 400 | 400 |
| 2004-07-19 | 0 | 0 | 0 | 0 |

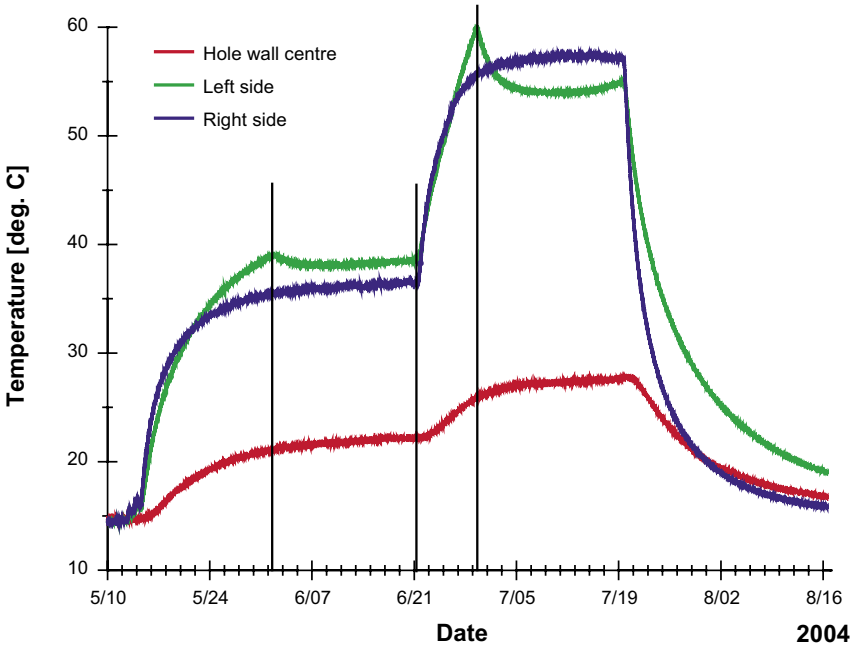


***Figure 4-1.*** *Temperature monitored at a depth of 3.5 m below the tunnel floor. The response of the reduction of the power input to the left side heater is obvious. The dates are indicated by vertical lines. Hole wall temperature from large hole DQ0063G01.*

The temperature of the water evacuated through the packer pipe next to the heater in KQ0065G03 was measured at 16.2°C on July 6th. The temperature increase was approximately 2°C compared with in-situ conditions and the flow rate was 5.36 l/min. This gives a cooling capacity of approximately 747 W. The temperature on the heater surface above the rock was at that time measured to be 250°C.

The temperature between the rock surface and the insulation between the heaters on the left side was measured on 9 occasions between June 23rd and July 6th. The average temperature was 36.5°C. The highest and lowest measured temperatures were 38.8 and 35.5°C, respectively.

# 5 Monitoring

## 5.1 Temperature

A plan view of the temperature monitoring positions is shown in Figure 5-1 and the monitored results are presented under each sub-section. All the depths given in the result graphs are related to the centre of the drift floor.

### 5.1.1 DQ0066G01

The temperatures in DQ0066G01, which was the confined hole, are approximately seven degrees lower than in the open hole DQ0063G01. This is probably due to the water that leaked between the rock wall and the confinement equipment. Most of the water leaking into the hole originates from its lower parts. The water was evacuated along the permeable textile straps. A constant-flowing water curtain was created along the borehole wall which cools it off. The total inflow to the hole is approximately 30 l/min.

From July 14 one can see anomalies in the temperature readings. This is due to the release of the confinement followed by the evacuation of the water from the hole. When the water was pumped out from the hole the temperatures on the hole wall approached the temperatures monitored in the other large hole. The pumping of the water was stopped when AE monitoring of the pressure release was finished. The hole then quickly became flooded resulting in cooling of the hole wall.

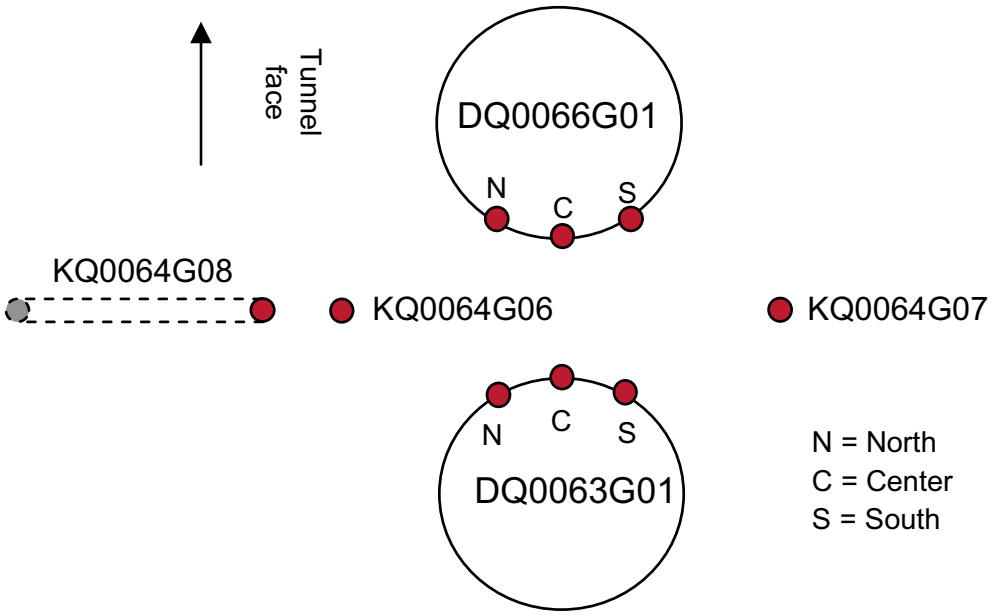


***Figure 5-1.*** *Positions of the thermocouples. The N, C, S markings are used to distinguish positions in the same large hole. Several sensors are placed below each of the marked positions.*

The temperature at position “S” is a few degrees lower than its symmetrical opposite at position “N”. Position “S” includes the measuring points that are closest to the heater in KQ0065G03, which is not completely inserted in the hole due to the water-bearing fracture intersecting at a depth of approximately 5 m. The “S” position is also close to a sub-vertical fracture from which approximately 2.4 l/min leaks into the hole, cooling down the rock some.

The measured temperatures are presented in Figure 5-2 to Figure 5-4.

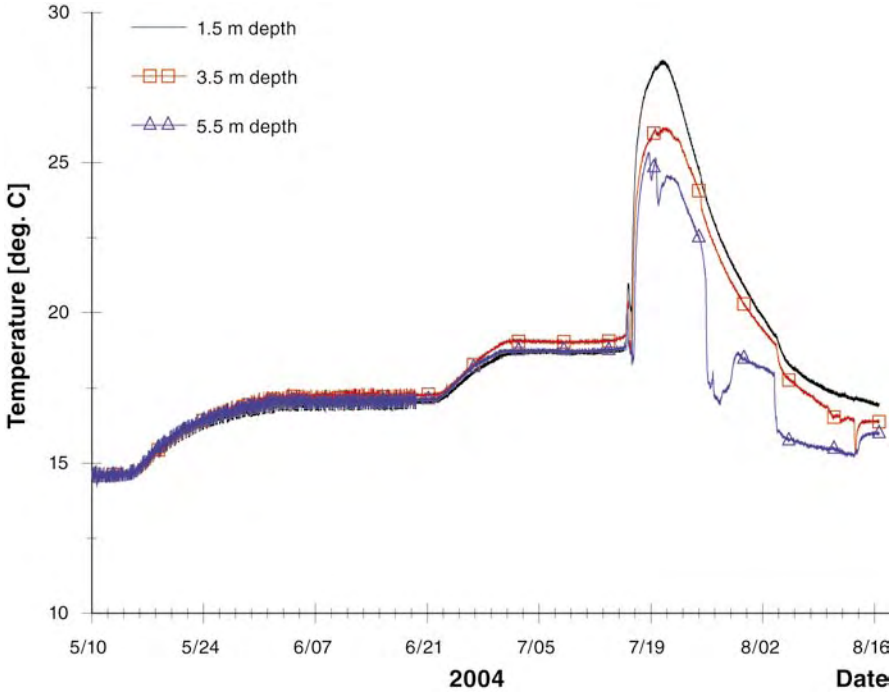


***Figure 5-2.*** *Measured temperatures in DQ0066G01 at position “N”.*

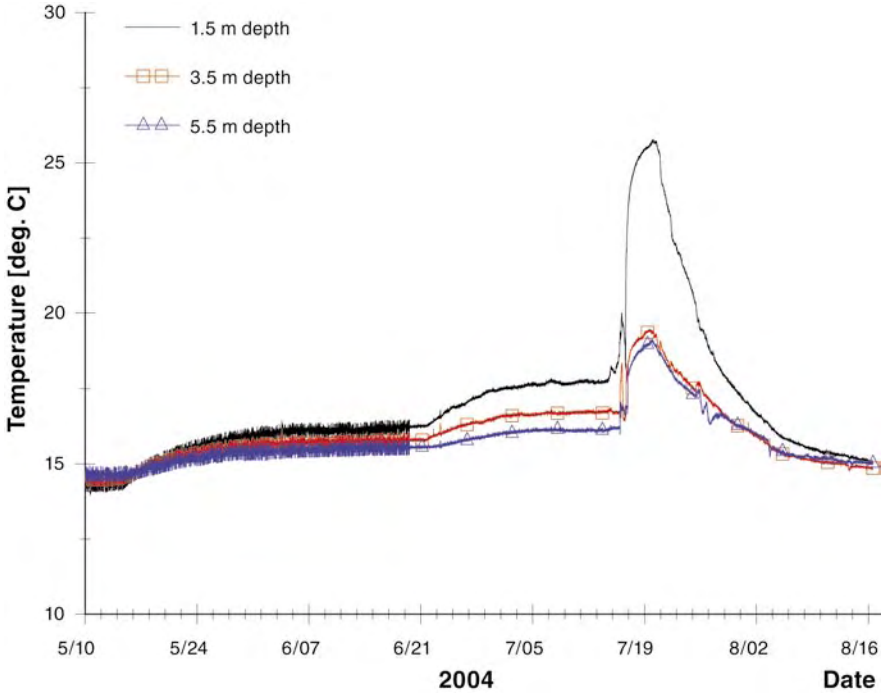


***Figure 5-3.*** *Measured temperatures in DQ0066G01 at position “C”.*

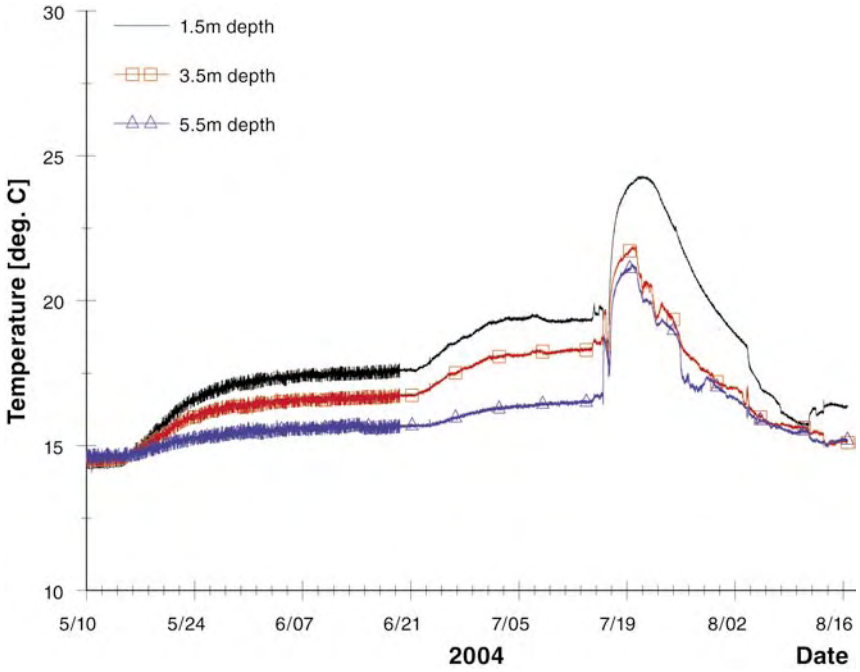


***Figure 5-4.*** *Measured temperatures in DQ0066G01 at position "S".*

### 5.1.2 DQ0063G01

The temperature readings in DQ0063G01 are quite uniform. The temperature at a depth of 5.5 m at position "S" is a bit lower than at position "N", most likely due to the not fully inserted heater in KQ0065G03.

The measured temperatures are presented in Figure 5-5 to Figure 5-7.

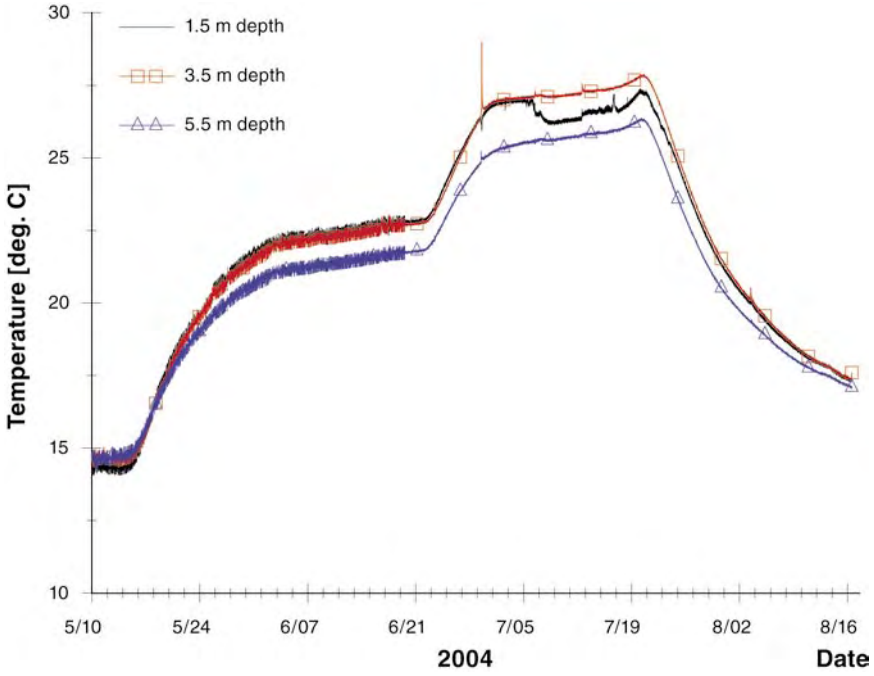


***Figure 5-5.*** *Measured temperatures in DQ0063G01 at position "N".*

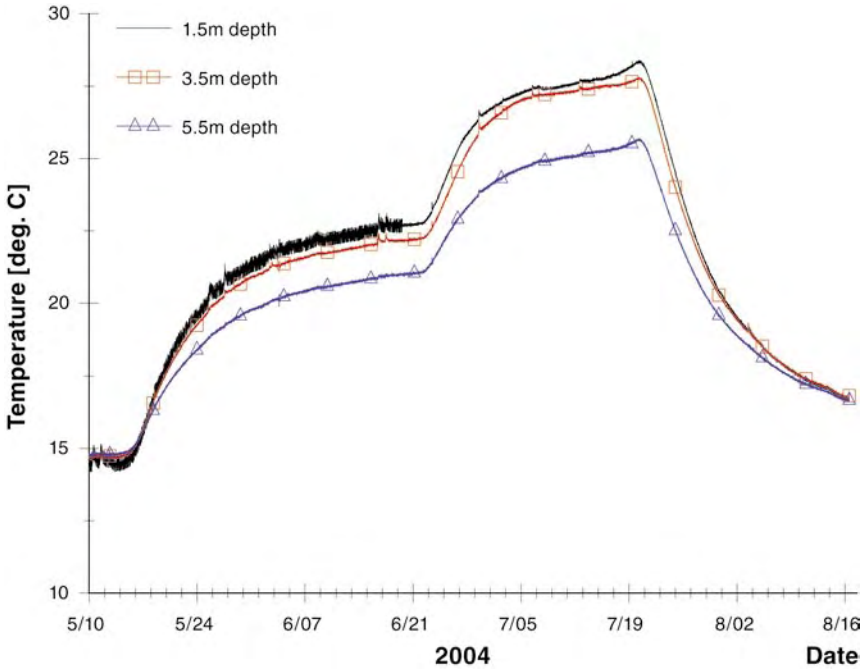


***Figure 5-6.*** *Measured temperatures in DQ0063G01 at position "C".*

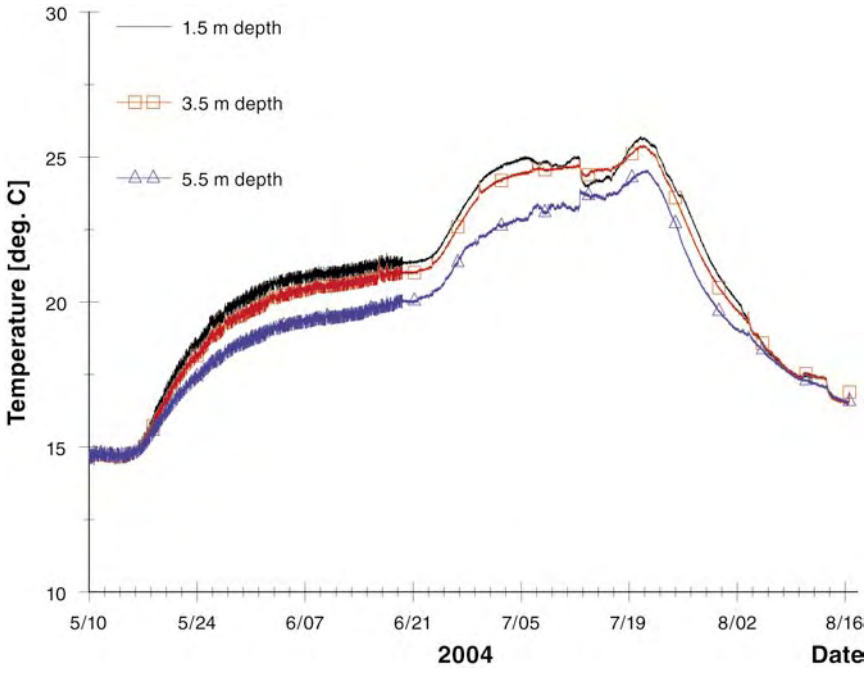


***Figure 5-7.*** *Measured temperatures in DQ0063G01 at position "S".*

### 5.1.3 KQ0064G06, between the heaters on the left side

This borehole is located midway between the tw o heater holes on the left side of the tunnel when looking at the face. The c/c distance between this hole and the heater holes is 0.40 m.

The measured temperatures are presented in Figure 5-8. When studying the results one can see that the temperature at 5.5 m depth is higher than at 3.5 m depth. This should not be the case since the thermocouple at 3.5 m is in the centre of the heated volume. No geological explanations have been found. The installation of the thermocouples was double checked before the heating started. The anomaly was noted after all the installations were removed again and a specific check could therefore not be done. Photographs of the installations does not indicate that the thermocuples were coupled to the wrong data taker. The other temperature readings from this borehole are therefore considered correct. It is recommended that the readings from the 3.5 m level not is used in analyses unless an explanation is found.

### 5.1.4 KQ0064G07, between the heaters on the right side

This borehole is located midway between the two heater holes on the right side of the tunnel when looking at the face. The c/c distance between this hole and the heater holes is 0.40 m. The temperature differences between the three different depths are greater here than on the left side, most likely due to the not fully inserted heater and the water-bearing fracture.

The temperature at a depth of 1.5 m was reduced for a few days starting on June 26. During this time steam was rising from the heater holes. The reduced temperature is probably due to the fact that the water in the holes started to boil. When all the water had evaporated the temperature started to increase again and that's what we can see on July 28.

The measured temperatures are presented in Figure 5-9.

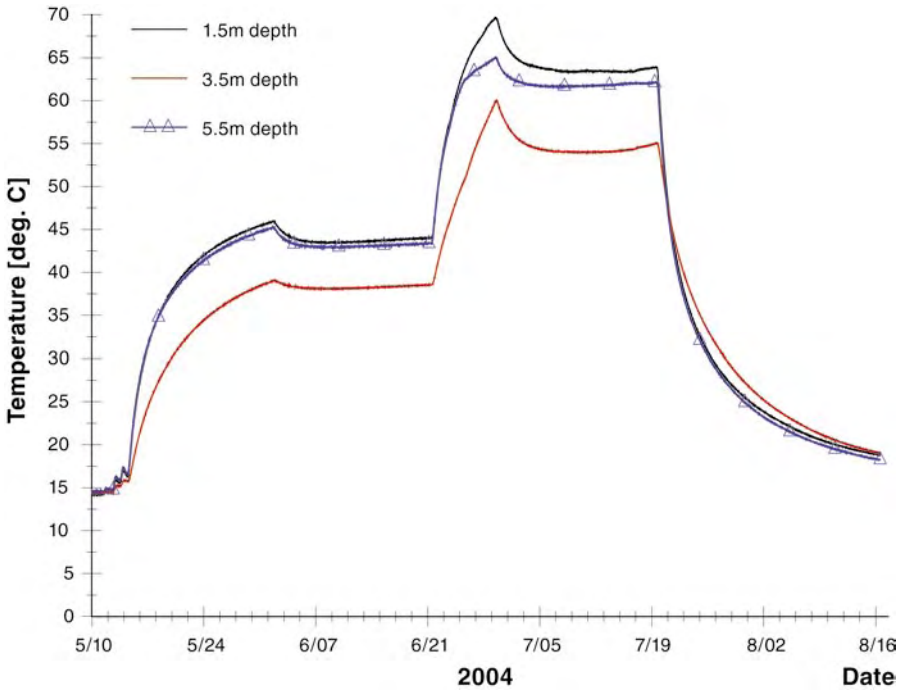


***Figure 5-8.*** *Measured temperatures in KQ0064G06.*

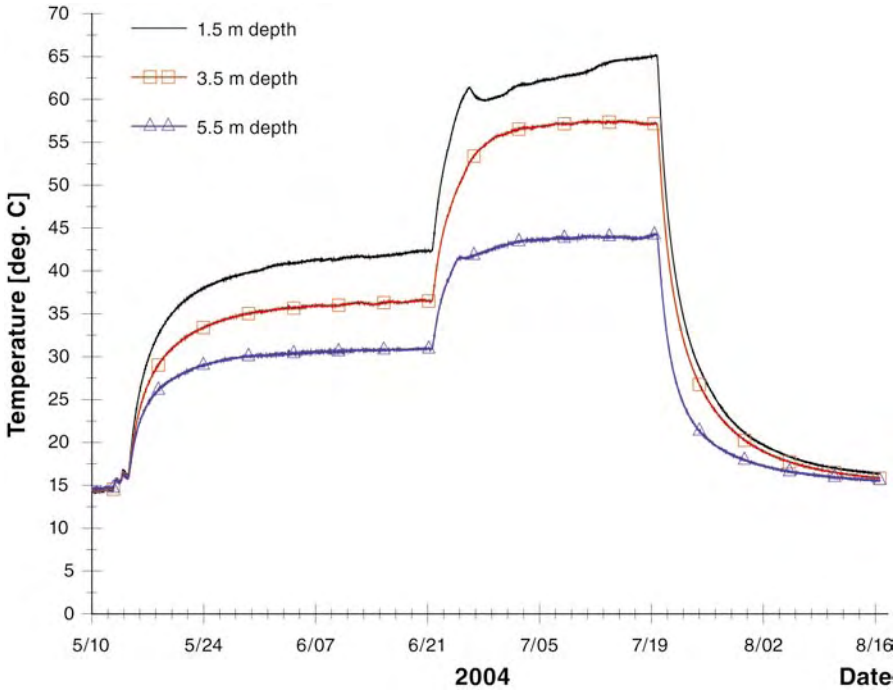


***Figure 5-9.*** *Measured temperatures in KQ0064G07.*

### 5.1.5 KQ0064G08, the inclined hole on the left side

KQ0064G08 was drilled to monitor temperatures a bit further away from the pillar and can be used for any calibration of temperature modelling that might be necessary at a later stage. The measured temperatures are presented in Figure 5-10.

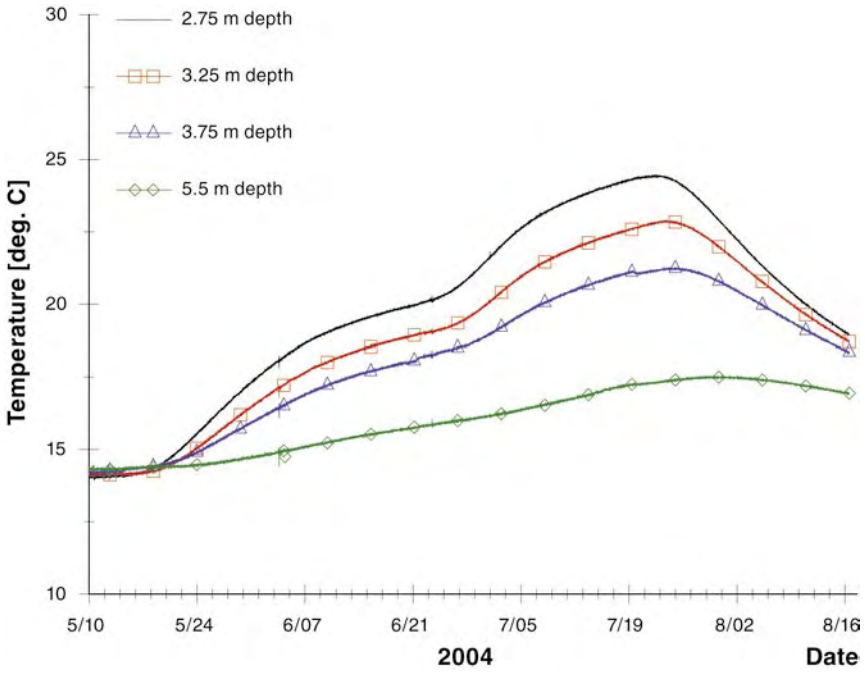


***Figure 5-10.*** *Measured temperatures in KQ0064G08.*

## 5.2 Displacement

The readings from the different LVDTs and the other transducers were stored in the data acquisition system once every minute. The time the displacements occurred is therefore known to the minute. The clock for this monitoring system and the one for the acoustic emission system differed less than 1 minute, depending on when in the experiment cycle the comparison is made. One can therefore say that the acoustic events that were picked up correspond to the displacements at that time.

In this section the displacements for selected instrument positions are plotted versus time. In Figure 5-12 to Figure 5-15 the displacements for the short range sensors at each instrumented level are presented. It is clearly seen that the largest displacement occur close to the pillar centre. Figure 5-16 to Figure 5-23 shows the displacements in more detail. The long range sensors are also included here. The instruments that have recorded very small displacements are not included here, but are presented in Appendix 2. Each plot contains one measurement position. On the three first instrument rows there are typically two instruments placed almost directly beneath each other at every measuring position and these are plotted together. The type of transducer at the upper and lower positions at each instrument level varies between the levels and is presented in Table 3-5. Figure 5-11 shows the temperature at a depth of 3.5 m in the boreholes between the heaters on each side and the temperature at the centre of the open large hole. The figure illustrates the changing stress situation in the rock mass during the heating phase.

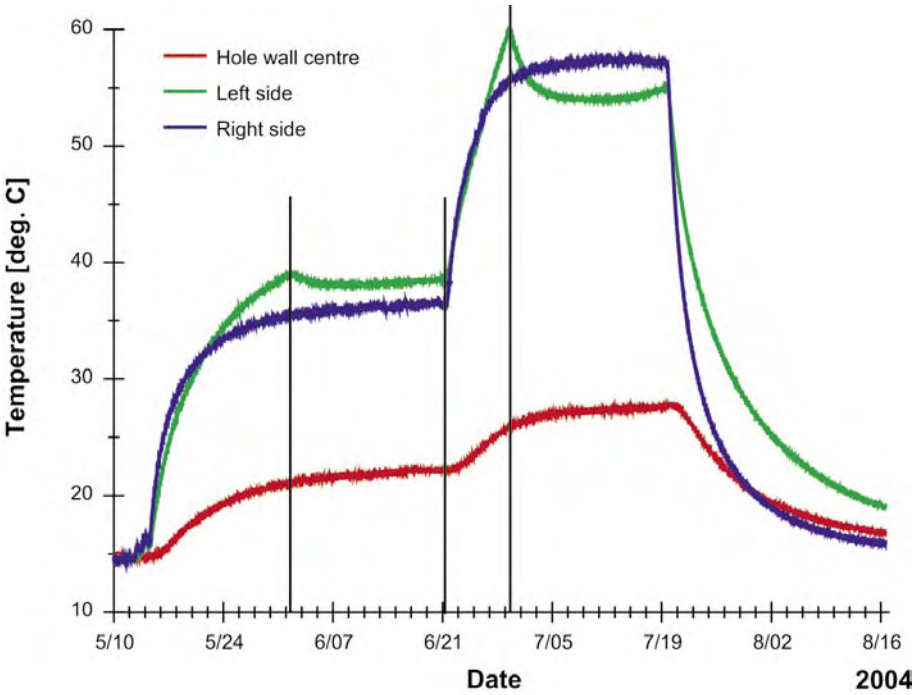


***Figure 5-11.*** *Temperature at depth of 3.5 m in the boreholes between the heater holes and in the centre of the open large hole.*

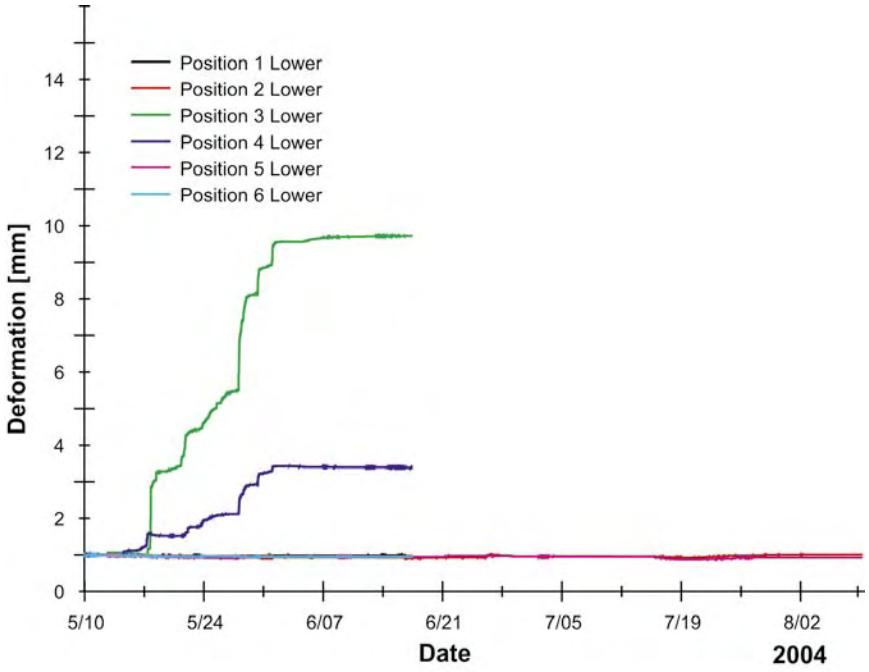


***Figure 5-12**. Deformation of the short range sensors at the 2.5 m instrument level.*

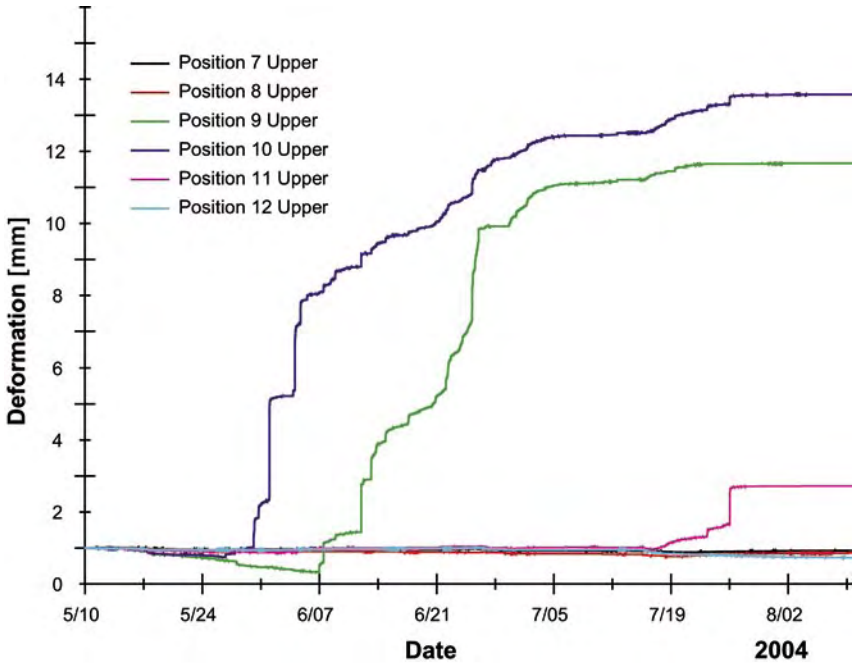


***Figure 5-13.** Deformation of the short range sensors at the 3 m instrument level.*

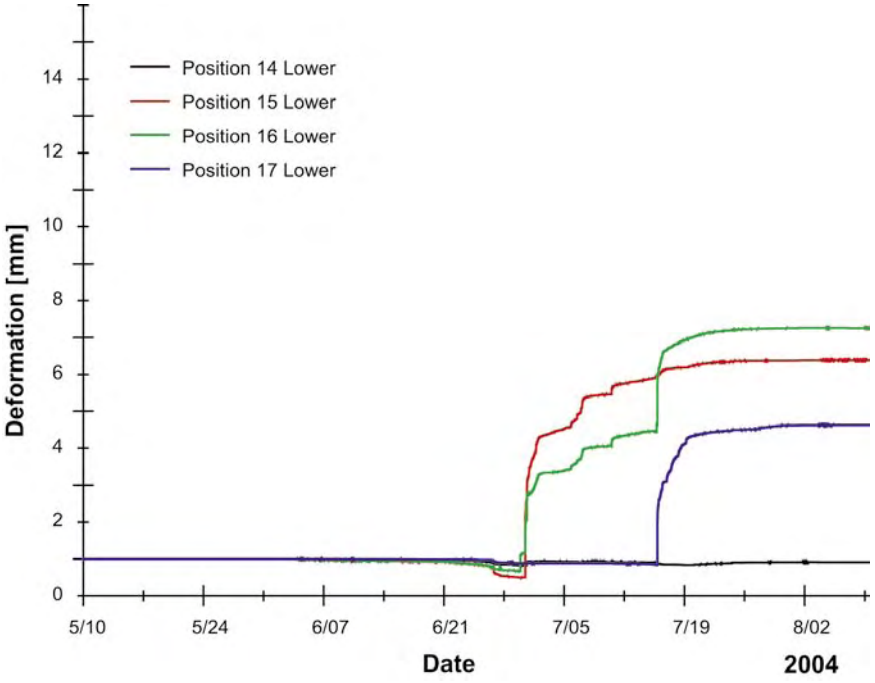


***Figure 5-14***. *Deformation of the short range sensors at the 3.5 m instrument level.*

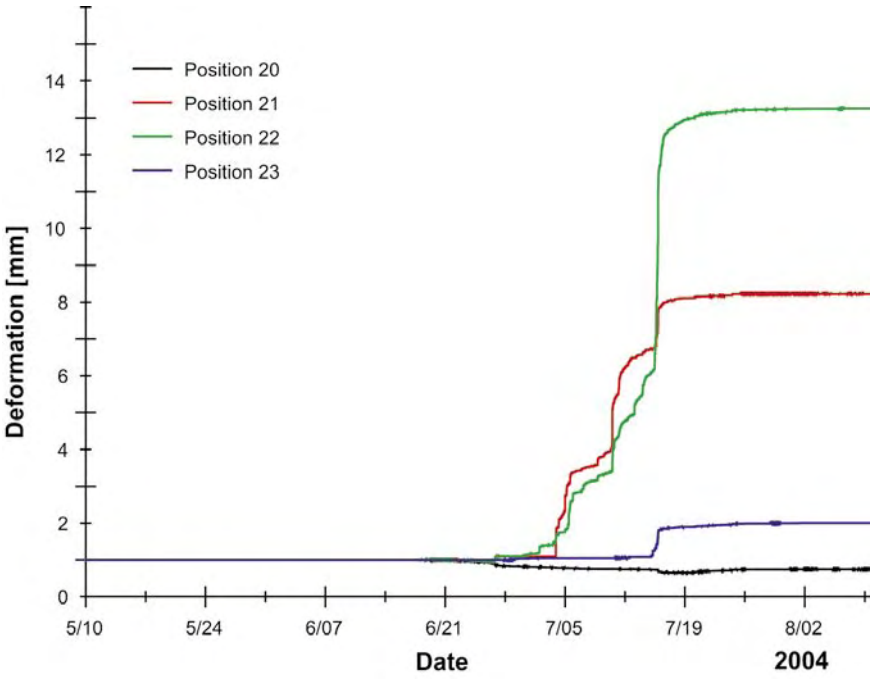


***Figure 5-15.*** *Deformation of the short range sensors at the 4.1 m instrument level.*

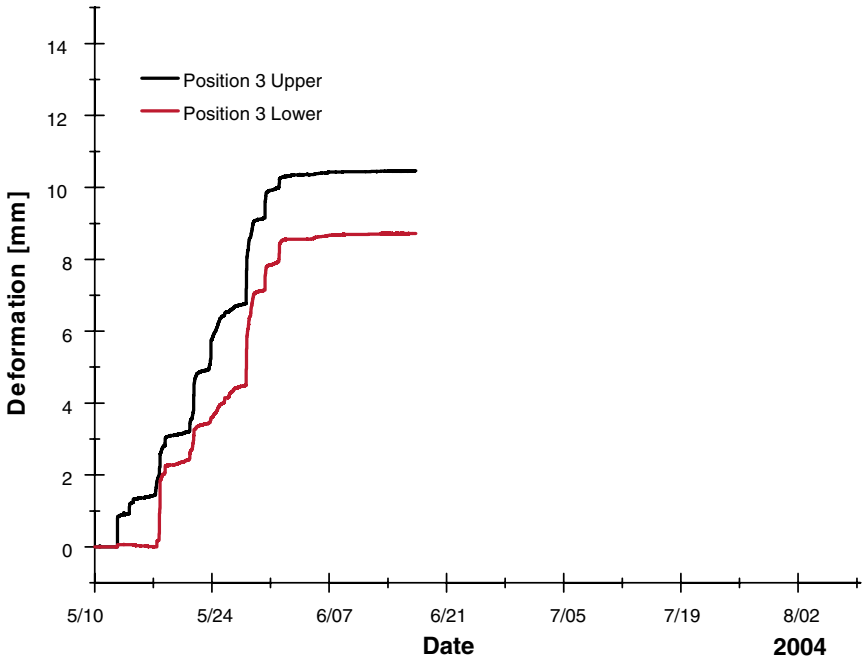


***Figure 5-16.*** *Deformations at instrument position 3.*

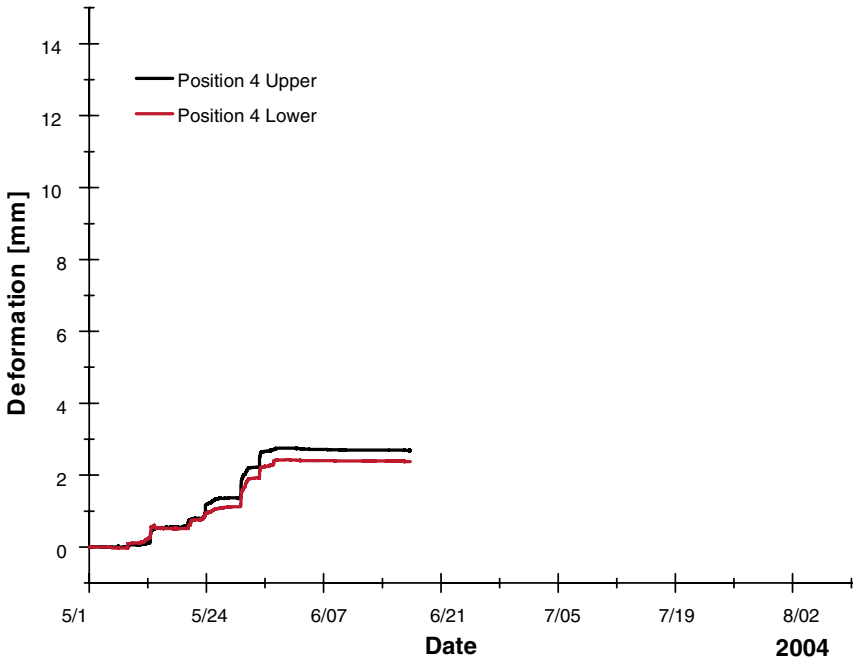


***Figure 5-17.*** *Deformations at instrument position 4.*

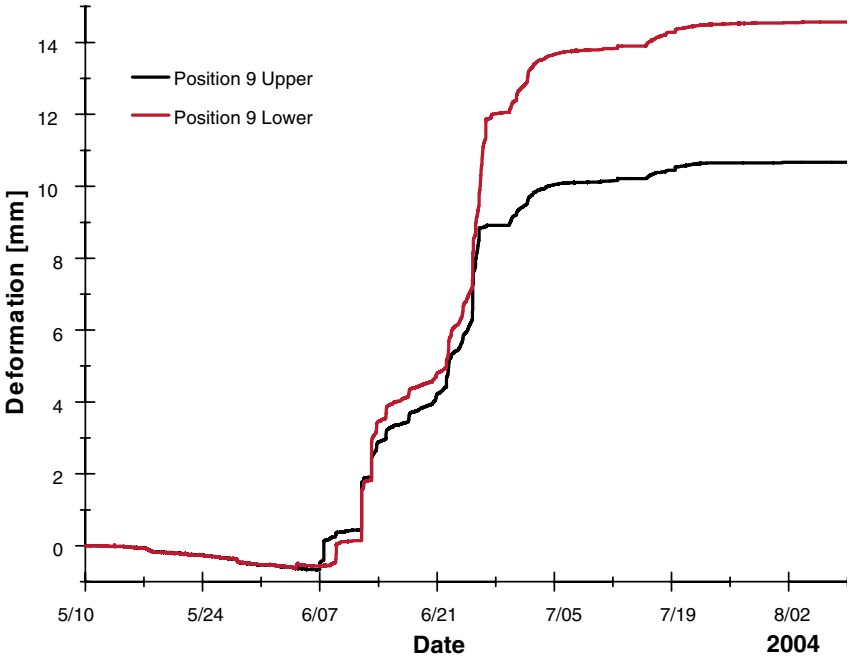


***Figure 5-18.*** *Deformations at instrument position 9.*

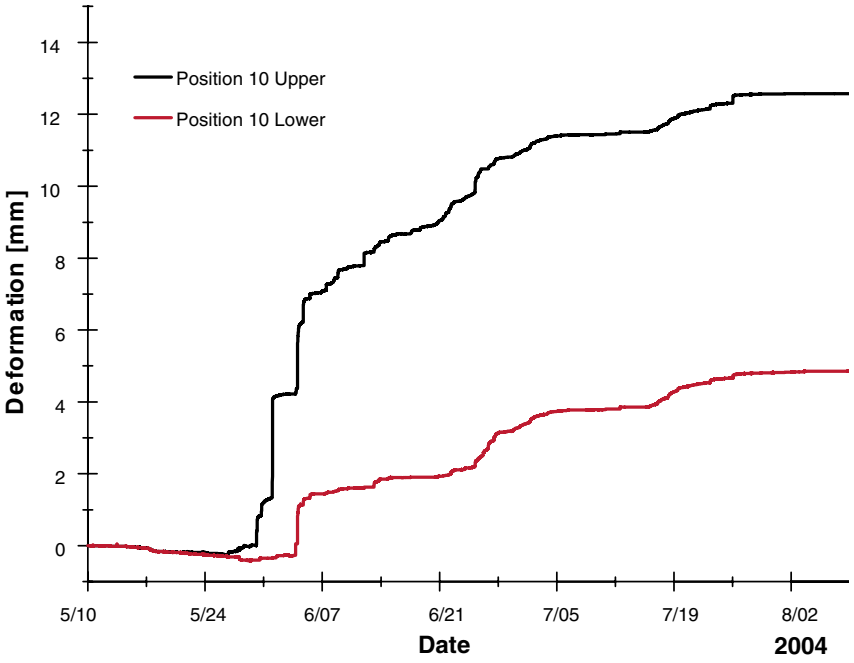


***Figure 5-19.*** *Deformations at instrument position 10.*

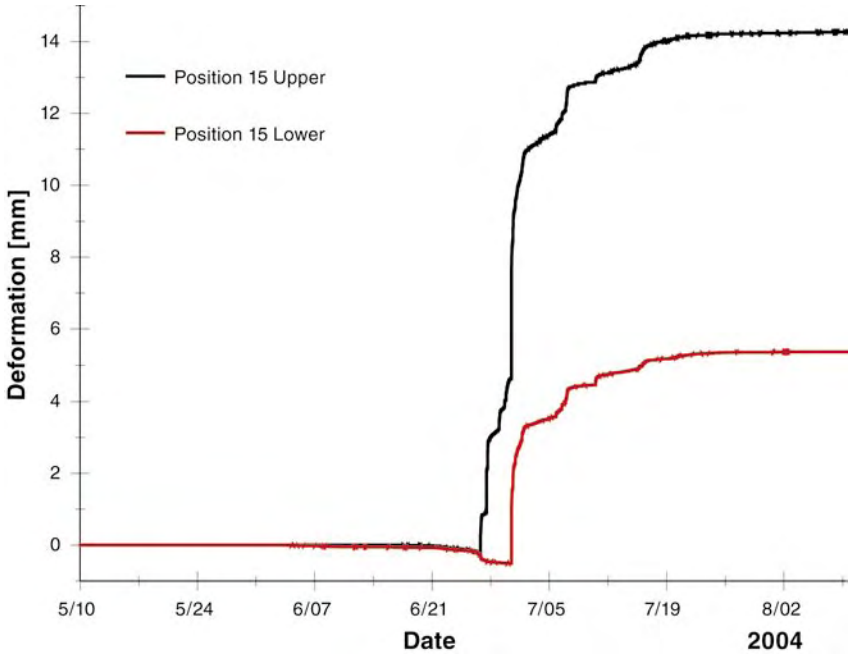


***Figure 5-20.*** *Deformations at instrument position 15.*

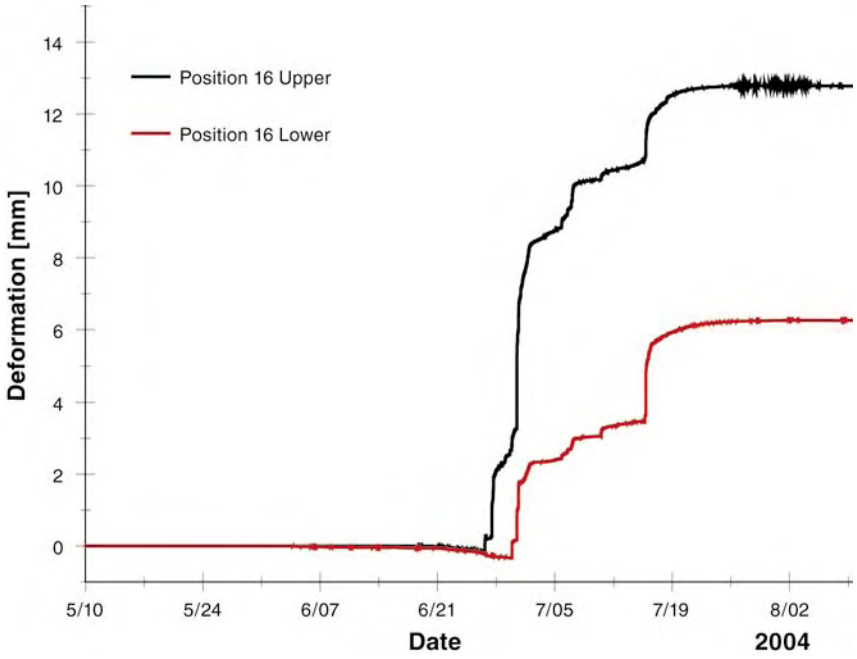


***Figure 5-21.*** *Deformations at instrument position 16.*

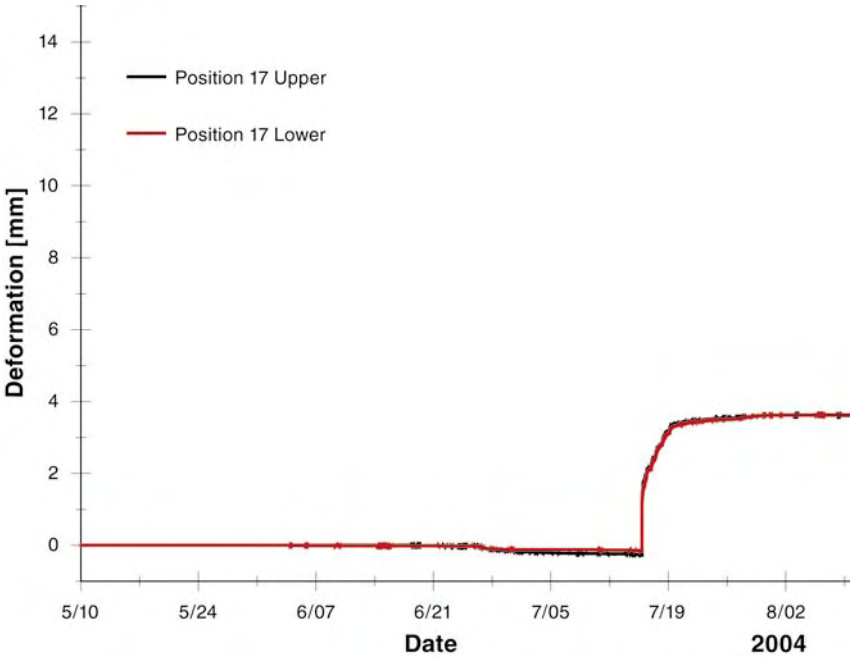


***Figure 5-22.*** *Deformations at instrument position 17.*

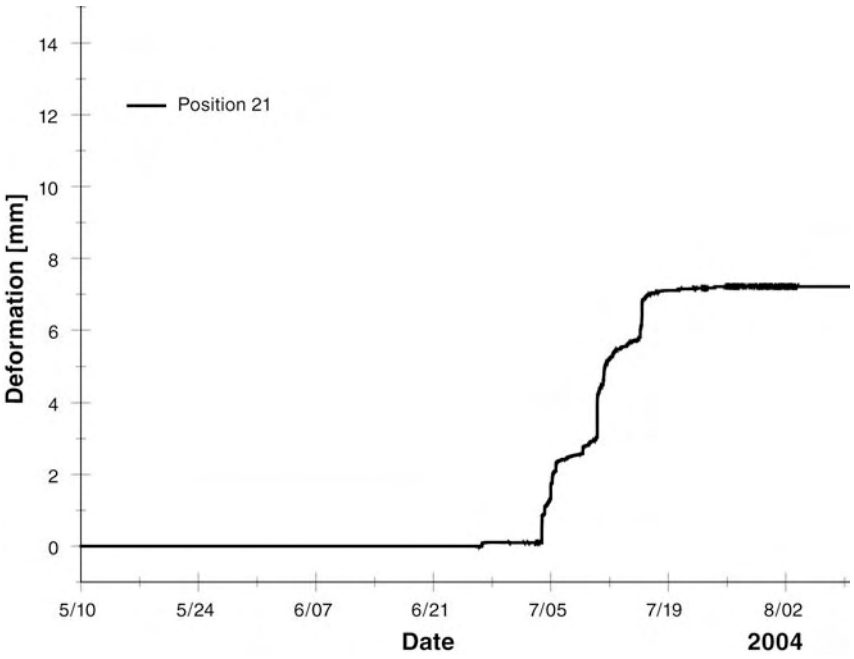


***Figure 5-23.*** *Deformations at instrument position 21.*

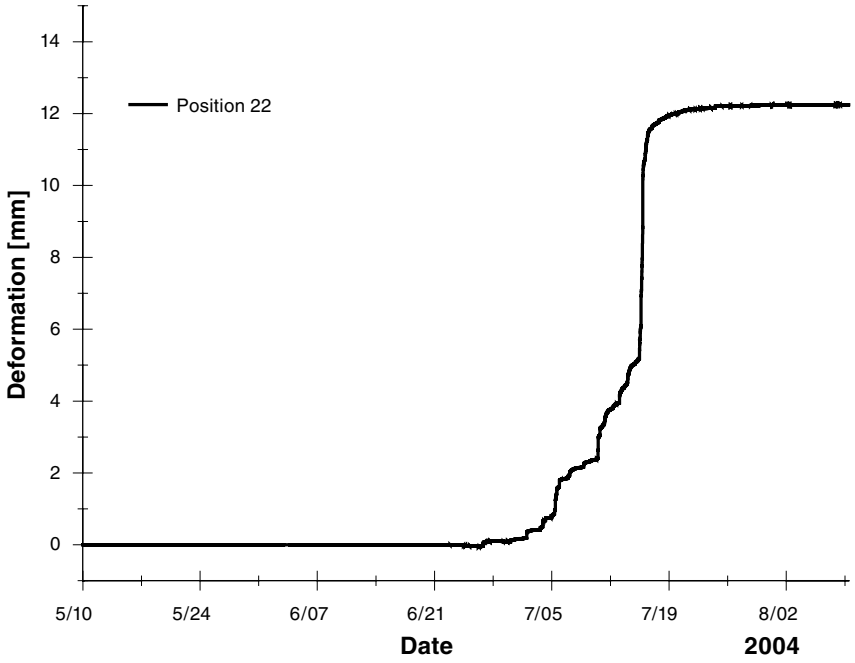


***Figure 5-24.*** *Deformations at instrument position 22.*

To get an understanding of the time it took for the notch to propagate down the hole, the displacements recorded on the left and right hand side of the centre pipe are presented in Figure 5-25 to Figure 5-28. The first two figures show plots for each of the instrument types on the left side, after which the plots from the right side are shown in the next two figures. The notch propagation is somewhat different between the two sides.

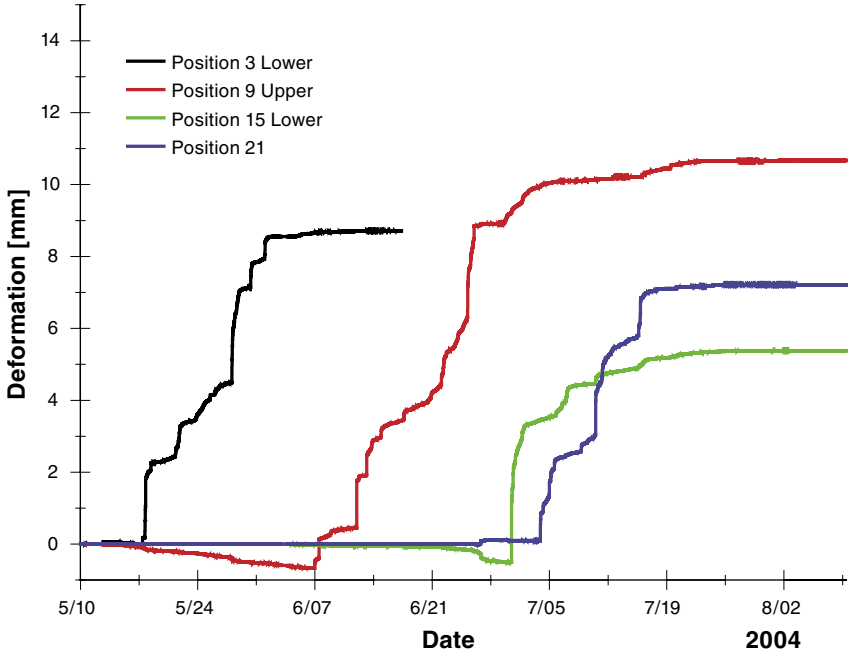


***Figure 5-25.*** *Deformation of the short-range sensors on the left side of the pillar centre.*

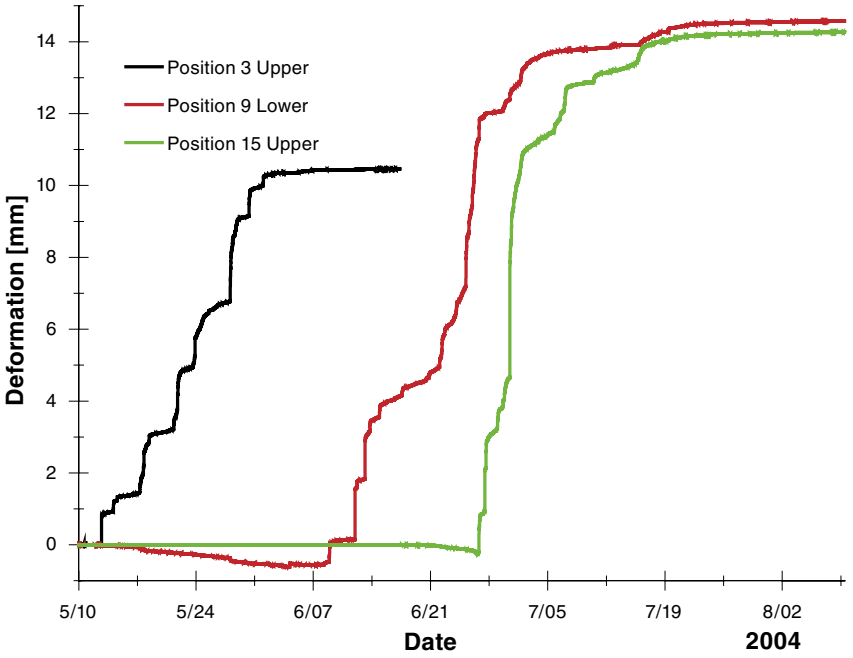


***Figure 5-26.*** *Deformation of the long-range sensors on the left side of the pillar centre.*

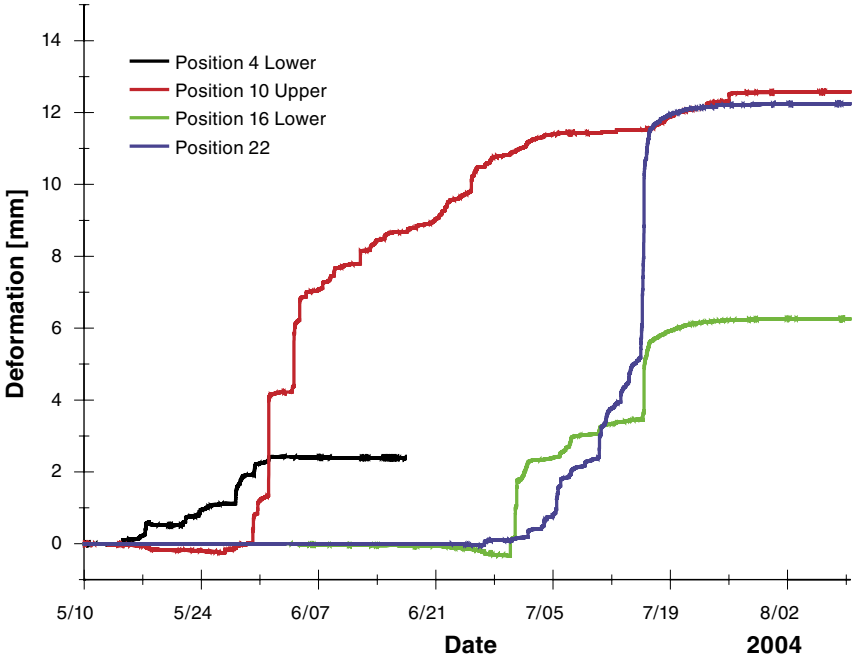


***Figure 5-27.*** *Deformation of the short-range sensors on the right side of the pillar centre.*

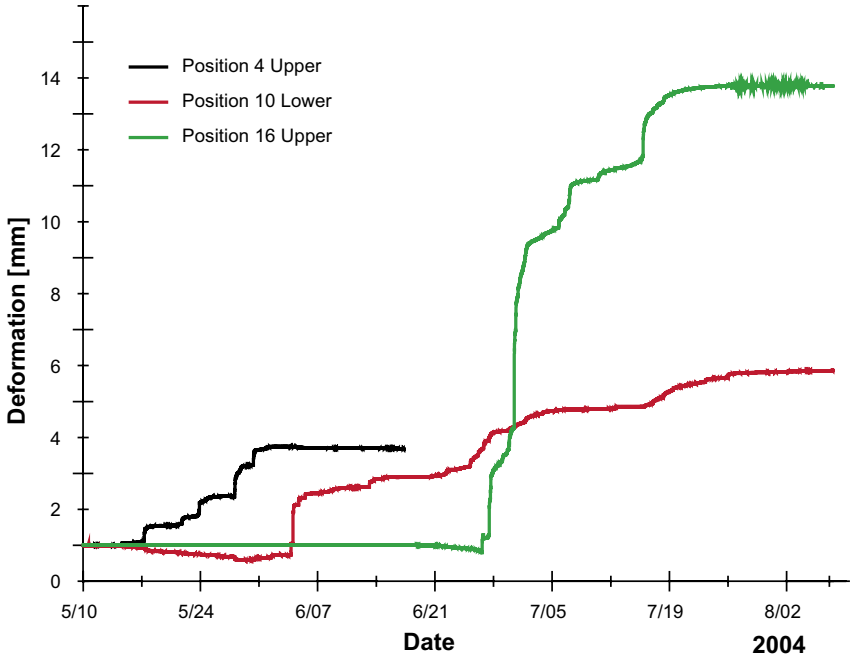


***Figure 5-28.*** *Deformation of the long-range sensors on the right side of the pillar centre.*

The rock at the centre instrument positions at depths of 3 and 3.5 m exhibits a radial expansion, contraction, before the dilatation is initiated. The reason for this is probably a 3-dimensional effect of the stress redistribution. When the rock above the LVDT is spalled, the stresses are forced deeper into the pillar, which relaxes the rock just below and causes the observed effect of a contraction. The propagation of the notch is also visible in the plots, since the upper instrument position reacts before the lower one at the same level. The fact that the instruments at a depth of 2.5 m don't indicate the contraction in the graphs is probably because they were installed so close to the pre-existing notch that the contraction may have taken place before the instruments were installed. These instrument positions will be further studied in the data analysis. The absence of contraction at the 4.1 m level is more difficult to explain. The spalling pattern is also quite different there. A weaker part of the rock started to spall from the 5 m level and propagated upwards. The two spalling fronts have created a complex geometry where the stresses are probably distorted. The contraction, radial expansion, of the spalling front is plotted in more detail in Figure 5-29 and Figure 5-30.

The LVDT placed along one of the larger fractures in the ductile shear zone indicated some movement along the plane of the shear zone. The deformation was quite small, approximately 0.5 mm. The plot is presented in Figure 5-31. The LVDT is extended which means that the right part of the shear zone has moved to the left.

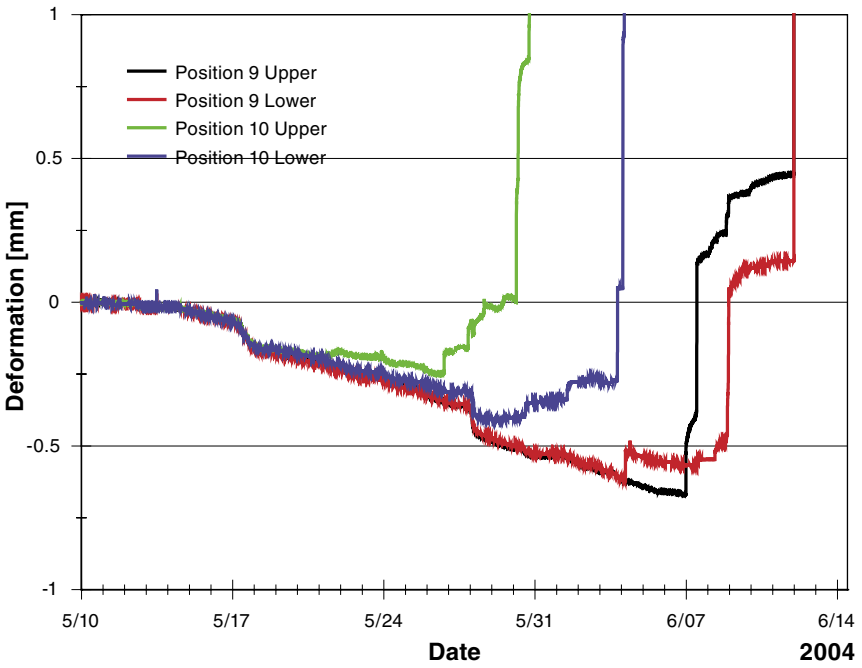


***Figure 5-29.*** *Contraction of rock before dilatation is initiated at 3 m level.*

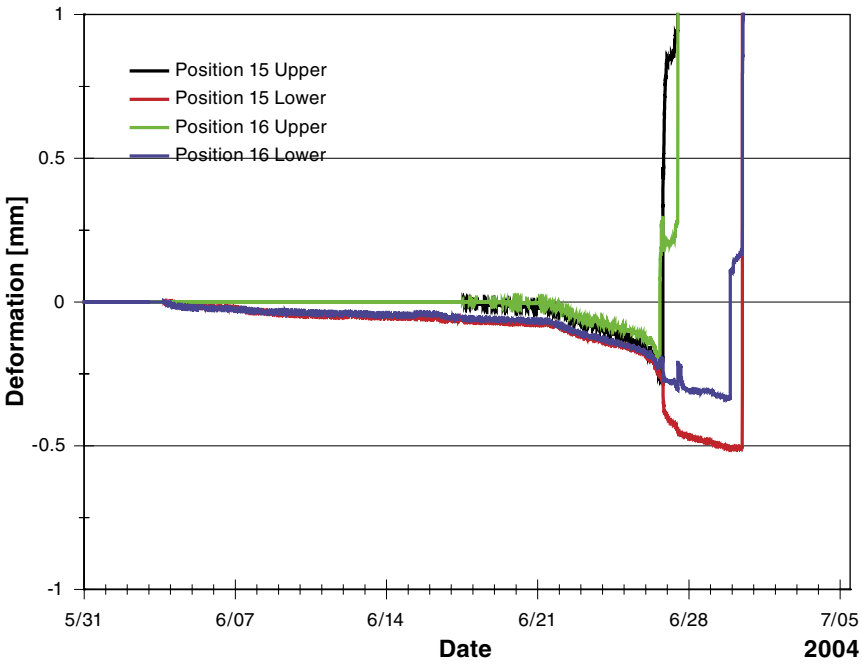


***Figure 5-30.*** *Contraction of rock before dilatation is initiated at 3.5 m level.*

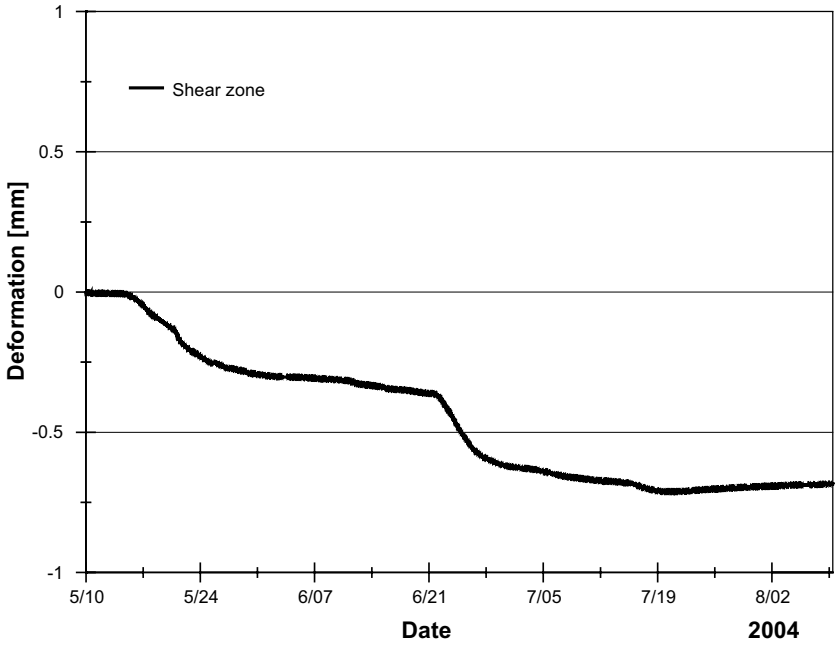


***Figure 5-31.*** *Deformations along the shear zone at the top of the pillar.*

## 5.3 Confinement

The confinement worked as planned. As expected, the pressure in the bladder increased with increasing temperature due to the volumetric expansion of the water, which also is evident when studying Figure 5-32. The pressure in the system had to be reduced on a number of occasions to keep the pressure close to the target pressure of 700 kPa. On one occasion the pressure increased at the same time as a cluster of acoustic events were recorded at a depth of 4.7 m on the confined hole's pillar side. At the end of the experiment, no physical trace of the acoustic cluster such as spalling or fracturing could be detected. It is nevertheless likely that a small displacement of the rock took place on that occasion that reduced the volume of the hole and hence increased the pressure in the hole. Since the system is stiff, very small changes in volume affect the pressure.

### 5.3.1 Release of confinement

The confinement pressure in the system was kept constant until July 14 (day 61). The temperature in the pillar had then been stable for about a week and a half. The on-going displacements were quite small in comparison with what had been measured previously, and the same was true for the acoustic emission hit frequency. It was decided that this was the steady state situation that we were waiting for and release of the confinement in the large hole DQ0066G01 could now be commenced.

The pressure was reduced in 50 kPa decrements. After each decrement the pressure was kept constant until the acoustic emissions indicated that the spalling in the rock had ceased again. The times of the pressure decrements are presented in Figure 5-33. In the log one can see that the pressure was dropped from 150 kPa to 0 in one decrement. This was not the intention. The reason was that the pressure transducer malfunctioned and recorded a pressure of 150 kPa even when it had been removed from the confinement equipment. The transducer was checked at the surface the next day and performed as it should. The reason for the malfunction is probably that a small part in the transducer jammed on that occasion. There is therefore no reason to believe that the previously recorded pressures are corrupt.

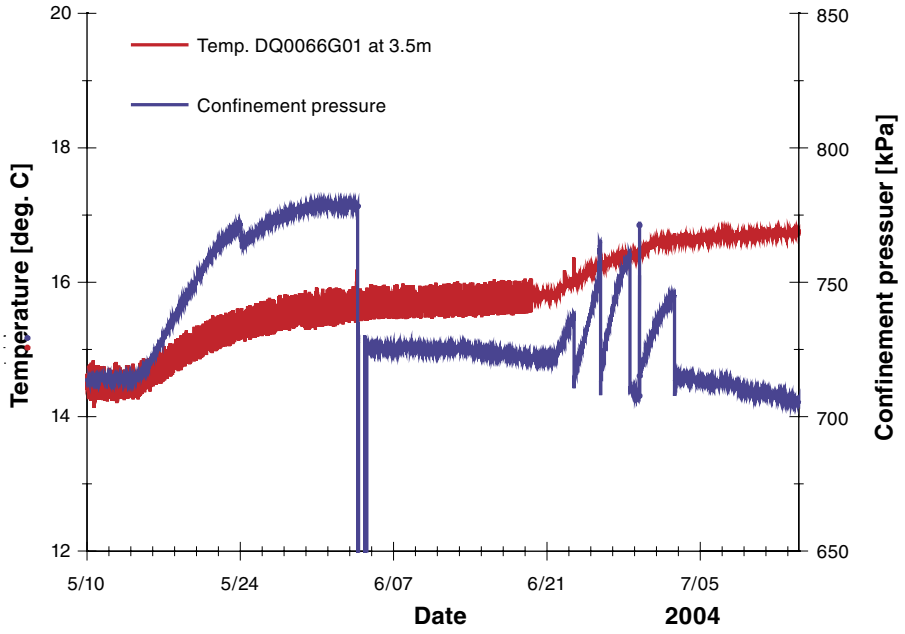


***Figure 5-32.*** *Confinement pressure and temperature on the hole wall in DQ0066G01 at a depth of 3.5 m. The temperature-pressure effect is quite clear, as well as the occasions when the pressure was adjusted. On June 4 the pressure did not fall, as dramatically as the graph indicates. The valve to the transducer was maintained and atmospheric pressure was logged just after the pressure decrease to 725 kPa.*

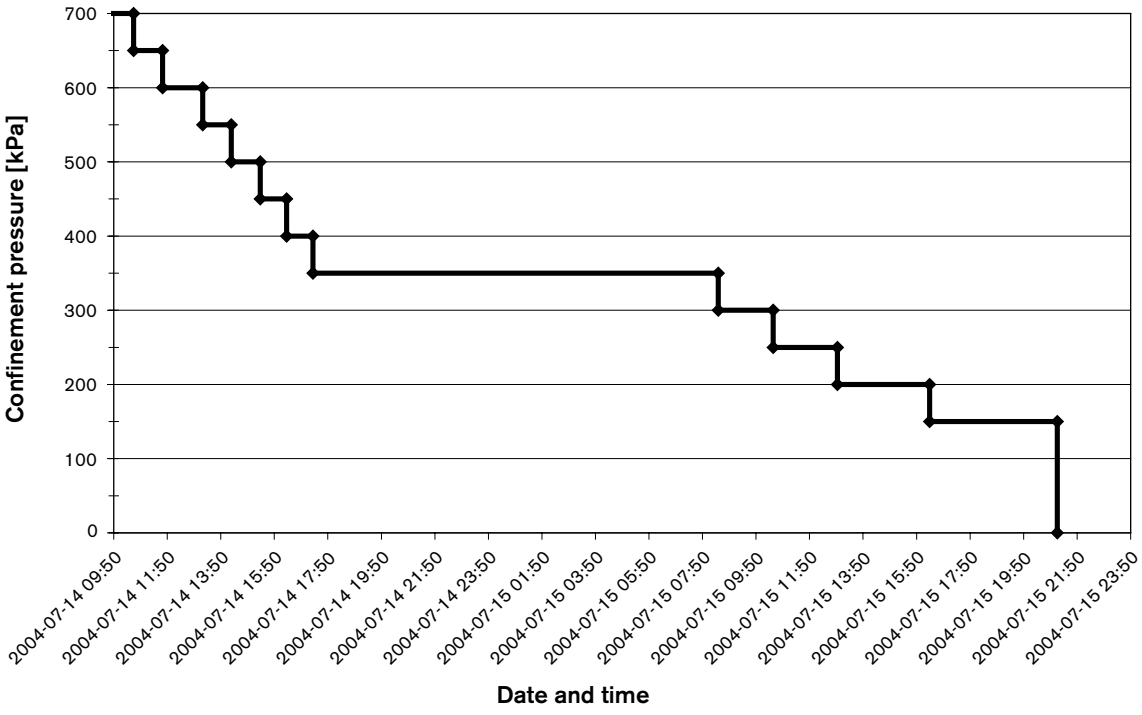


***Figure 5-33.*** *Graph of confinement pressure versus time during confinement release in DQ0066G01.*

The pressure decrease led to displacements in the open hole, which can be seen in the displacement plots in Section 5.2.

The volume of the water released from the confinement bladder was measured for each pressure drop. The volumes and times are presented in Appendix 3. It can be seen in the appendix that the pressure increased and that additional volumes of water had to be released to maintain the target pressure. The reason for the pressure increase in the system after a pressure decrement has not been investigated yet. One explanation that occurred to the author at the time of the writing of this report is that the textile straps may act like springs and try to contract to their original length when the pressure is reduced. A contraction of the straps would lead to a pressure increase. Another, more far-fetched explanation has to do with water inleakage. Some of the water leaking into the hole flows between the textile straps and the rock wall. The flow resistance exerts a pressure on the textile straps and the bladder. The pressure and flow of the leaking water and the flow resistance reach an equilibrium, which includes a certain pressure on the bladder that is transferred into the system.

## 5.4 Spalling

Sketches of the propagation of fracturing and spalling were made on 15 different occasions during the experiment. The rock wall was photographed on most of these occasions as well as at some additional times.

Two types of sketches were made. One type was on a more detailed scale and includes the fracturing around the LVDT positions. The other type was on larger scale and shows the depth and width of the spalled zone. Both types of sketches include observations made during the visit in the hole.

When the heaters had been turned off and the rock mass had cooled down, the slabs created by the spalling was carefully removed. The slabs were collected in approximately 0.5 m sections. All the slabs from one section were collected in a separate basket. Almost 0.1 $m^3$ of slabs was removed.

Laser scanning of the pillar wall in the open hole was performed before and after the slabs from the spalling were removed. The result of the latter scanning is presented later in this chapter. The scaning result gives the final size of the spalled zone and the volume of spalled rock in 0.05 m increments.

The characterisation of the spalling is presented in chronological order in this chapter, but first a summary is given of general spalling observations.

### 5.4.1 General spalling observations

As the v-shaped notch migrated down the borehole, the rock behaviour can be summarized in five different observations.

1. Below the notch tip small rock slabs (chips) started to form, the first indication of dilation. These chips were roughly a quarter of a fingernail in size and very thin. After a while, larger thin chips of coin size became visible.
2. Discrete fractures started to form. The fractures became the borders of slabs and ranged in length from a few centimetres to approximately 10 cm.
3. More fractures formed, creating larger slabs beneath the ones already formed. In the end, many slabs were located beneath each other. The dilatation of the rock wall increased as the slabs formed. The total deformation was the sum of the distances between each slab.

4. The notch was located at a certain hole depth until the rock approximately 20 cm above it had reached a spalled width at the hole surface of 40–50 cm. The notch now migrated a bit further and remained there until the spalled width above it reached 40–50 cm.
5. When spalling occured at discrete positions at the hole wall (outside the propagating notch) it was mostly initiated in preexisting fractures located in weaker parts of the rock.

The template used for the sketches of the spalling is presented in Figure 5-34. The four instrument levels are indicated and each instrument position is marked with a black circle. Instrument positions #1–6 is at the 2.5 m level. Positions #7–12, 13–18 and 20–23 are found on the respective following levels. The grid is not included in all figures below to make them easier to read. The instrument positions are though always included. If not otherwise stated lines represents spalling fractures in the figures.

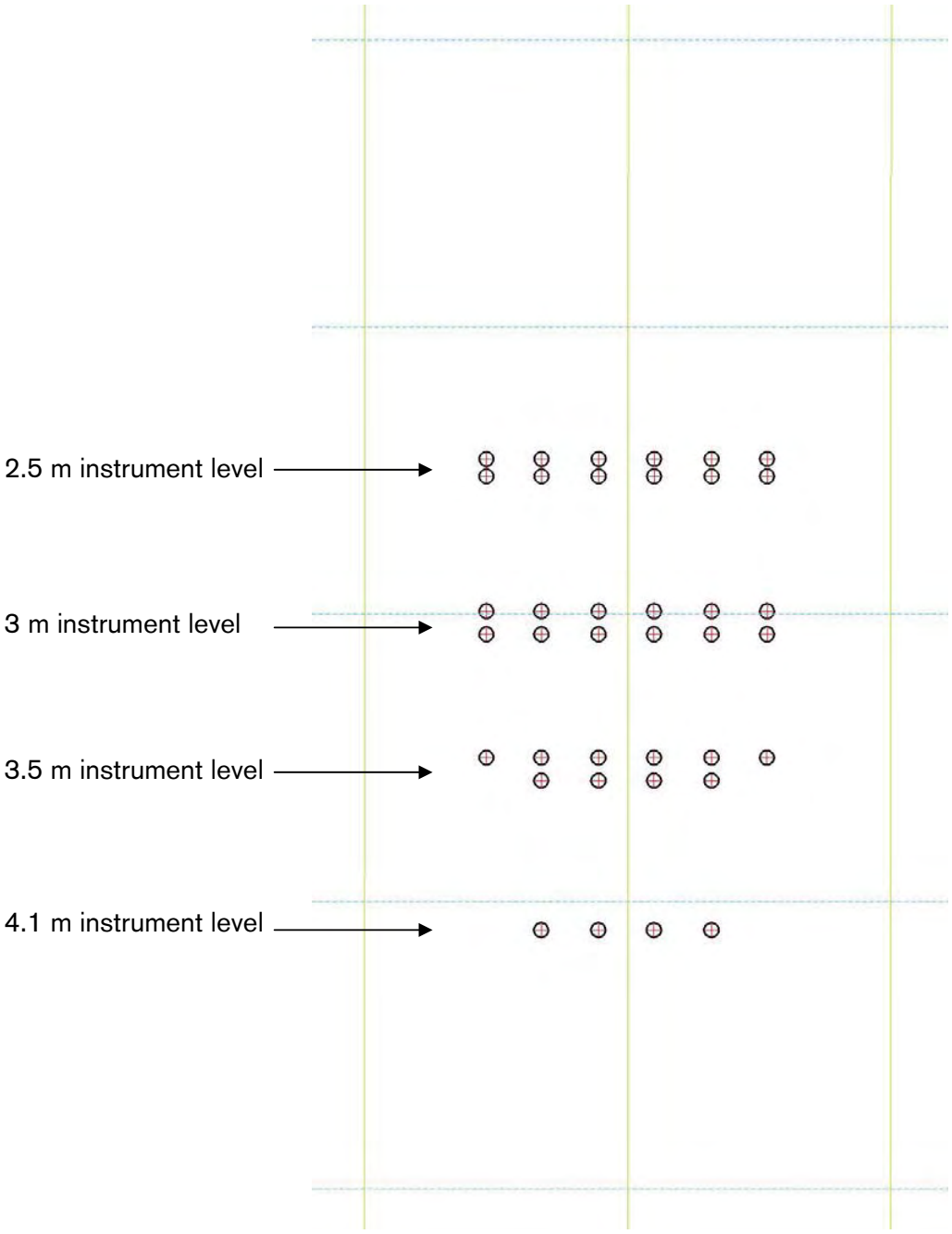


***Figure 5-34.*** *Template used for the spalling including the sensor positions. The grid spacing is 1 m and the horizontal line corresponds to the hole depths.*

### 5.4.2 April 26, 2004

When drilling of the large hole to host the instrumentation was finished, spalling had propagated down 1.95 m from the borehole collar. Installation of the LVDTs and thermocouples was finished on April 22. During installation the spalling slowly propagated down the hole. On one occasion the sound of breaking rock was heard and a very small piece of rock was ejected. It is likely that the spalling propagation was due to the small temperature fluctuations in the hole originating from people working there when the supporting structure was assembled etc. This indicates the delicate equilibrium at the notch tip. This conclusion has been drawn based on a long history of very limited acoustic emission events in the hole. The events started to be picked up when the work in the hole had been going on more regularly for a couple of weeks.

The first sketch of the spalling front was made on April 26. The spalling had then propagated close to the first instrument level.

The sketches from April 26 to May 14 (when the heating started) are summarized in Figure 5-35.

### 5.4.3 March 5, 2004

During the weekend April 30 to May 3 spalling occurred and the notch moved down between the instrument positions #3 and #4 (the locations of the instrument positions are given in Table 3-5). The spalling could be correlated with acoustic signals and with small deformations. It is clear that the extent of the spalling was affected by the force applied to the rock by the springs in the LVDT sensors. As can be seen in Figure 5-35, the fracturing occurs around the steel plates. This is also the first time that small radial expansion displacements (contraction) directed into the pillar were noticed.

### 5.4.4 May 12, 2004

Practically no displacements or any acoustic events of importance took place until May 12. In the afternoon, the AE system started to pick up events and at the same time position #3 was displaced almost 1 mm. A visit was therefore made in the hole and the new fracturing was sketched. The summary sketch in Figure 5-35 shows that a small slab was created beneath the #3 instrument plate. The slab was terminated close to instrument plate #4 where the force from the LVDT spring was probably large enough to suppress the spalling.

### 5.4.5 May 14, 2004

In the early morning and early afternoon of May 14, acoustic events and displacements at position #3 were picked up again. No new fractures were observed in the hole, but an increase of the dilatation of the old slabs was clearly visible.

The sketches from April 26 to May 14 are summarized in Figure 5-35, see how the spalling front propagates downwards.

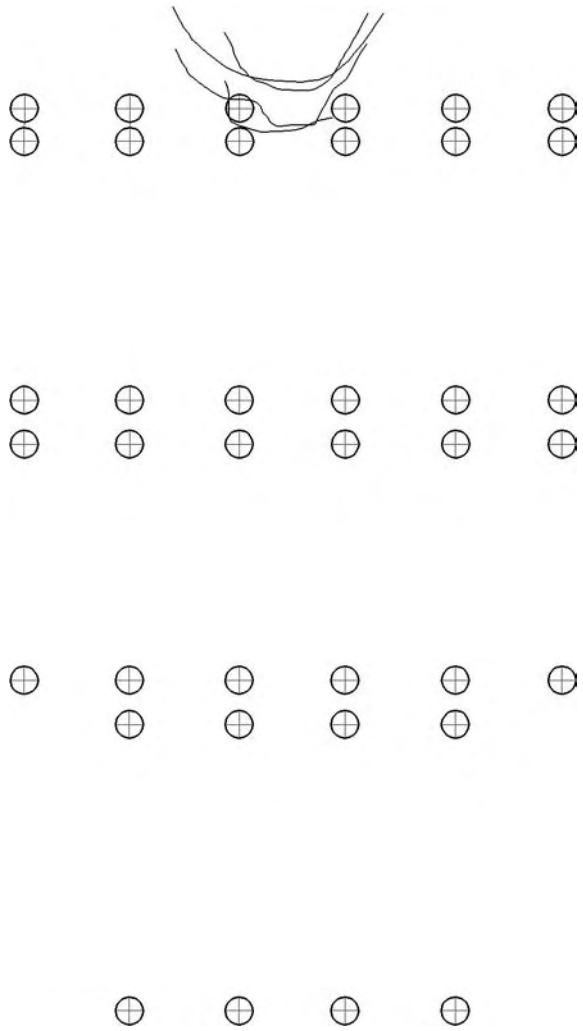

***Figure 5-35.*** *Summary sketch of the spalling observations between April 26 and May 14. The lines represents fractures.*

### 5.4.6 May 18, 2004

The acoustic activity picked up again May 17 and continued with quite a high event frequency until the beginning of June. This having been said, no general comments will be made on AE activity in the following sub-chapters.

In connection with the acoustic activity on May 17, displacement on the mm scale were observed with both sensor types at position #3. Displacements on the sub-mm scale were recorded with both of the sensors at position #4. The onset of negative displacements was monitored at positions #9 and #10.

Fracturing/slabbing associated with the other recordings includes a slab that was created beneath the short-range sensor at position #3. Fractures from that slab extended down the hole approximately 15 cm, where chipping occurred in a small mylonitized (dashed line) area. Still no fractures go past any of the sensors at position #4. The increasing dilation of the previously formed slabs is clearly visible. The dilatation of the fractures was approximately 1–2 mm.

The sketch from May 18 is shown in Figure 5-36. The spalling propagation was photographed for the first time during this hole visit. Two of the photographs are shown in Figure 5-37.

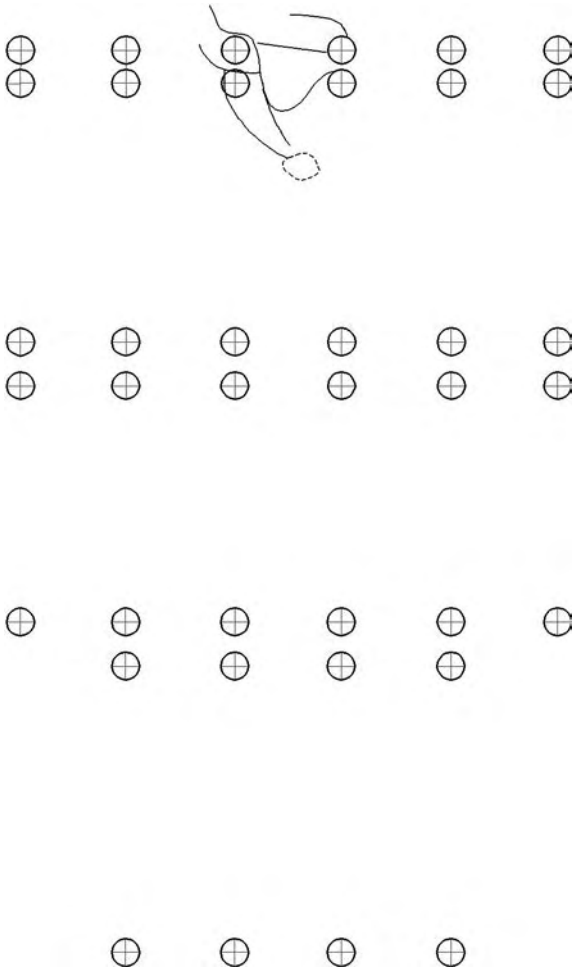

***Figure 5-36.*** *Spalling observations, May 18. Dashed line, chipping in mylonitized area.*

***Figure 5-37.*** *May 18. Photographs of the pillar wall. Left: close-up of position #3 (2.5 m level); the short-range LVDT is the right one. Right: photograph from below along the centre of the pillar (pos #3 to the left and pos #4 right of the pipe).*

### 5.4.7 May 25, 2004

The downward spalling propagation was very small on this date compared with the earlier observation dates. The slabs already formed continued to dilate, however, on May 25 a slab fell off the borehole wall. The upper part of the slab was attached to the rock wall and the lower part was forced to dilate by the underlying slabs (the long line in the figure). The edge of this slab was dilated between 10 to 20 mm. The slab was broken in a thin sub-horizontal pegmatite vein at the upper end of the long line.

When the hole was mapped that day, the increasing dilatation was obvious. Chipping continued in the thin mylonite band and the dilatation of the fractures from the rock wall was 5 to 10 mm. Figure 5-38 presents the spalling observations and Figure 5-39 shows photographs of positions #3 and #4.

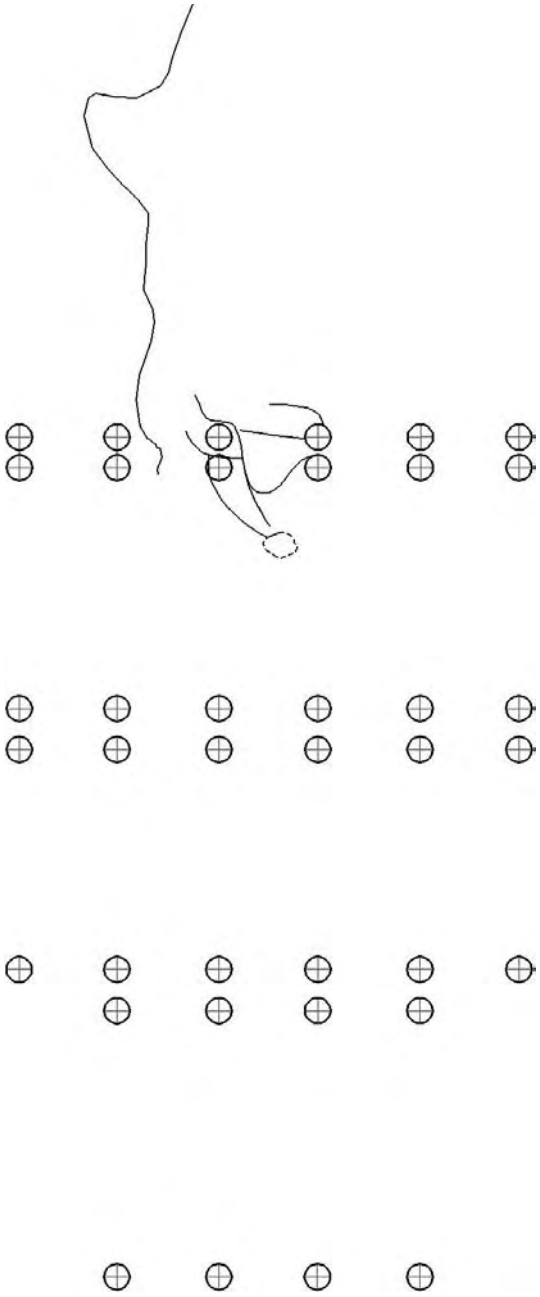

***Figure 5-38.*** *Spalling observations May 25.*

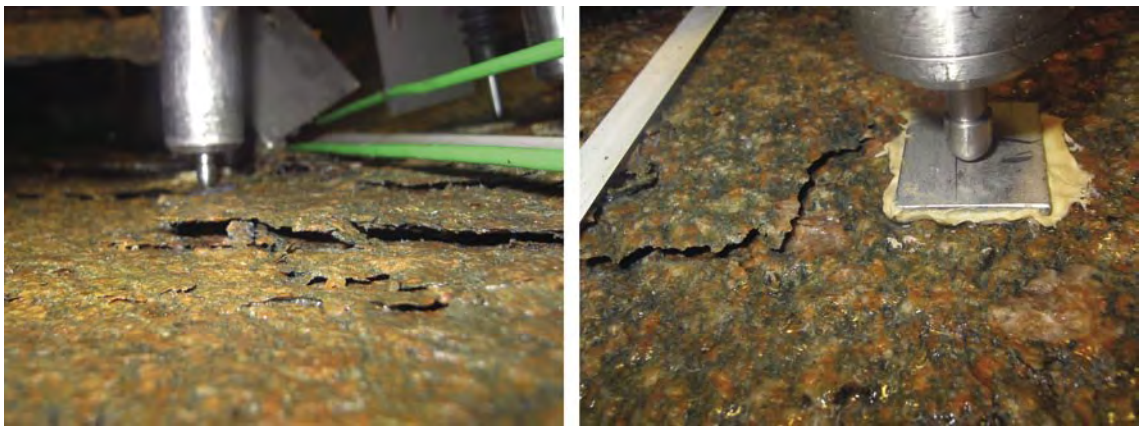

***Figure 5-39.*** *May 25. Photograph of the short-range sensors at positions #3 (left) and #4 (right).*

### 5.4.8 May 27–28, 2004

The hole was accessed again on the 27th to fit new sensor clamps. Mapping was done at the same time. Close to the instruments on the 3 m level there was chipping in the very centre of the pillar (dashed area). At one location along the mylonite band between the instrument levels, 1–2 mm thick chips were formed in the weaker mylonitized rock (oval area).

On May 28, displacements on the mm scale occurred at both the 2.5 and 3.0 m levels. A check was made in the hole but no new fractures were seen. There were some small additional chips between positions #9 and #10 (3 m level). Generally larger dilatation at almost all existing fractures was observed, Figure 5-40. A photograph of sensor position #3 is presented in Figure 5-41.

### 5.4.9 June 2, 2004

Chips had now formed around the centre instruments at the 3 m level between positions #9 and #10. Areas with small chips as well as increased dilatation in the preexisting spalling fractures were observed as well as drummy areas (inside dashed line) in Figure 5-42. A sub vertical granite vein above position #4 is drunny and small chips is formed around it. The dilatation of the long fracture above position #2 is approximately 20 mm. The photographs in Figure 5-43 shows the fracturing at position #10, which was not present at the previous hole visit. The figure also shows position #3.

### 5.4.10 June 8, 2004

The spalling had now propagated below the instrument level at 3 m. A drummy area was formed between the instrument levels at 2.5 and 3 m (large dashed area). Chipping had occurred between the instrument positions #10 and 11 (small dashed ovals). Small chippings in a limited area were observed at the centre of the pillar just below the 3 m instrumentation level (oval dashed area). The spalling is illustrated in Figure 5-44 and photographs of the spalling at the 2.5 and 3 m levels are presented in Figure 5-45.

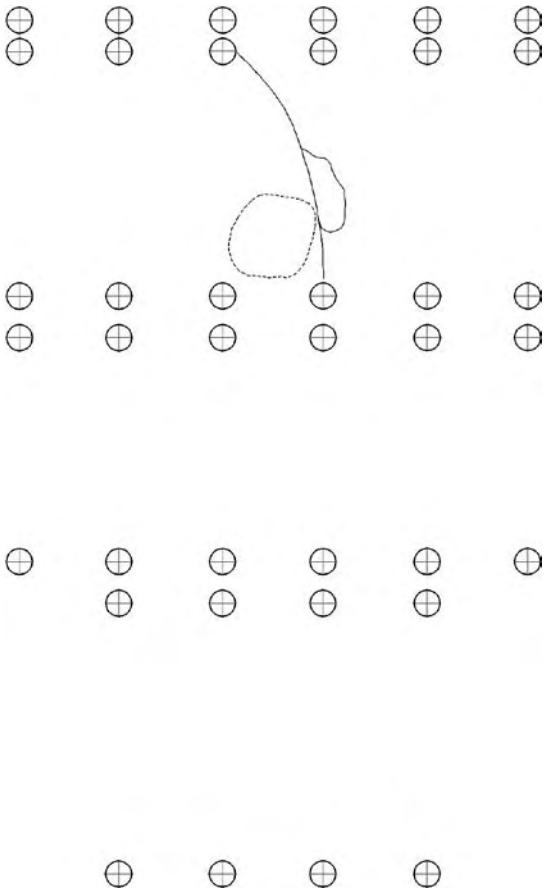

***Figure 5-40***. *Spalling observations May 27. Dashed area – chipping. Oval area chips in mylonitized rock.*

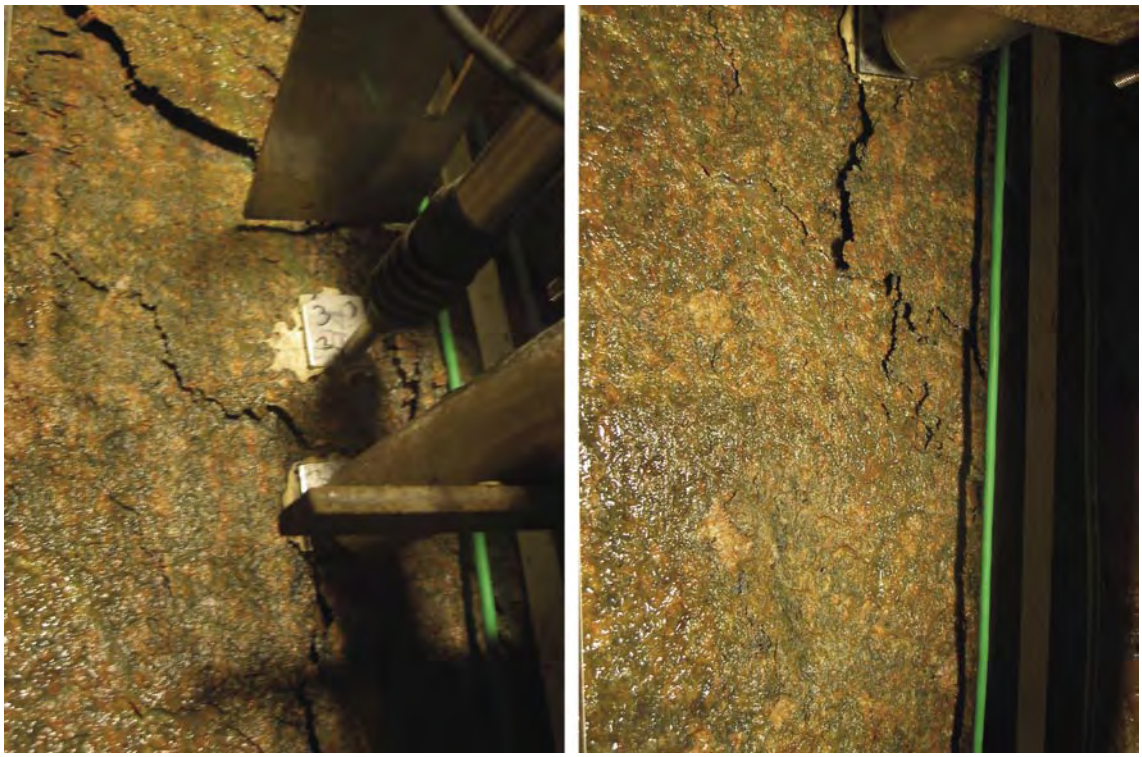

***Figure 5-41.*** *May 27. Photograph of position #3, left both sensors and right below the short range sensor.*

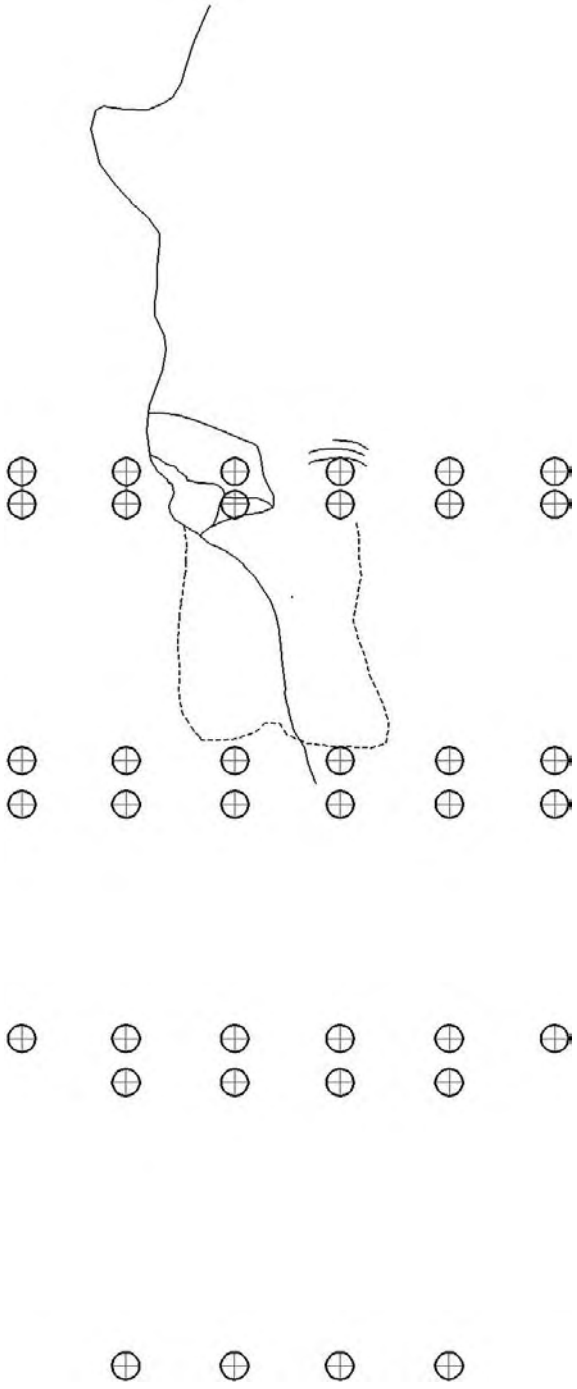

***Figure 5-42.*** *Spalling observations on June 2. Small chips and drummy inside spalled line.*

***Figure 5-43.*** *June 2. Photograph of spalling/fracturing at positions #3 (left) and #10 (right).*

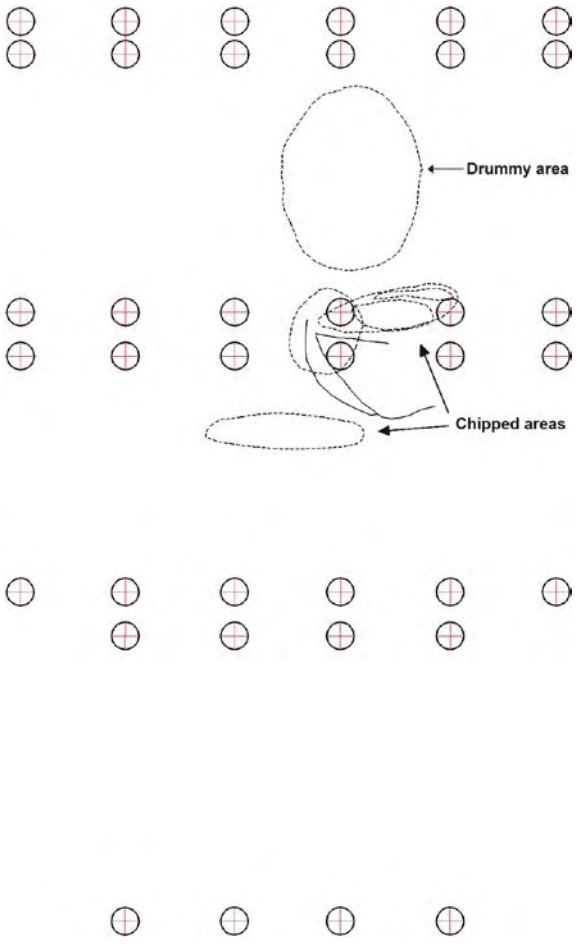


***Figure 5-44.*** *Spalling observations on June 8.*

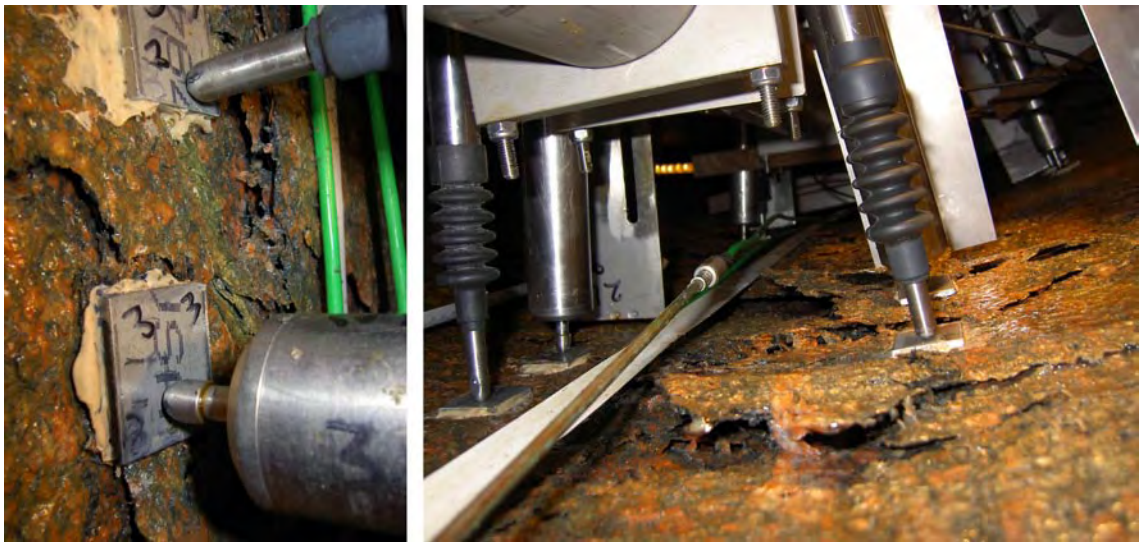

***Figure 5-45.*** *June 8. Photographs of spalling/fracturing at position #3 (2.5 m level) and between positions #9 and #10 at the 3 m level. In the right photograph position #9 is to the left.*

### 5.4.11 June 16, 2004

The major difference since the last spalling observation was that the spalled zone had widened in the horizontal direction at 3 m. Thin finger nail sized chips was formed between the pillar centre and the long curved dashed line, Figure 5-47. Small areas with limited spalling were observed just above 4 m and at approximately 4.5 m depth (dashed lines). At 4.5 m the spalling was associated with an inclusion of greenstone. Just above 5 m depth spalling was initiated in mylonitized rock close to an existing fracture. The dilatation of the fractures above the 3 m instrument level lies between 10 to 20 mm. The spalling is illustrated in Figure 5-46 and Figure 5-47. Photographs of the spalling at the 2.5 and 3 m levels are shown in Figure 5-48.

### 5.4.12 June 23, 2004

Chipping had now occurr ed slightly to the left of the pillar centre at between the 2.5 and 3 m instrument levels in the area created by the lines. The chips there were thin with a width of approximately 5–10 and length of 10 centimetres. The dilatation of the fractures above the 3 m instrument level lies between 10 to 20 mm. The spalling is illustrated in Figure 5-49 and photographs of the spalling at the 2.5 and 3 m levels are shown in Figure 5-50.

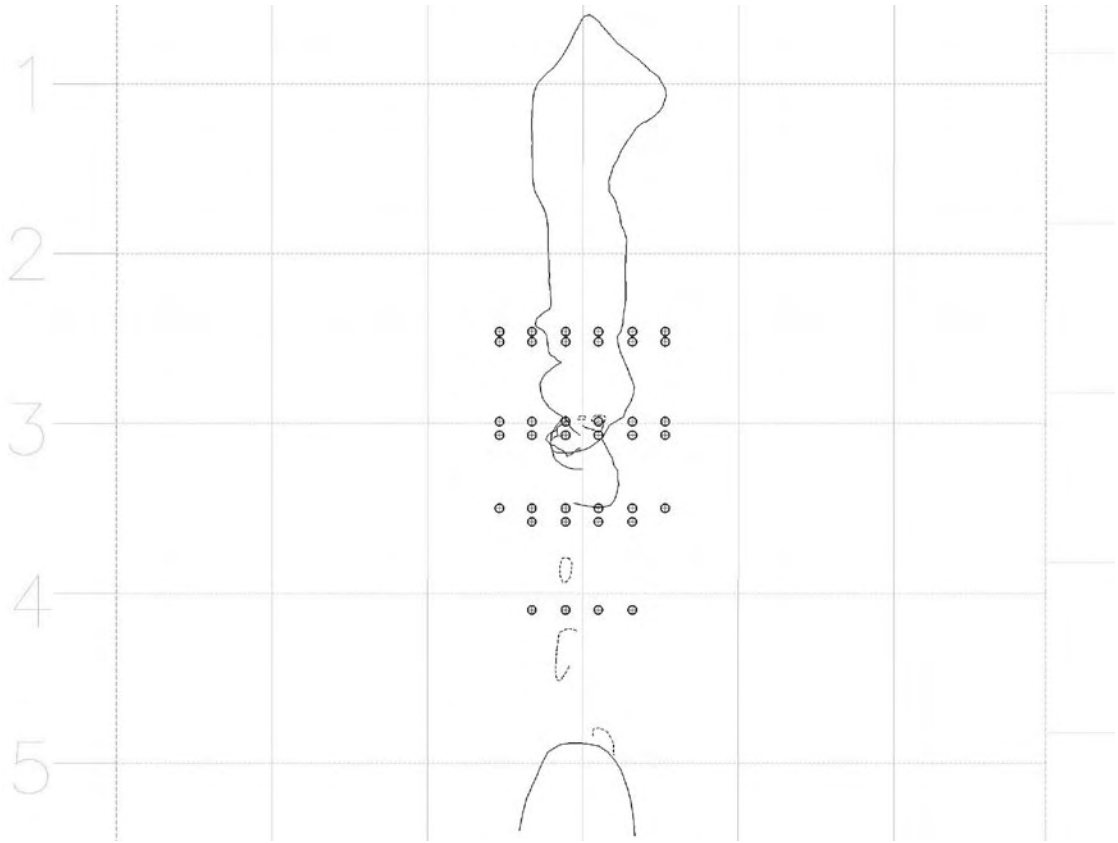


***Figure 5-46.*** *General extent of spalling on June 16.*

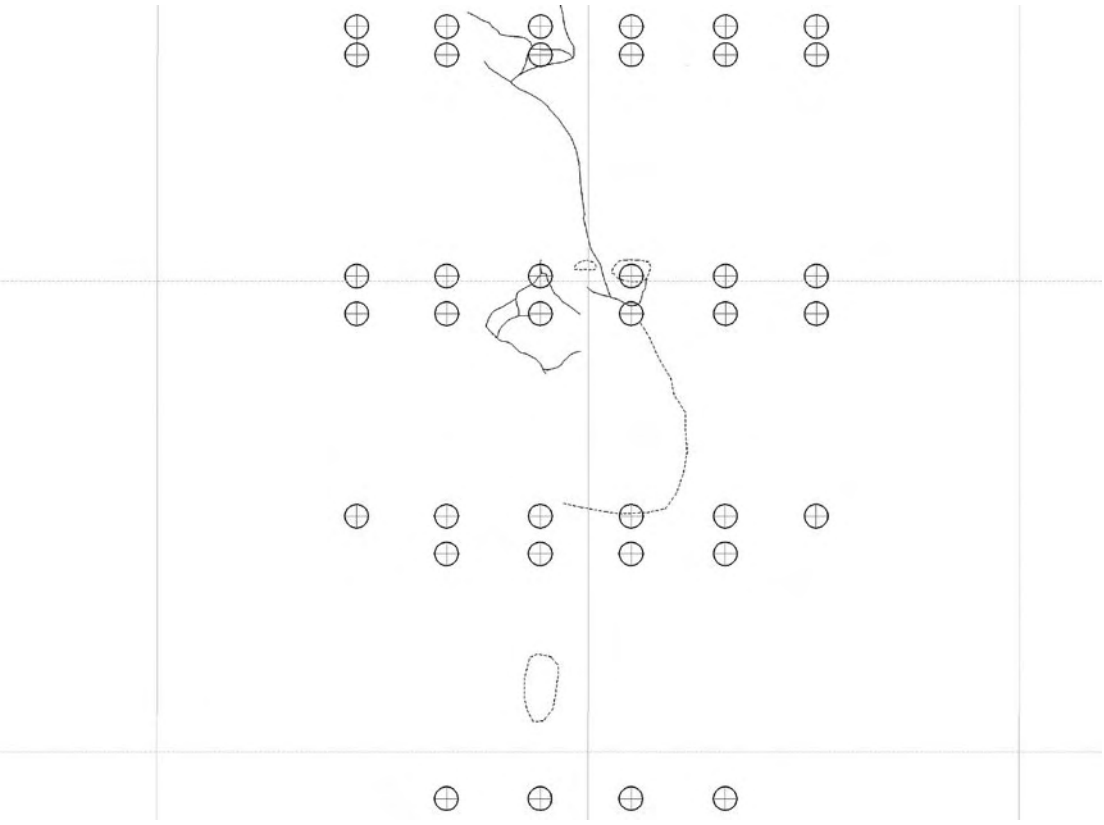

***Figure 5-47.*** *Detailed spalling observations on June 16. At 3 m depth a small rock fragment had fallen of at the very pillar centre (dashed oval).*

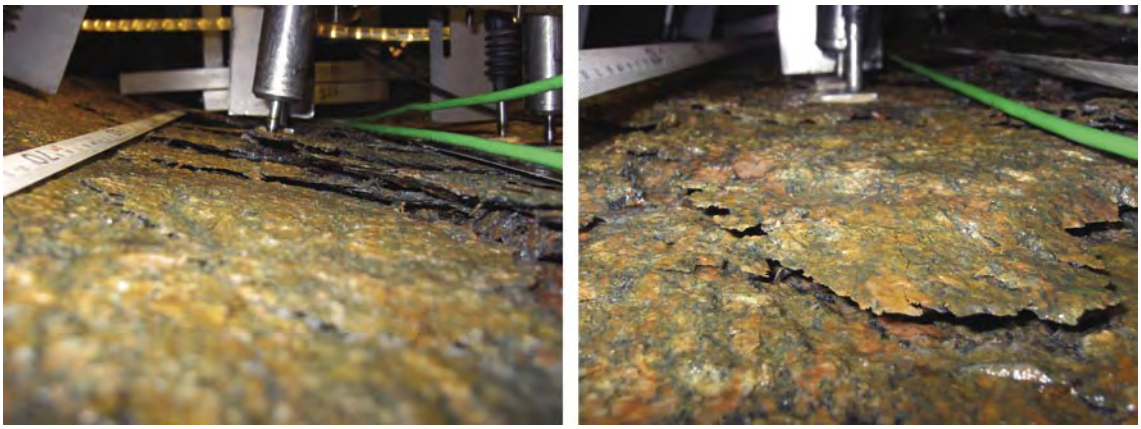

***Figure 5-48.*** *June 16. Photographs of spalling/fracturing at position #3 on the 2.5 m level (left) and at position #9 on the 3 m level (right).*

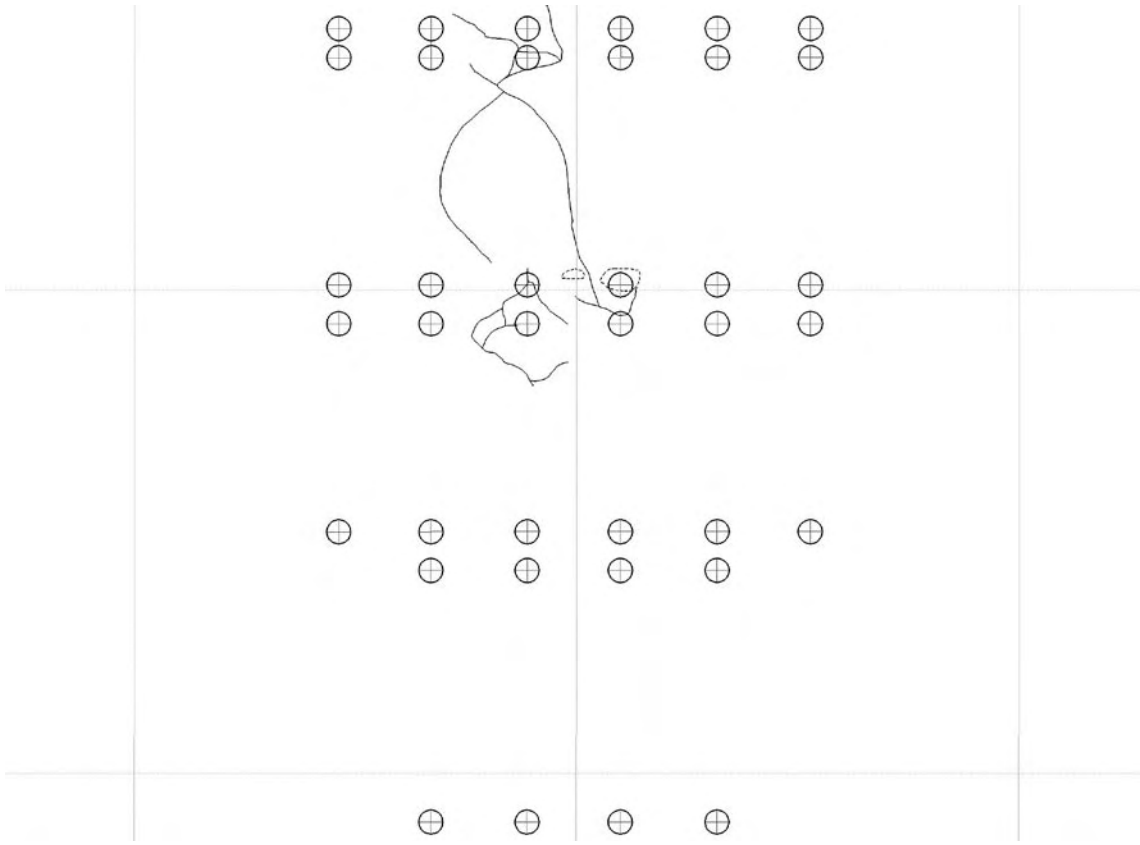

***Figure 5-49.*** *General extent of spalling on June 23.*

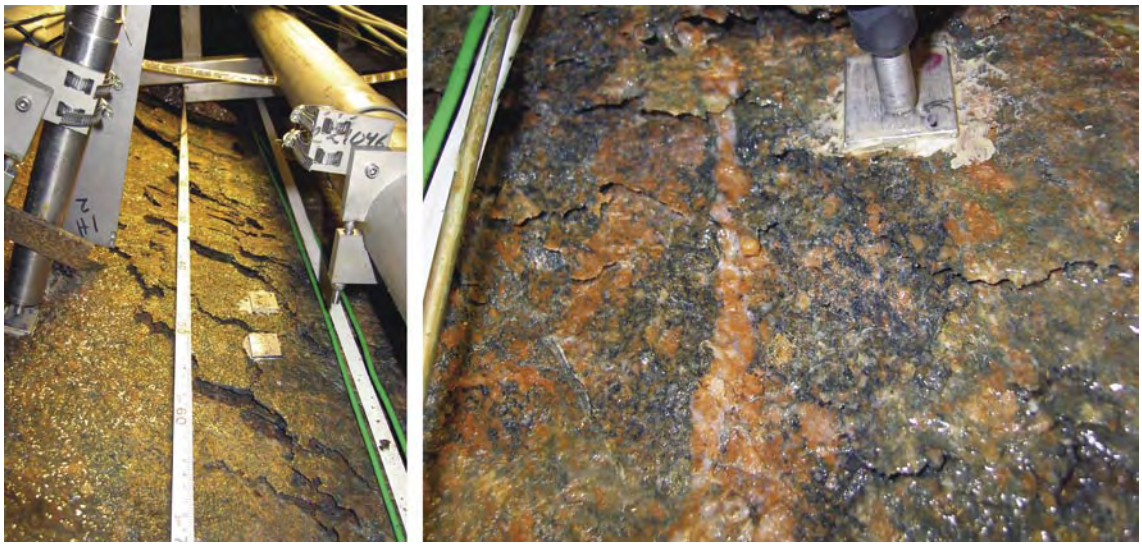

***Figure 5-50.*** *June 23. Photographs of spalling/fracturing at position #3 on the 2.5 m level (left) and at position #10 on the 3 m level (right).*

### 5.4.13 June 29 2004

Now the spalling had propagated to the 3.5 m instrument level. The spalled zones at approximately 4 and 4.5 m had the same area but were more spalled. The oxidized and mylonitinized part of the pillar at approximately depth of 5 m had continued to spall. The spalling had propagated upwards and had reached a hole depth of 4.2 m. The notches in the two spalling fronts seemed to be moving directly against each other. Quite a lot of small fractures are formed around instrument position #10 lower. The U-shaped line at the 3.5 m instrument level contains thin chips from coin size and up. The spalling is illustrated in Figure 5-51 and Figure 5-52. Photographs of the spalling at the 2.5 and 3 m levels are shown in Figure 5-53. Nothing seems to have happened in the upper part of the pillar.

### 5.4.14 July 6, 2004

The upper and lower spalling fronts were now joined. Additional fracturing was observed at the 3, 3.5 and 4.1 m instrument levels as well as at a depth of 5 m close to a fracture trace. The spalling is illustrated in Figure 5-54 and Figure 5-55. Photographs of position #10 and #16 in Figure 5-56.

### 5.4.15 July 12, 2004

A few new fractures were observed. Dilatation was increased at most locations, but fracture propagation had probably almost ceased due to the fact that the temperature was reaching a constant level and hence very small additional thermal stresses were being added.
The spalling is illustrated in Figure 5-57.

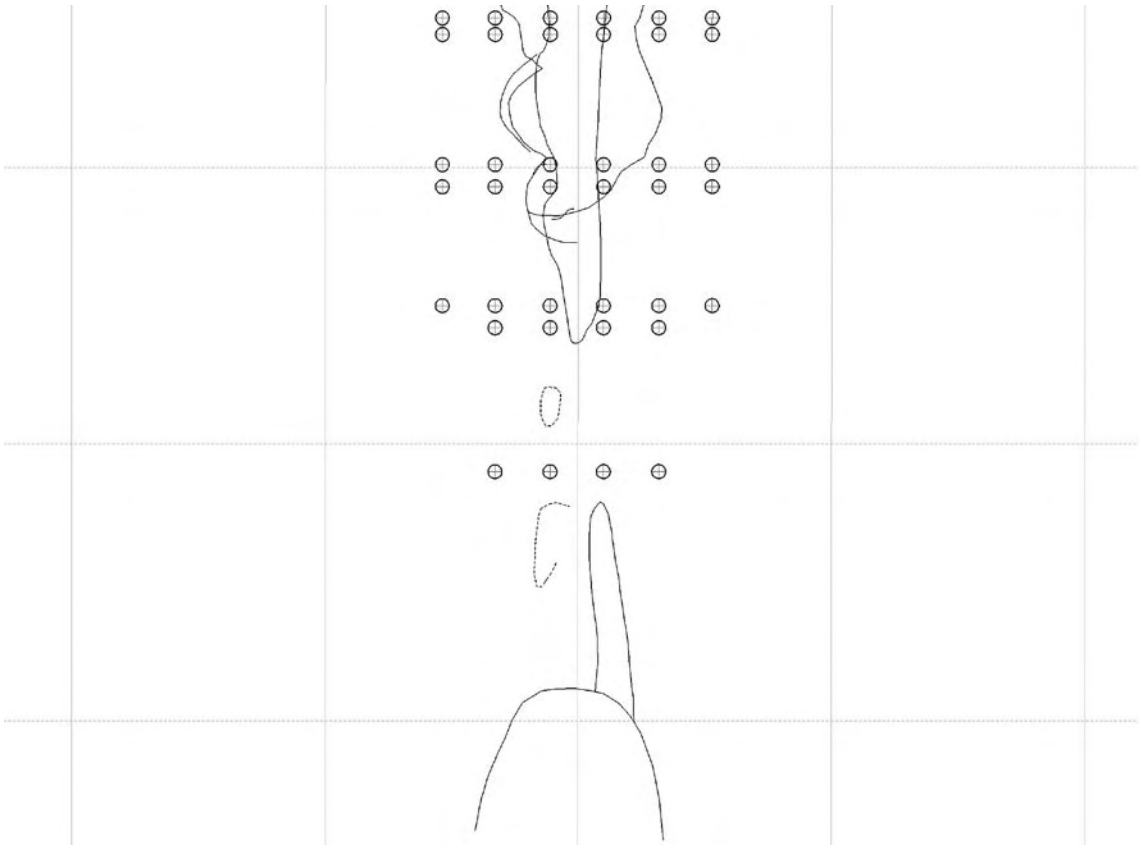

***Figure 5-51.*** *General extent of spalling on June 29.*

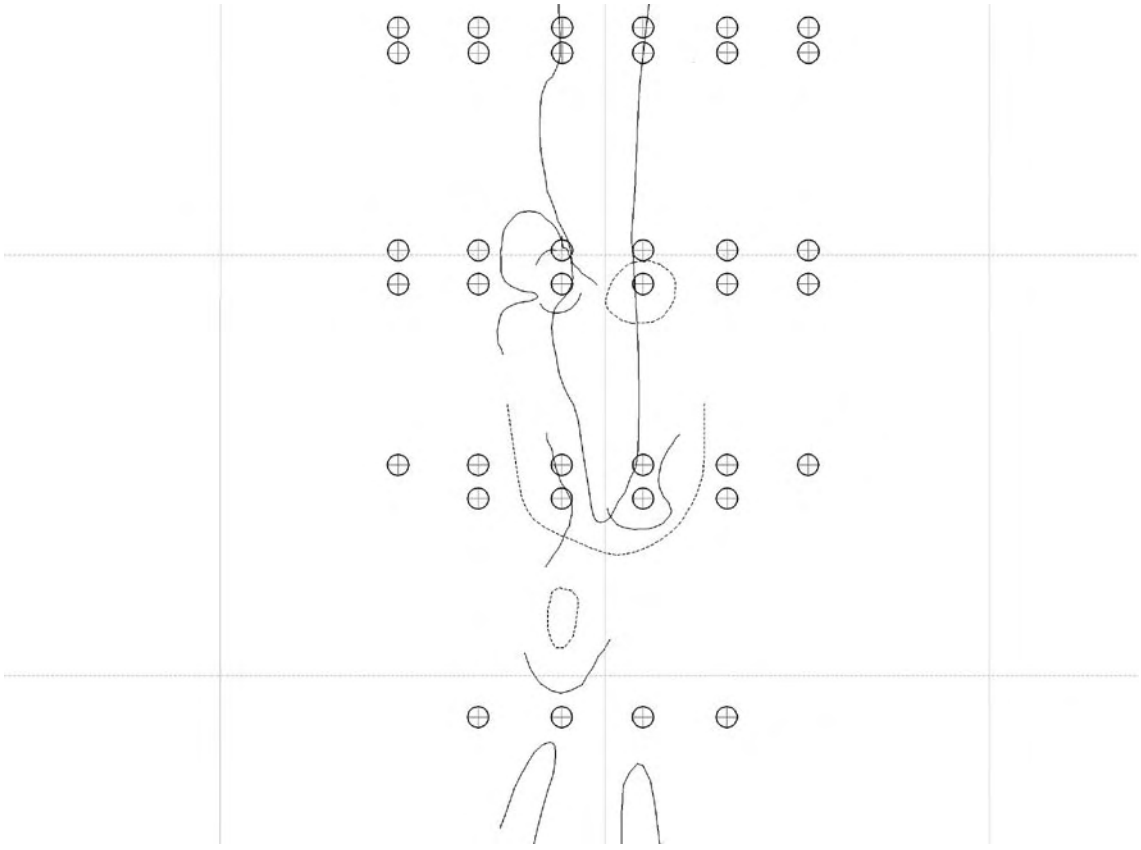

***Figure 5-52.*** *Detailed spalling observations on June 29.*

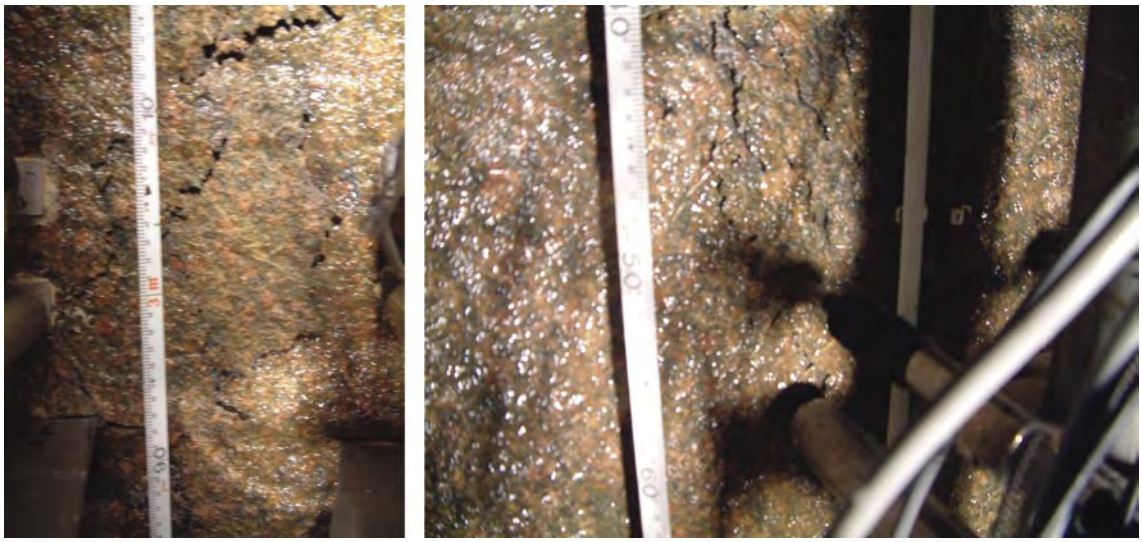

***Figure 5-53.*** *June 29. Photographs of spalling/fracturing at position #9 at the 3 m level (left) and at position #15 at the 3.5 m level (right).*

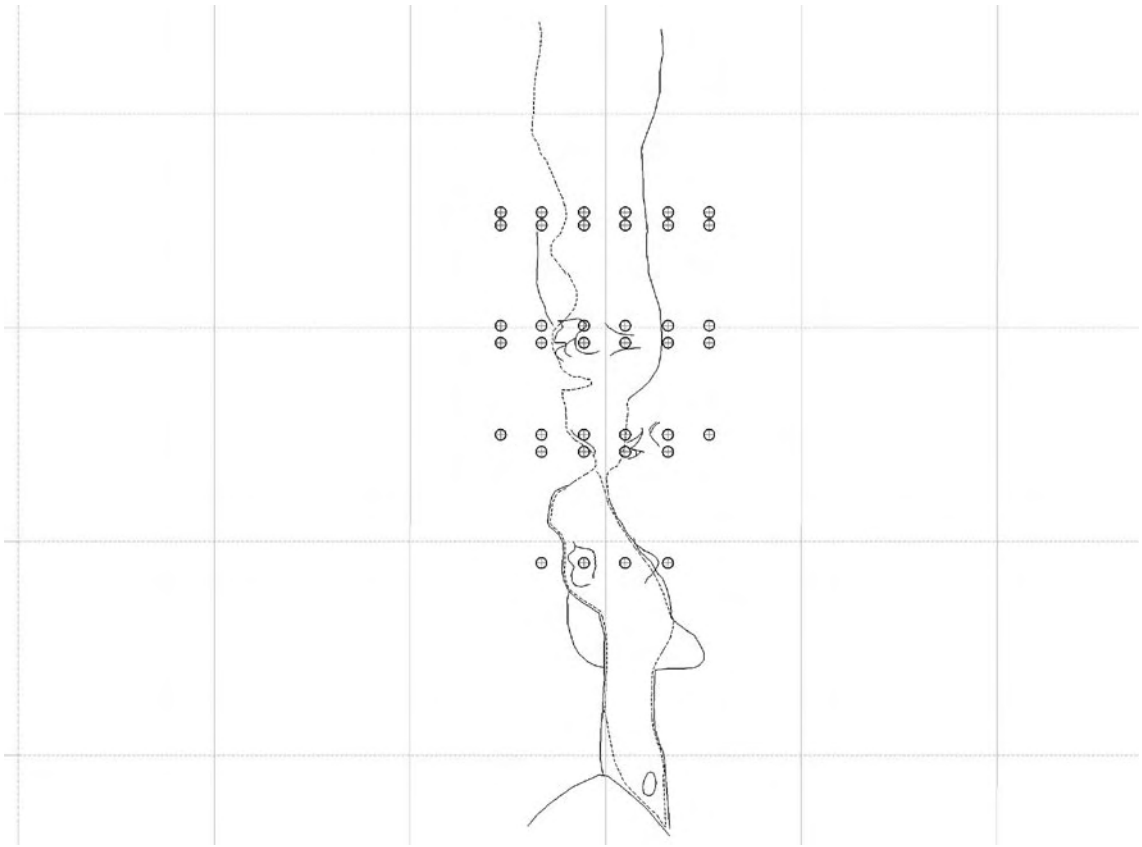

***Figure 5-54.*** *General extent of spalling on July 6.*

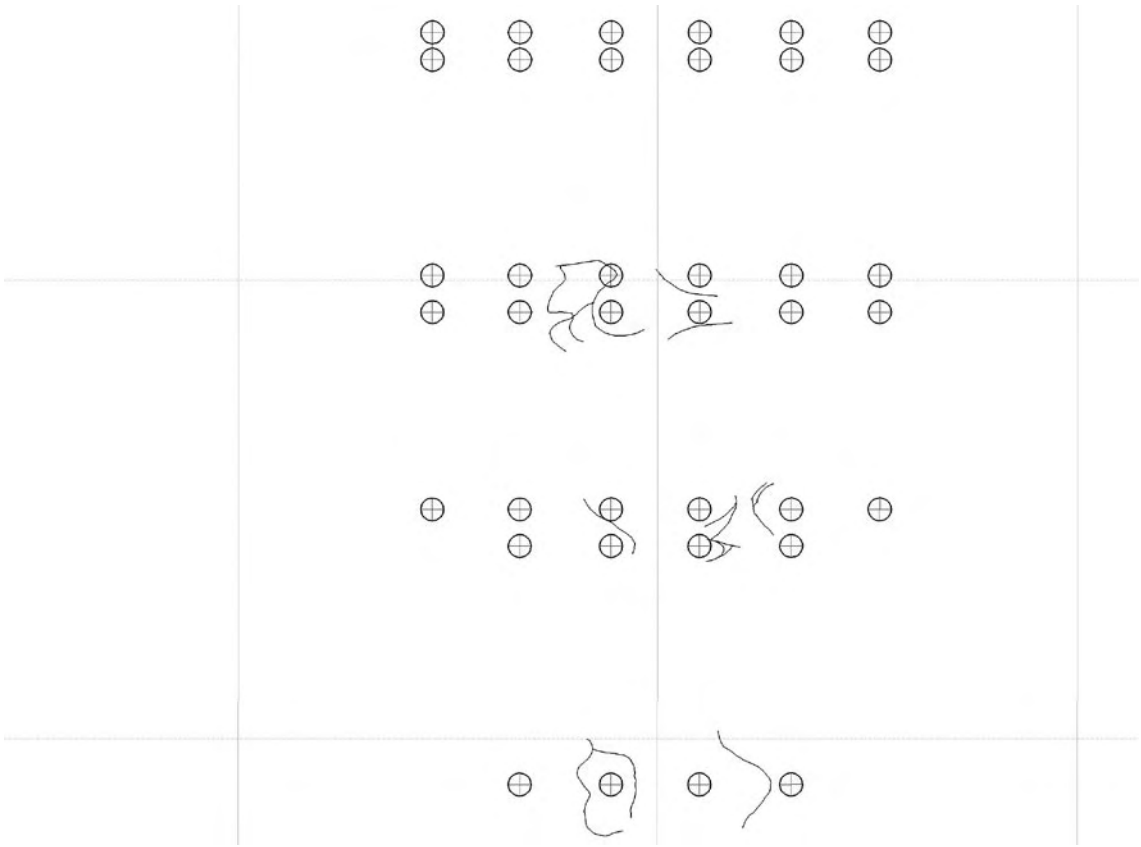

***Figure 5-55.*** *Detailed spalling observations on July 6.*

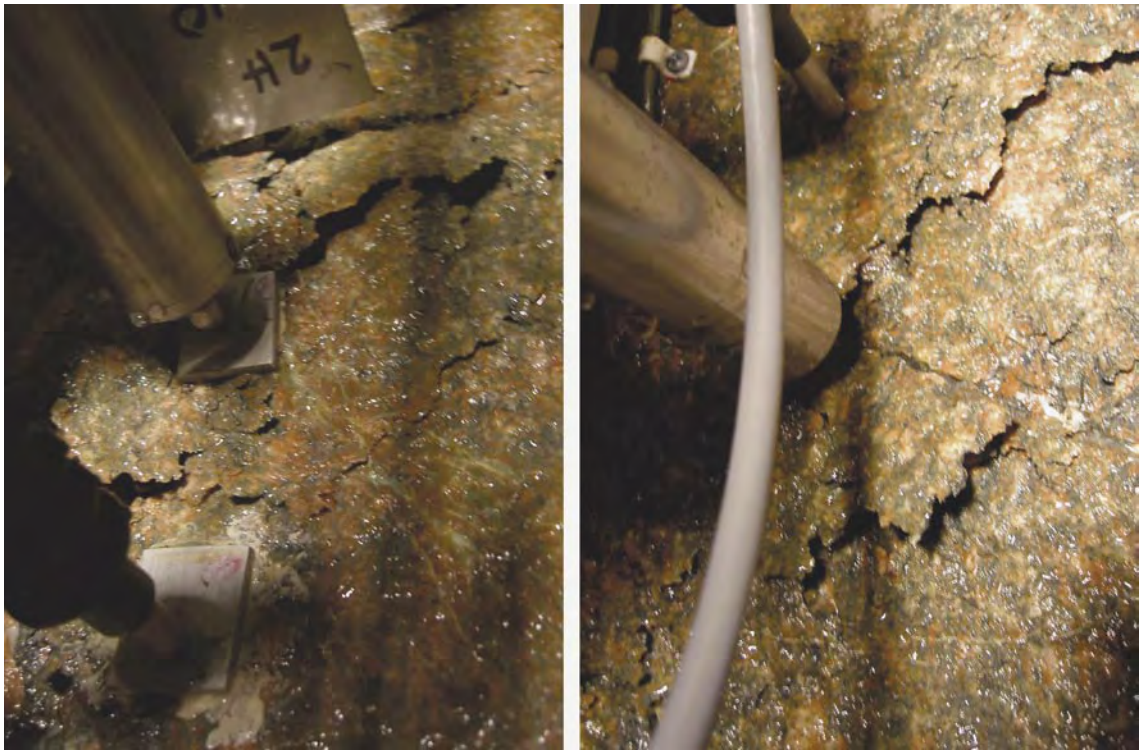

***Figure 5-56.*** *July 6. Photographs of position #10 (left) and position #16 (right).*

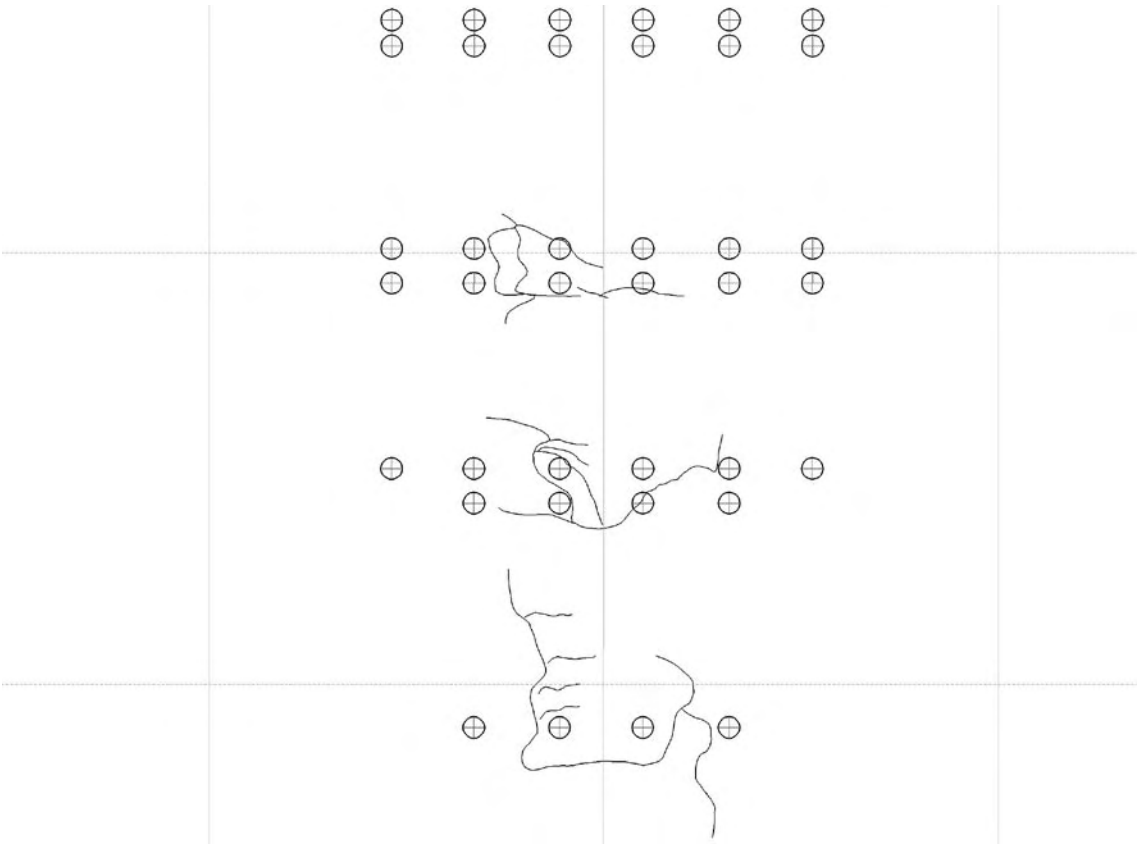

***Figure 5-57.*** *Spalling observations July 12.*

## 5.5 Removal of spalled slabs

When the heaters had been turned off and the rock had cooled down, the slabs formed during the spalling process were removed. The observations made during this work are presented in this section. Since spalling was progressing downwards, the slabs were firmly attached at their upper end. The work of removing the slabs therefore started at the bottom of the hole. All the loose slabs were removed from an approximately 0.5 m long section before work started on the following 0.5 m section. The observations are therefore listed from the bottom of the hole and up.

The process of removing the slabs was quite easy. The tip of a flat screwdriver was carefully inserted in the opening between two slabs. The screwdriver was then turned to widen the gap between the chips. This was done until the slab could be gripped with the fingers and lifted into the plastic container.

### 5.5.1 Depth 4.9 to 4.3 m

From 4.9 to 4.5 m the rock seemed to have moved along an existing fracture and looked crushed. The chipping was more pronounced further up the hole, and between each of the larger slabs there was a thin zone with fractured rock. On the slab's surfaces there were many small thin chips on a mm scale. The slabs appeared to have been formed along invisible weakness planes. The surface was slightly undulating and the shape seemed to be determined by small-scale geology such as feldspar eyes etc.

A small pit with relatively small chips on a mm to cm scale was created at a depth of 4.2 m approximately 0.5 m to the left of the notch in a small body of fine-grained greenstone. It looks like the greenstone was stiffer than the surrounding rock mass and attracted stresses until it failed, Figure 5-58.

Generally there are more small chips beneath and between the larger chips than could be seen from the surface. The chip size decreases closer to the notch. Its centre is quite crushed and consists of small fragments on a mm scale. The notch has followed an undulating path as it worked its way down the hole. This indicates that it followed the easiest way down. This is in itself an indication that the process has been quite slow since there has been time for the notch to move through the weaker parts of the rock instead of going the shortest way. That would probably have been the case if the process had been instantaneous.

All chips that were created in intact rock have very thin edges and are thicker in the centre. The thickness can be a few centimetres with edges thinner than half a millimetre. It is likely that the chips have been formed by pure normal displacement without shearing. The occurrence of shearing would probably have broken the thin edges of the chips/slabs.

No fractures could be found in the pillar wall after removal of the slabs. At some locations, pre-existing fractures have halted the growth of the spalling slabs. Where fracture growth has taken place in intact rock, a quite smooth and curved surface sub-parallel to the borehole wall remains.

Another interesting phenomenon occurred at this level as well. Some weaker rock was located at a depth of approximately 5 m. Spalling was initiated there on around June 16 and propagated upwards in the hole. The major spalling front was then at a depth of approximately 3 m in the hole. The upward-moving spalling reached a depth of about 4.1 m, where it joined the major spalling front. It is interesting to note the formation of the chips in the upward-moving front. Their loose end points upwards, in the opposite direction of the other spalled areas. It can be concluded that the spalling direction determines the geometry of the chips, which is also logical. A photograph of these chips is shown in Figure 5-59.

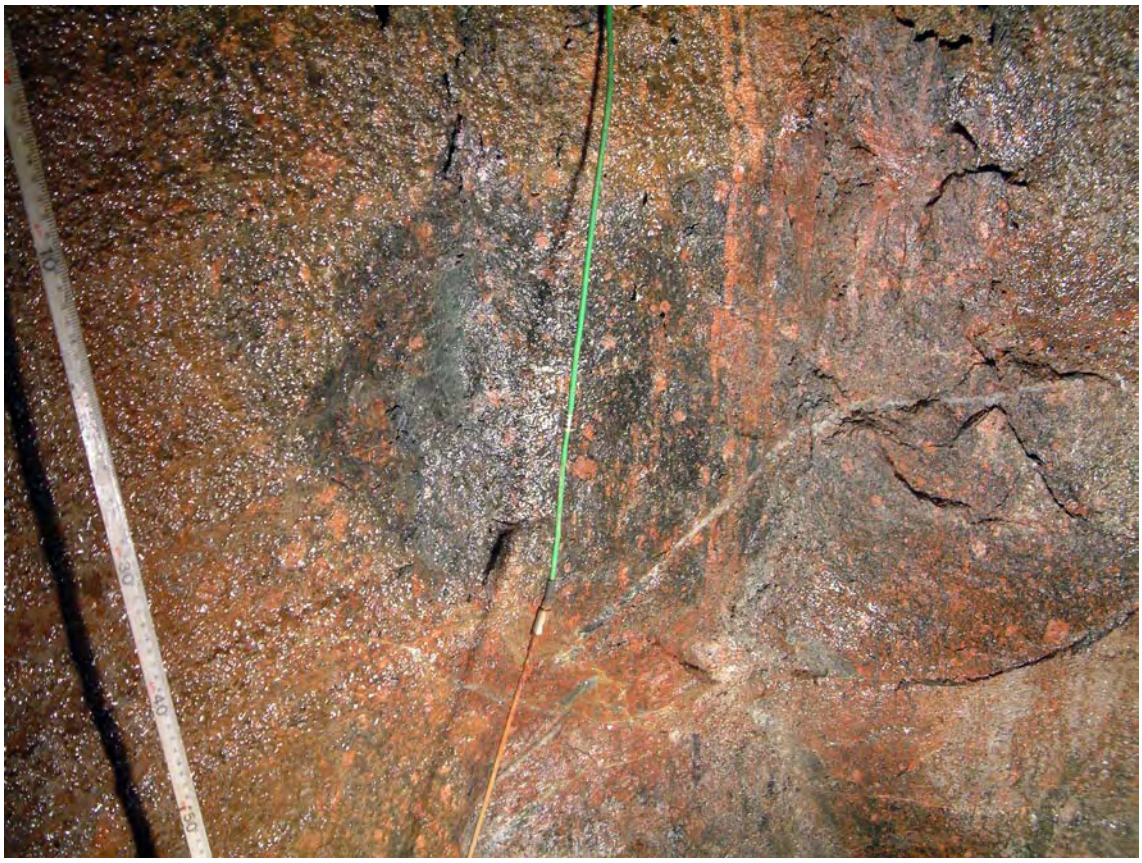

***Figure 5-58.*** *The greenstone body that created a small pit in the rock wall.*

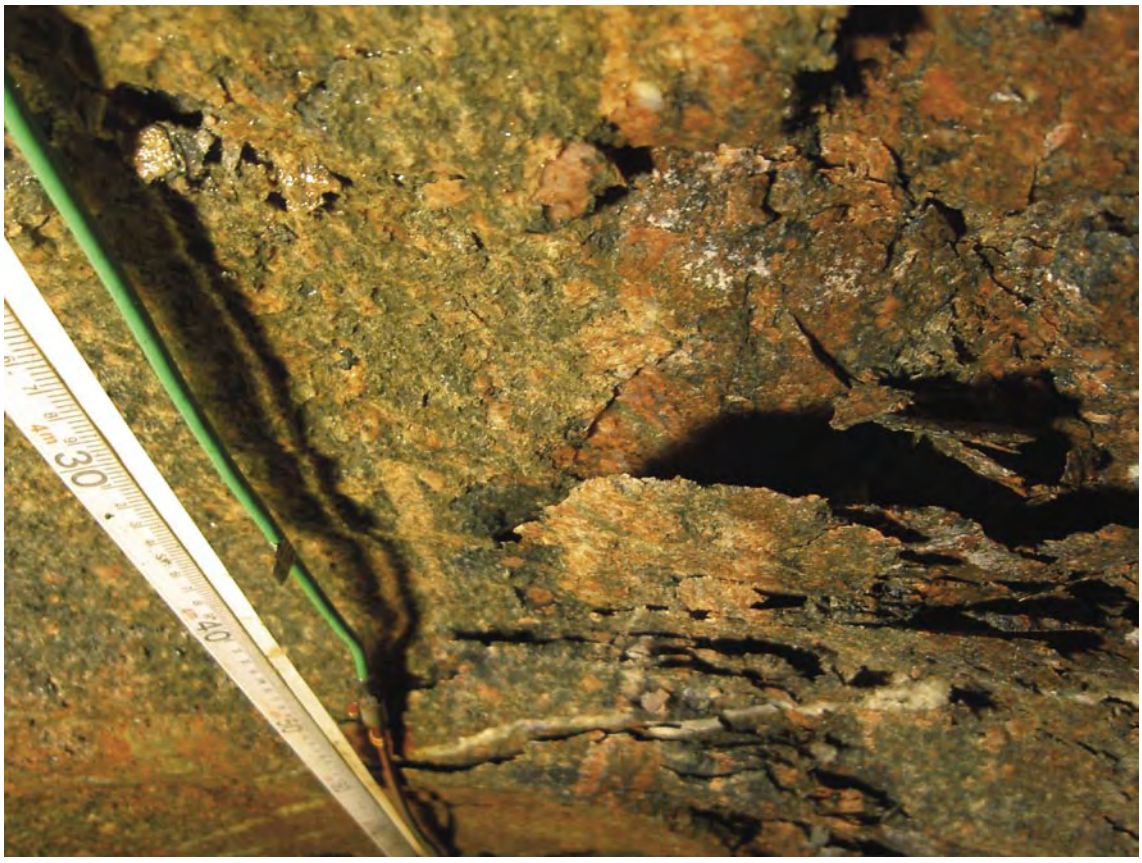

***Figure 5-59.*** *Photograph of the upward-pointing chips, looking downwards.*

### 5.5.2 Depth 4.3 to 3.7 m

On the surface there are very loose small chips, and beneath those the slabs become quite large, Figure 5-60. When a chip is removed one can see the typical small chips of mm scale that are present on almost all fracture surfaces. The chips in the notch are very small. The rock right next to it is however intact, which indicates that crushing in the notch and not pre-existing fracturing is the cause of the small chips. Another indication of crushing is grey dust in the centre of the notch. It is likely that this dust originates from a crushing process. It is very unlikely that the dust originates from drilling and has been transported there by water during the spalling process. The thin chips in the centre of the notch striking almost directly eastward in the Äspö 96 co-ordinate system or 45 degrees relative to the tunnel axis. The small chips are interlocked and quite difficult to remove.

At 4.2 m a chip with an arched shape was removed. This was the first chip of that shape that was found. The others have been flattish. If the remaining chips from 3.7 m and up are viewed from below, clear indications of arching can be seen. The displacement of the individual chips is also quite clear, Figure 5-61.

***Figure 5-60.*** *Photograph of rock wall at depth of approximately 4 m. The small cm-scale chips on top of the larger chips are clearly visible.*

***Figure 5-61.*** *Photograph taken from below of chips at 3.7 m and up. The dilatation and curvature of the slabs can be seen.*

### 5.5.3 Depth 3.7 to 3.3 m

Here as well there are small mm-scale chips on top of larger chips at the surface. The geometry looks the same as in the lower part of the hole (except at the very bottom where more crushing occurred). Rock slabs are arranged like fish scales on top of one another. All the scales are attached at their upper end, and the lower end is normally displaced. All the way from the bottom the centre of the notch is coloured greyish by the crushed rock powder. There are sub-vertical fractures going straight into the pillar in parts of the section. They strike approximately N105E.

Quite a lot of chips were removed up to 3.2 m. There are sub-horizontal chlorite-filled fractures in the section. The chips broke along these fractures when they were removed and subjected to a momentum. This determined the size of the removed chips in the longitudinal direction.

When looking at the notch surface to the left and right of the centre at 3.7 m one can see the arching, the chips are small but they are arched. There is a distinct difference at the very centre of the notch. The chips there are very small, on a cm scale, interlocked and difficult to remove. The rock behind is drummy but the fracturing is behind the slabs that can be removed (no fracture traces seen). The full extent of the spalling can therefore not be excavated. The notch at 3.4 to 3.5 m is not as crushed as it is below, instead the surface is smooth, Figure 5-62. This might be due to the fact that the full extent of the spalling not has been excavated and that the crushed centre is somewhere beneath.

From lower parts of the spalling up to a depth of 4.1 m in the hole, the complete notch surface is quite smooth and arched, even in the very centre. Between 4.1 to 3.6 m (especially between 4.3 to 4.1 m) there are fractures in the notch centre. The fractures enter the notch from the left, striking N075E. Above 3.6 m the fractures have changed direction and now enter the notch from the right, striking N145E, almost perpendicular to the tunnel axis. This part of the rock is much more oxidized than the other parts.

The remaining chips from 3.3 m and up in the hole are dilated on their left side while the right side is attached to the rock wall, Figure 5-63.

***Figure 5-62.*** *Photograph of the smooth arched notch at a depth of 3.7 m.*

***Figure 5-63.*** *Photograph of the slabs with a free left surface and the right side attached to the rock wall. The depth at the bottom of the photograph is 3 m.*

### 5.5.4 Depth 3.3 to 2.7 m

Almost all of the slabs between depths of 2.7 and 3.3 m have a free left edge and are attached to the rock on the right side, Figure 5-63. The slabs also have a larger area then in the previous sections and there are fewer cm scale chips. The slabs are more interlocked here than in the previous sections. One has to work one's way up and down the section to remove one chip that locks other chips into place. The dust from the crushed rock is present in the centre of the notch.

Between 3 and 3.2 m, the fractures entering the notch centre strike approximately N125E, almost parallel to the major principal stress direction. These fractures disappear above 3 m.

The steel plates glued to the rock wall for the LVDTs at the 3 m instrument level were removed. The upper plate in position #9 was attached to a chip covering its entire surface. The chip thickness was a few mm. A diagonal fracture divided the chip below the lower plate into two pieces. The right part of the chip was still glued to the plate and its thickness was about 15 mm.

The upper plate at position #10 fell down almost by itself. The back of the plate was covered with thin rock fragments. The lower plate at the same position also came down very easily. A thin rock chip was still attached to the entire back of the plate.

Both of the plates at position #11 were located at the same chip, whose thickness was about 10 mm.

Between 2.8 and 2.9 m, the slabs increase in thickness quite rapidly. The left edge is very thin and the right side, which is attached to the rock wall, is about 20 mm thick.

The notch surface between 3.2 to 2.7 m is quite smooth, Figure 5-64, especially above 3 m, and arching of the chips is visible. The slabs closest to the hole surface are the largest, after which the slabs decrease in size only to increase again at the notch bottom. It is mainly the slabs closer to the tip of the notch that are arched. As the 2.5 m instrument level is approached, an excellent view is obtained of the slabs beneath instrument position #3, Figure 5-65.

The slabs on the right side of the pillar centre at a depth of approximately 2.6 m and higher up have a larger area and are more tightly interlocked. The left side was therefore removed first, since it was easier to remove. On the right side there was one obvious difference compared with the other sections observed. The very small chips that have been present on the hole surface are not there and the usual cm-scale chips are very few in number. It would appear that the larger slabs were created instantaneously with no time for the small chips to grow in an increasing stress environment.

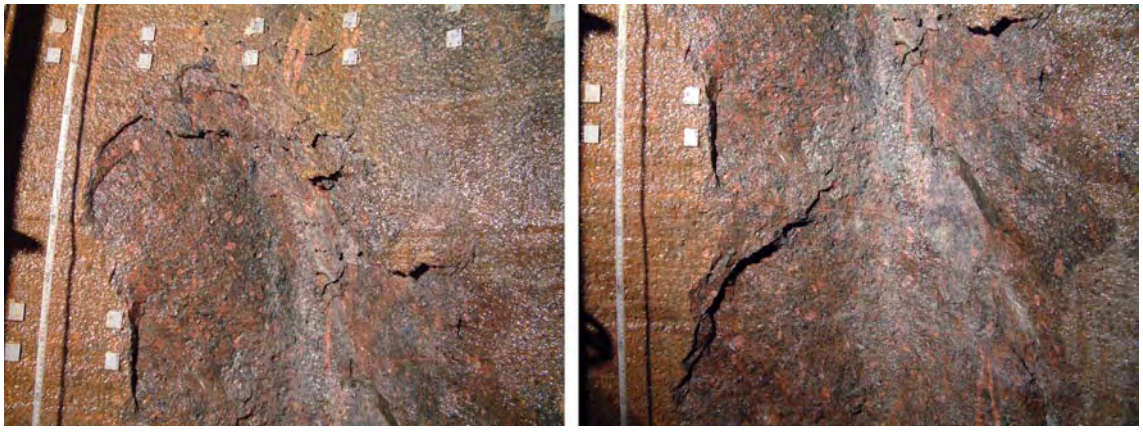

***Figure 5-64.*** *Photographs of the smooth notch surface. The upper two rows of steel plates in the left photograph are from the 2.5 m instrument level.*

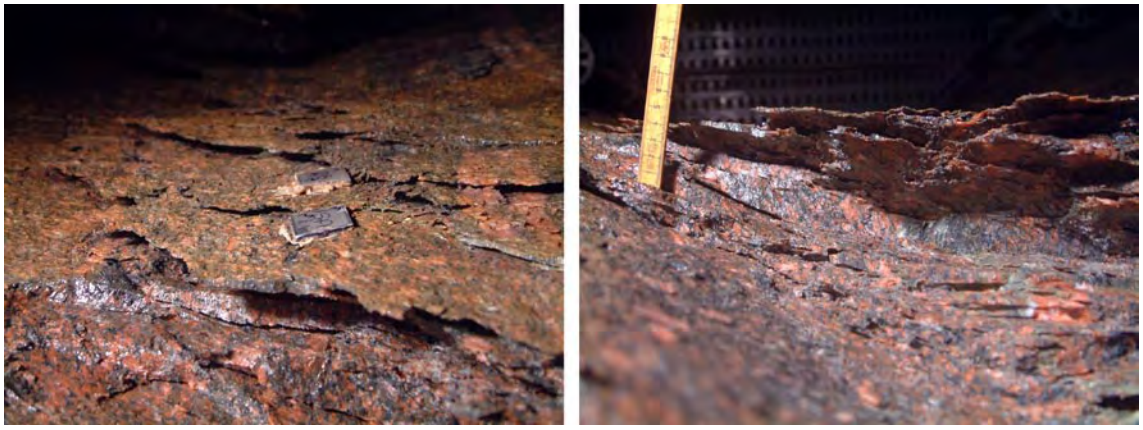

***Figure 5-65.*** *Photograph of the steel plates at instrument position #3 (left) and a photograph taken directly from below at the same location.*

### 5.5.5 Depth 2.7 to 2.1 m

In this section the fracture pattern becomes quite different from what has been seen deeper down in the hole. Fractures come in from the left with a large angle in relation to the tunnel axis. The slabs created become curved when they approach the centre of the pillar. In the deepest part of the notch the fracturing is very intense, and mostly cm-sized rock fragments were removed. Almost no slabs could be removed from the right side of the pillar, and the slabs on the left side were quite interlocked, Figure 5-66.

The slab to which the upper and lower steel plates at position #2 were glued was removed. The boundary fracture for the slab was beneath the centre of the upper plate and to the left of the lower plate. The lower plate fell off when the slab was removed. The rock behind the slab was not drummy. That slab is probably the only one that is formed at position #2.

The upper steel plate in position #3 was attached to quite a large slab. The slab is approximately 20 cm long and 15 cm wide with an oval shape. The slab's thickness is at a maximum 15 to 20 mm. The steel plate at position #3 lower came loose with a chip of approximately the same size as the plate. The chip was wedge-shaped and had a thin point ending about 1 cm above the plate. The chip's base was located at the lower end of the chip. The base thickness was approx 5 mm.

The same pattern regarding the distribution of the chip sizes is evident here as well. Beneath the larger slabs located closest to the hole periphery there is a zone with more intensely fractured rock (smaller chip size). Deeper into the notch the chip size then increases again.

The upper steel plate at position #4 fell down during work on nearby slabs. The plate was attached to a very thin chip. The lower plate at position #4 was easy to remove from the rock wall and it was drummy underneath.

***Figure 5-66.*** *Photograph at depth of approximately 2.5 m showing the right side of the pillar, where almost no slabs could be removed.*

### 5.5.6 Depth 2.1 to 1.6 m

This section enters the part of the hole that was spalled during the drilling. The initial spalling reached a depth of 1.95 m and is illustrated by the photograph in Figure 5-67.

The angle of the fracture entering the pillar from the left is now smaller, and the fracture strikes N080E. The right side of the pillar is drummy, but no rock fragments could be removed. The curvature of the slabs is more pronounced here. A beautifully arched chip from the centre of the notch was retrieved between 2 and 1.6 m, Figure 5-68.

While a chip close to 1.6 m was being removed, a number of large slabs between 1.6 to 1.1 m fell down to the bottom of the hole.

### 5.5.7 Depth 1.6 to 1.1 m

Like at 3.6 m, the fracturing angle is larger and more perpendicular to the tunnel axis. The complete spalled volume cannot be excavated, Figure 5-69. There seem to be fractures behind the wall, indicated by drumminess. The opposite edge of these fractures cannot be seen. They may, however, originate from a depth of 2.5 m, where fracture traces are visible that could continue behind the rock wall up to this level. The notch is located in a local inclusion of greenstone. The powder probably originating from crushed rock is clearly visible.

***Figure 5-67.*** *Photograph of the initial spalling in DQ0063G01 that occurred during the drilling.*

***Figure 5-68.*** *Photograph of the location of the arched chip and the chip itself.*

***Figure 5-69.*** *Photograph of the fractures and slabs between 1.6 and 1.1 m.*

### 5.5.8 Depth 1.1 to 0 m

From the beginning of the hole and down to 0.7 m, no spalling has occurred. The reason is probably softening of the rock mass in the floor from the excavation (Excavation Damaged Zone) as well as displacement along the ductile shear zone at the top of the pillar. Between 0.7 and 1.1 m, very little spalled rock was removed. However, the total volume of spalled rock in that region due to the drilling is in the same range as for the lower parts of the hole, where thermal effects triggered the spalling.

## 5.6 Extent of spalled and drummy area

Before the heating started and after the removal of the chips/slabs, the parts of the pillar wall that were spalled and drummy were mapped. Every 10 cm, the extent of the spalling and the drummy length was measured to the left and right of the centre line of the pillar. The individual points were connected by straight lines. A screwdriver was tapped against the rock wall to map the drummy zones. Spalling was defined as the parts of the rock wall where chips/slabs had fallen off or been removed. The results of the mapping, including the location of the notch after heating, are presented in Figure 5-70. The notch is located very close to the left boundary of the drummy area after heating. This is an effect of the induced fractures coming in from the left described in the sections about the removal of the slabs. Only the very superficial slabs created on the right side could be removed. The fractures from the left therefore continue beneath the rock surface, making it drummy.

Laser scanning was performed in the hole after the slabs were removed. A 3D survey of the spalled zone was thereby obtained. This survey was used to make a more precise drawing of the extent of the notch. In Figure 5-71 this drawing is superimposed on a photograph of the pillar wall. The laser scan was also used to measure the horizontal contour of the spalled zone. Spalling depth was plotted in intervals of 5 cm. The volume of spalled and removed rock over the depth of the notch is presented in Figure 5-72. The total spalled volume is approximately 0.1 $m^3$. In Figure 5-73 the spalled volume is presented together with the spalled area.

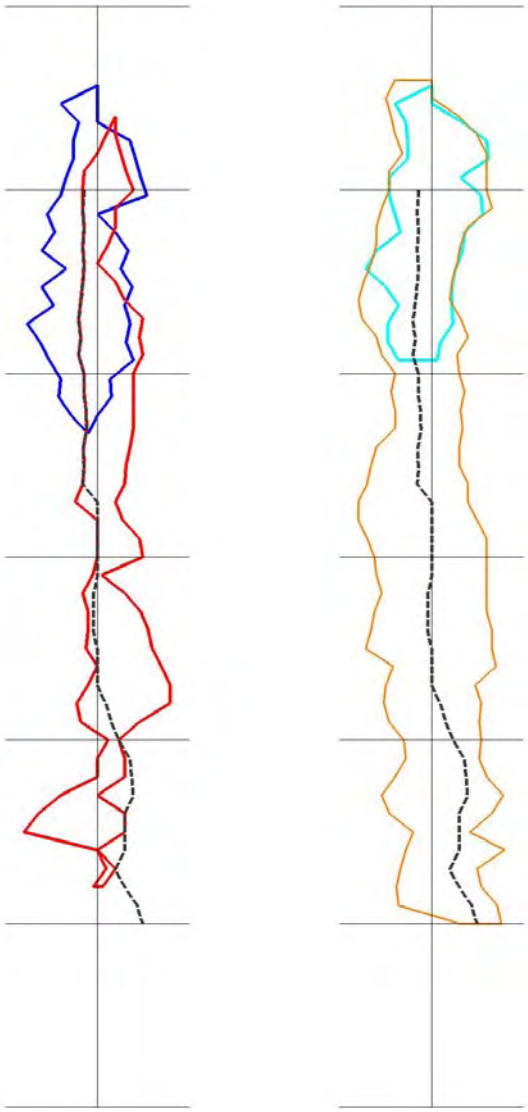

***Figure 5-70.*** *Left: mapping of the drummy areas before and after heating. Blue area before and red area after heating. Right: mapping of the spalled areas before and after heating. Turquoise area before and orange area after heating. The dashed line in both figures is the location of the deepest part of the notch after heating.*

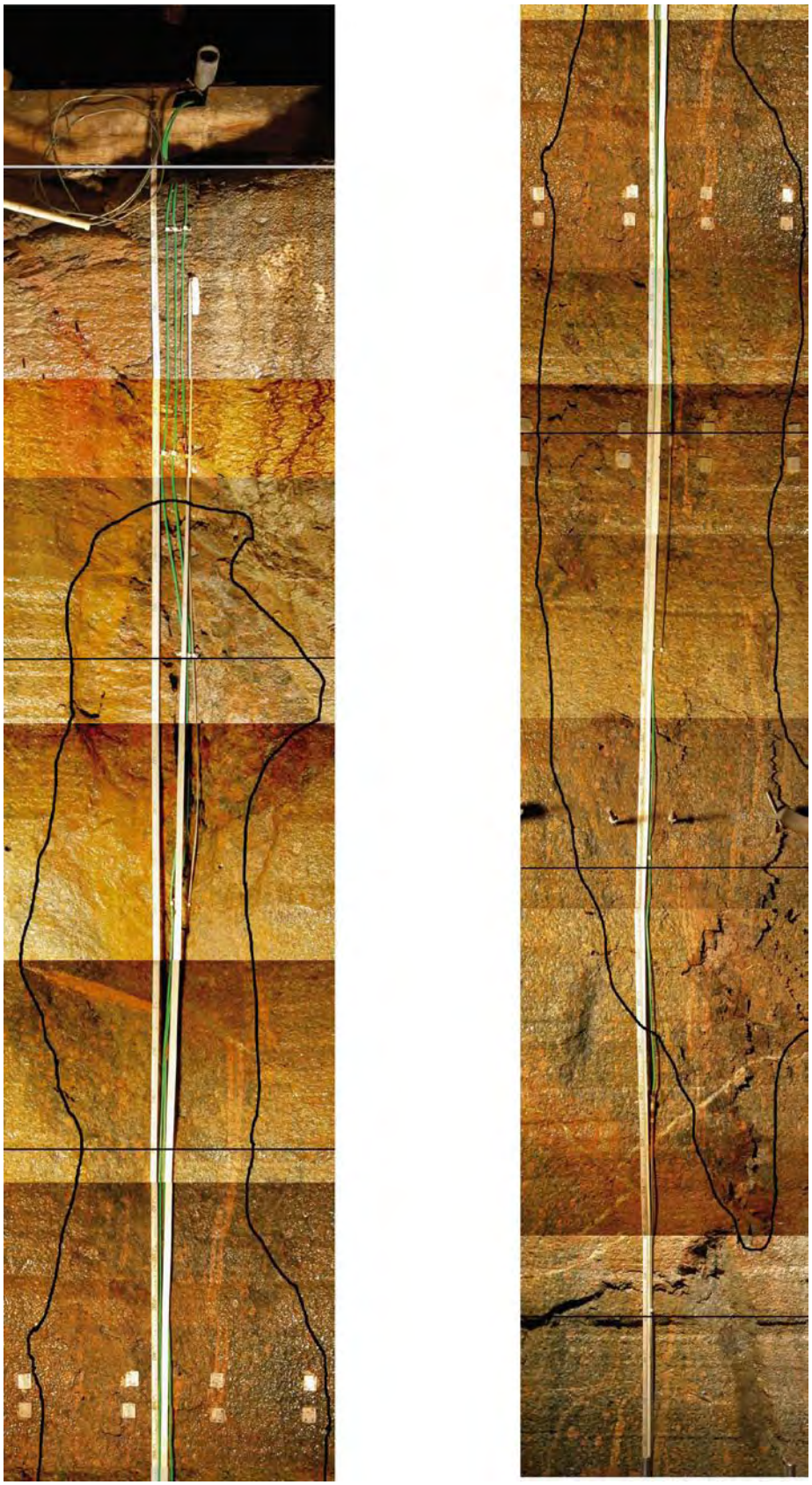

***Figure 5-71.*** *The final extent of the notch superimposed on a photograph of the pillar wall. The horizontal lines are metre markers.*

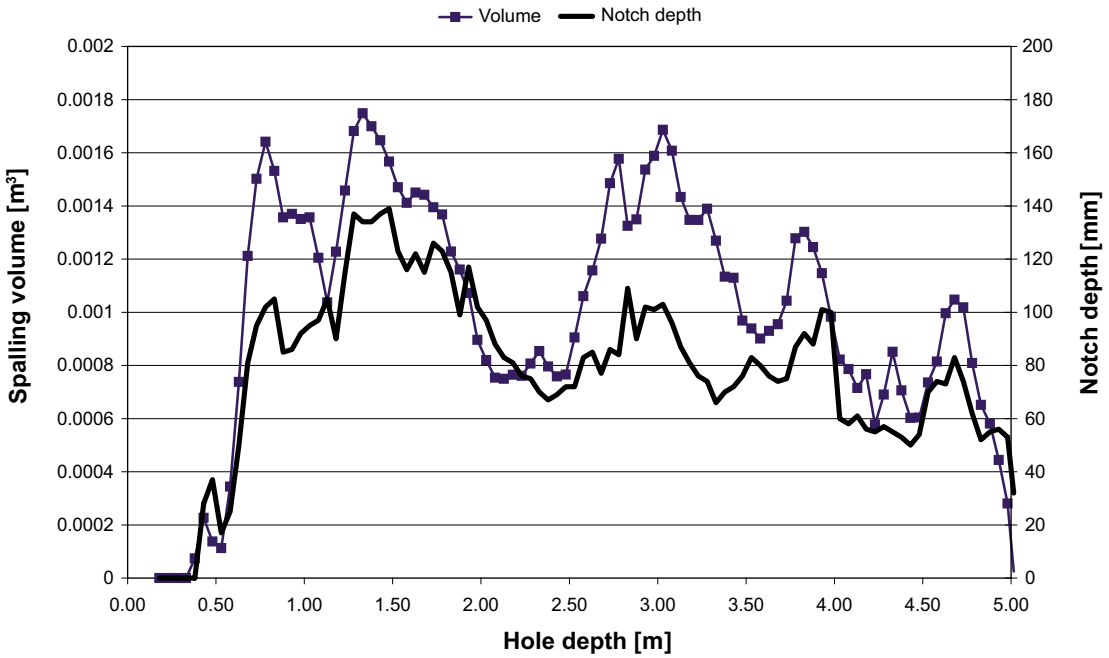


***Figure 5-72.*** *The volume of spalled and removed rock and the depth of the notch. The volume is presented in 50 mm increments.*

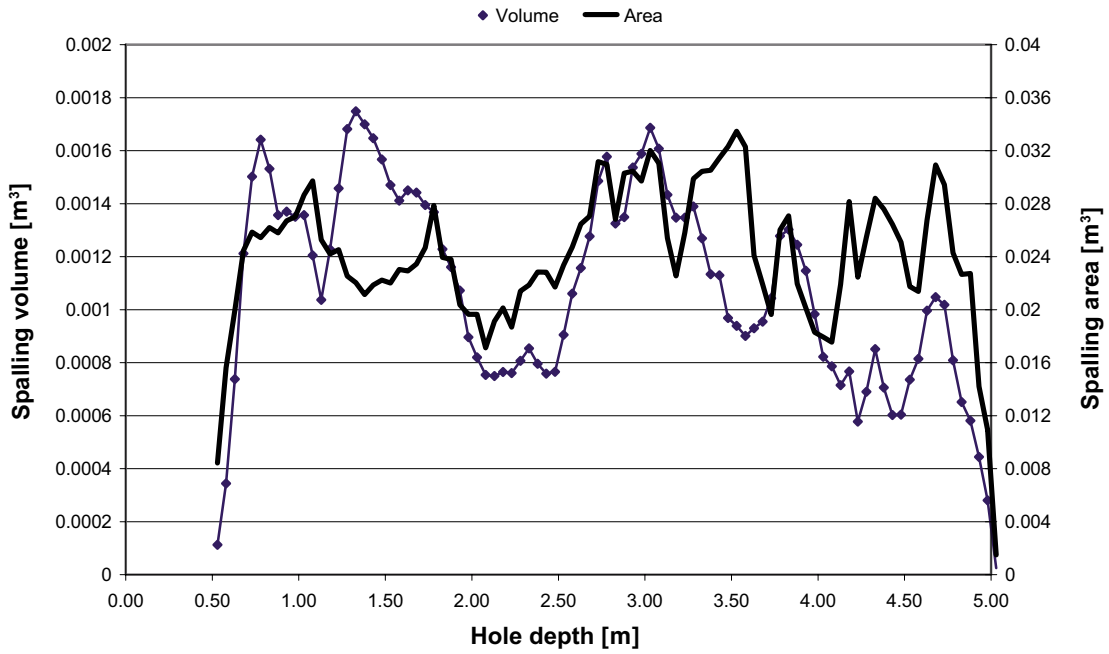


***Figure 5-73.*** *The volume and the area of the spalled and removed rock. Both presented in 50 mm increments.*

# 6 General summary

This section presents a general overview of the monitored acoustic emissions in relation to displacements for instrument levels three and four. Some of the work planned during the integrated analysis that will be reported at a separate occasion is also described. Some of the preliminary analyses done are also presented in /Andersson 2005/.

## 6.1 Acoustic emissions and displacements

The acoustic emissions can be related to actual monitored deformations during the whole experiment. However, with the current state of knowledge about the results it is not possible to determine an acoustic density that can be related to a specific deformation. As can be seen in the sample figures, these two parameters do not quite agree at all times, but it is nevertheless clear that the two are related. The acoustic emissions within instrument levels 2 and 3 (2.90–3.17 m and 3.40 to 3.67 m) are sorted out in Figure 6-1 and Figure 6-2. All acoustic events between those two levels are included. Only the LVDTs that account for the major displacement during the specific periods are presented. The figures show quite clearly how there is a deformation with a cluster of AE events followed by a reasonably quiet period. What happens is that the rock fails and the stresses are re-distributed. The stresses have to be built up by the increasing thermal load until the ultimate strength of a portion of the rock is reached and failure occurs again. The temperature of the rock at the approximate depth is shown in Figure 5-11.

One thing must be borne in mind when comparing the acoustic emission density and the displacement for a given area/rock volume. As spalling progresses, the slabs area decreases but the thickness increases deeper into the notch. It is therefore possible that acoustic events/deformations above or below the studied zone affect the displacements at the LVDTs. In this case they will not show up on the accumulated acoustic emission curve for the zone, since they have been filtered out. Caution is therefore necessary when studying the relationships in detail.

Photographs of the instrument positions were taken during visits in the hole. To exemplify the development of the notch, photographs taken at the approximate same positions at two different dates are compared in Figure 6-3 and Figure 6-4.

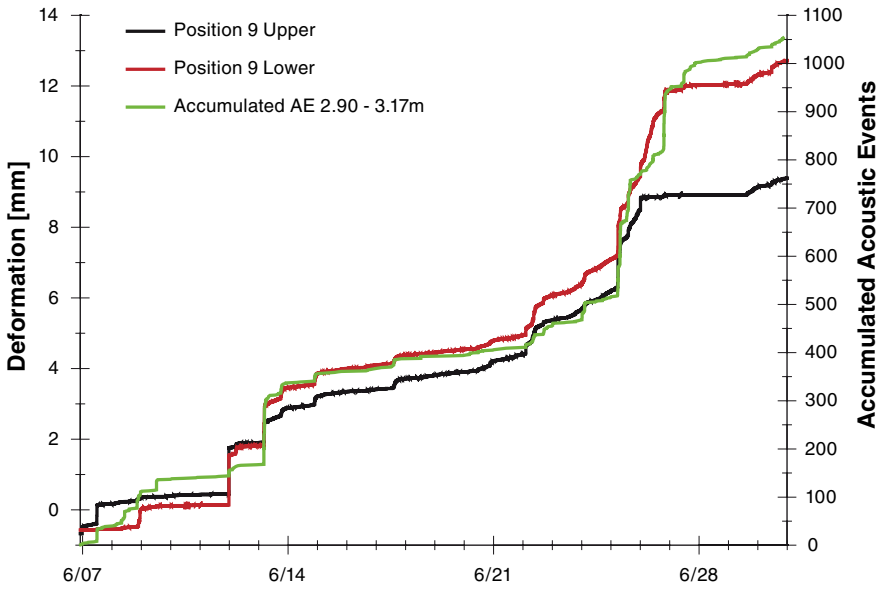


***Figure 6-1.*** *Deformations at upper and lower instrument positions #9. All the accumulated acoustic events at that instrument level (2) are also included.*

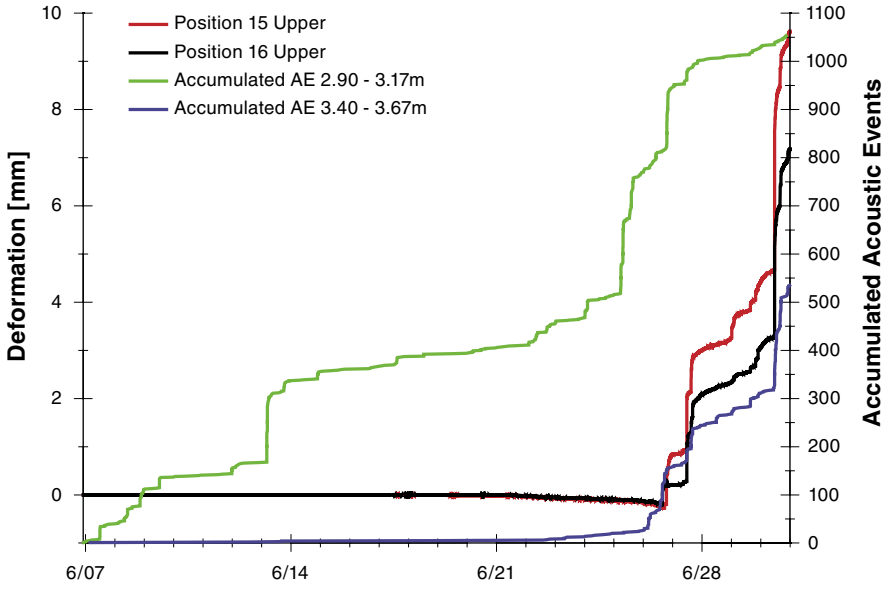


***Figure 6-2.*** *Deformations at upper instrument positions #15 and #16. All the accumulated acoustic events at that instrument level (3) are also included. The acoustic emissions from the second level are also included for comparison.*

***Figure 6-3.*** *Photograph of instrument position #9 was taken on June 2nd (left) and on June 16th (right).*

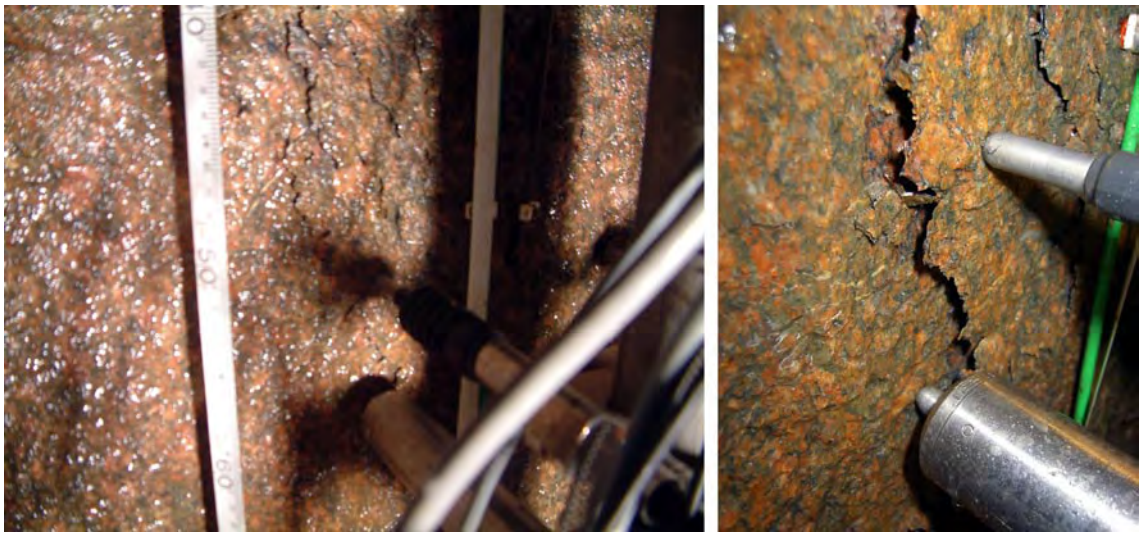

***Figure 6-4.*** *Photograph of instrument position #15 was taken on June 29th (left) and on July 12th (right).*

## 6.2 Confinement

The confinement pressure was released in 50 kPa decrements. There was in principle no response in the rock mass until the confinement pressure was in the range between 150 to 250 kPa. The fact that the acoustic and displacement response occurred in the open and not the confined hole indicates the importance of geometry. In the open, spalled hole there was a delicate equilibrium between the strength of the rock and the stresses. The small stress change caused by the change of confinement pressure in the other hole triggered the failure process. The extremely limited response in the confined hole may be due to the fact that the hole wall still had a circular geometry that redistributed the stresses evenly and did not create a deviating stress field large enough to initiate failure.

## 6.3 Spalling strength

A preliminary analysis has been performed of the spalling strength of the rock. First the stresses acting at the level where the initial spalling after boring stopped were calculated. This was straightforward since only the geometry-induced stresses had to be taken into account. At a depth of 1.95 m, where the initial spalling stopped, the stress at the notch tip was 117 MPa.

When the LVDTs at a certain level start to record displacements, the notch can be said to have reached that level. The thermal stress contribution for the whole experiment time has been back calculated and is presented in /Fälth et al. 2004/. The thermal stress is added to the static stress and the spllaing strencth at the insturment levels is calculated. Preliminary assessments of the thermal contribution indicate that the spalling strengths at instrument levels number 2, 3 and 4 are 121, 128 and 123 MPa respectively. The spalling strength is relatively close to the values determined in the virtually unfractured Lac du Bonnet granite. A spalling strength of 120 MPa is reported for that rock by /Martin and Read 1996/. This indicates that it is the properties of the intact rock and the mineral grains that control the onset of spalling.

# 7 Planned work

The Äspö Pillar Stability Experiment has generated a large, high-quality data set. Parts of the data set will be further studied on behalf of SKB. Three main topics will be investigated:

1. The data sets from displacement and acoustic emission monitoring will be integrated. The objective will be to study notch development in relation to stresses, displacements and acoustic emission. Efforts will be made to correlate spalling damage with acoustic density at that location.
2. How yielding occurs in the fractured rock as the notch tip advances will be studied. Numerical modelling will be used to try to replicate the contraction of the rock recorded before the notch reaches an instrumented location.
3. Spalling strength will be determined. The thermally induced stress will be modelled and superimposed on the pillar stress created by the chosen geometry. The LVDTs will be used to determine the exact times when the notch reaches a certain depth. The stress at that location will then be calculated and the spalling strength can be determined.

# 8 Äspö Pillar Stability Experiment reports

A number of working reports and publications have been produced during the planning, modelling, design and characterization phase of the experiment. These are listed below.

**Andersson J C.** Äspö Pillar Stability Experiment, Feasibility Study. SKB IPR-03-01, Svensk Kärnbränslehantering AB.

**Andersson J C.** Äspö Pillar Stability Experiment, Summary of preparatory work and predictive modelling. SKB R-03-02, Svensk Kärnbränslehantering AB.

**Andersson J C, Martin C D, Christiansson R.** SKB's Äspö Pillar Stability Experiment, Sweden. In the proceedings of Gulf Rocks 2004, the 6th North American Rock Mechanics Symposium (NARMS), Houston, Texas, June 5–9, 2004.

**Andersson J C, Rinne M, Staub I, Wanne T, Stephansson O, Hudson J A, Jing L (ed.).** The on-going pillar stability experiment at the Äspö Hard Rock Laboratory, Sweden. In the proceedings of GeoProc 2003, International conference on coupled T-H-M-C processes in Geo-systems: Fundamentals, Modelling, Experiments & Applications. KTH, October 13–15, 2003, Stockholm, Sweden, p 385–390.

**Andersson J C, Martin C D, Sugawara K, Obara Y, Sato A (ed.).** Stress variability and the design of the Äspö Pillar Stability Experiment. In the proceedings of the third international symposium on rock stress. RS Kumamoto '03, 4–6 November 2003, Kumamoto Japan, p 321–326.

**Andersson J C.** Äspö Pillar Stability Experiment. In the proceedings of the 40th Rock Mechanics Meeting, Stockholm March 14, 2005. Edited by SveBeFo, Swedish Rock Engineering Research.

**Barton N.** Äspö Hard Rock Laboratory, Äspö Pillar Stability Experiment, Q-logging of the APSE tunnel at Äspö, For rock quality assessment and for development of preliminary model parameters. SKB IPR-04-07, Svensk Kärnbränslehantering AB.

**Bjelkström E, Ekblad A.** Djupförvarsteknik. Äspö Pillar Stability Experiment. Riskbedömning samt rekommendationer för sprängningsarbeten vid utbyggnad av nya tunnlar inom 450 m nivån, Äspö HRL. SKB TD-02-19, Svensk Kärnbränslehantering AB.

**Eng A, Andersson J C.** Äspö Pillar Stability Experiment. Description of the displacement and temperature monitoring system. SKB IPR-05-19,
Svensk Kärnbränslehantering AB.

**Fransson Å.** Äspö Hard Rock Laboratory. Äspö Pillar Stability Experiment. Core boreholes KF0066A01, KF0069A01, KA3386A01 and KA3376B01: Hydrogeological characterization and pressure responses during drilling and testing. SKB IPR-03-06, Svensk Kärnbränslehantering AB.

**Fredriksson A, Staub I, Janson T.** Äspö Hard Rock Laboratory. Äspö Pillar Stability Experiment. Design of heaters and preliminary results from coupled 2D thermo-mechanical modelling. SKB report IPR-03-03, Svensk Kärnbränslehantering AB.

**Fredriksson A, Staub I, Outters N.** Äspö Pillar Stability Experiment, Final 2D coupled thermo-mechanical modelling. SKB R-04-02, Svensk Kärnbränslehantering AB.

**Fälth B, Kristensson O, Hökmark H.** Äspö Hard Rock Laboratory, Äspö Pillar Stability Experiment. Thermo-mechanical 3D back analyze of the heating phase. SKB IPR-04-19, Svensk Kärnbränslehantering AB.

**Hardenby C.** Äspö Pillar Stability Experiment. Geological mapping of the pillar. SKB IPR-05-24, Svensk Kärnbränslehantering AB.

**Haycox J R, Pettitt W S, Young R P.** Äspö Pillar Stability Experiment. Acoustic Emission and Ultrasonic Monitoring. SKB R-05-09, Svensk Kärnbränslehantering AB.

**Magnor B.** Äspö Hard Rock Laboratory. Äspö Pillar Stability Experiment. Geological mapping of tunnel TASQ. SKB IPR-04-03, Svensk Kärnbränslehantering AB.

**Olsson M, Niklasson B, Wilson L, Andersson J C, Christiansson R.** Äspö HRL Experiences of blasting of the TASQ tunnel. SKB R-04-73, Svensk Kärnbränslehantering AB.

**Pöllänen J, Rouhainen P.** Äspö Hard Rock Laboratory. Difference flow measurements in boreholes KA3386A01, KF0066A01 and KKF0069A01 at the Äspö HRL. SKB IPR-02-55, Svensk Kärnbränslehantering AB.

**Pöllänen J, Rouhainen P.** Äspö Hard Rock Laboratory. Difference flow measurements in borehole KA3376B01 at the Äspö HRL. SKB IPR-03-07, Svensk Kärnbränslehantering AB.

**Rinne M, Baotang S, Lee H-S.** Äspö Hard Rock Laboratory. Äspö Pillar Stability Experiment. Modelling of fracture stability by Fracod. Preliminary results. SKB IPR-03-05, Svensk Kärnbränslehantering AB.

**Rinne M, Lee H-S, Shen B.** Äspö Pillar Stability Experiment, Modelling of fracture development of APSE by FRACOD. SKB R-04-04, Svensk Kärnbränslehantering AB.

**Sjöberg J.** Äspö Hard Rock Laboratory. Äspö Pillar Stability Experiment. 3D overcoring rock stress measurements in borehole KA3376B01 at Äspö HRL. SKB IPR-03-16, Svensk Kärnbränslehantering AB.

**Staub I, Janson T, Fredriksson A.** Äspö Hard Rock Laboratory. Äspö Pillar Stability Experiment. Geology and properties of the rock mass around the experiment volume. SKB IPR-03-02, Svensk Kärnbränslehantering AB.

**Staub I, Andersson J C, Magnor B.** Äspö Pillar Stability Experiment, Geology and mechanical properties of the rock in TASQ. SKB R-04-01, Svensk Kärnbränslehantering AB.

**Wanne T, Johansson E.** Äspö Hard Rock Laboratory. Äspö Pillar Stability Experiment. Coupled 3d thermo-mechanical modelling. Preliminary results. SKB IPR-03-04, Svensk Kärnbränslehantering AB.

**Wanne T, Johansson E, Potyondy D.** Äspö Pillar Stability Experiment, Final Coupled 3D thermo – mechanical modeling.

**Preliminary Particle** – mechanical modeling. SKB R-04-03, Svensk Kärnbränslehantering AB.

# 9 References

**Andersson J C, 2003a.** Äspö Pillar Stability Experiment, Feasibility Study. SKB IPR-03-01, Svensk Kärnbränslehantering AB.

**Andersson J C, 2003b.** Äspö Pillar Stability Experiment, Summary of preparatory work and predictive modelling. SKB R-03-02, Svensk Kärnbränslehantering AB.

**Andersson J C, Martin C D, 2003.** Stress variability and the design of the Äspö Pillar Stability Experiment. In the proceedings of the third international symposium on rock stress. Edited by: Katsuhiko Sugawara and Yuozo Obara and Akira Sato. RS Kumamoto '03, 4–6 November 2003, Kumamoto Japan, p 321–326

**Andersson J C, Martin C D, Christiansson R, 2004.** SKB's Äspö Pillar Stability Experiment, Sweden. In the proceedings of Gulf Rocks 2004, the 6th North American Rock Mechanics Symposium (NARMS), Houston, Texas, June 5–9, 2004.

**Andersson J C, Rinne M, Staub I, Wanne T, 2003.** The on-going pillar stability experiment at the Äspö Hard Rock Laboratory, Sweden. In the proceedings of GeoProc 2003, International conference on coupled T-H-M-C processes in Geo-systems: Fundamentals, Modelling, Experiments & Applications. Edited by: Stephansson, O. and Hudson, J.A. and Jing, L. KTH, October 13–15, 2003, Stockholm, Sweden, p 385–390, Svensk Kärnbränslehantering AB.

**Andersson J C, 2005.** Äspö Pillar Stability Experiment. In the proceedings of the 40th Rock Mechanics Meeting, Stockholm March 14, 2005. Edited by SveBeFo, Swedish Rock Engineering Research group.

**Eng A, Andersson J C, 2004.** Äspö Pillar Stability Experiment. Description of the displacement and temperature monitoring system. SKB IPR-04-15, Svensk Kärnbränslehantering AB.

**Fälth B, Kristensson O, Hökmark H, 2004.** Äspö Hard Rock Laboratory, Äspö Pillar Stability Experiment. Thermo-mechanical 3D back analyze of the heating phase. SKB IPR-04-19, Svensk Kärnbränslehantering AB.

**Hardenby C, 2005.** Äspö Pillar Stability Experiment. Geological mapping of the pillar. SKB IPR-05-24, Svensk Kärnbränslehantering AB.

**Haycox J R, Pettitt W S, Young R P, 2005.** Äspö Pillar Stability Experiment. Acoustic Emission and Ultrasonic Monitoring. SKB R-05-09, Svensk Kärnbränslehantering AB.

**Janson T, Stigsson M, 2002.** Test with different stress measurement methods in two orthogonal bore holes in Äspö HRL. SKB R-02-26, Svensk Kärnbränslehantering AB.

**Magnor B, 2004.** Äspö Hard Rock Laboratory. Äspö Pillar Stability Experiment. Geological mapping of tunnel TASQ. SKB IPR-04-03, Svensk Kärnbränslehantering AB.

**Martin C D, Read R S, 1996.** AECL's Mine-by Experiment: A test tunnel in brittle rock. In Proc. 2nd North American Rock Mechanics Symposium, Montreal Edited by M. Aubertin, F. Hassani, and H. Mitri. Vol 1 pp 13–24, A.A. Balkema, Rotterdam.

**Olsson M, Niklasson B, Wilson L, Andersson C, Christiansson R, 2004.** Aspö HRL Experiences of blasting of the TASQ tunnel. SKB R-04-73. Svensk Kärnbränslehantering AB.

**Staub I, Andersson J C, Magnor B, 2004.** Äspö Pillar Stability Experiment, Geology and mechanical properties of the rock in TASQ. SKB R-04-01, Svensk Kärnbränslehantering AB.

# Appendix 1

**Filtered time intervals**

| Time turn OFF | Time turn ON |
|---|---|
| 2004-05-12;15:20:00 | 2004-05-12;16:00:00 |
| 2004-05-14;15:00:00 | 2004-05-14;16:20:00 |
| 2004-05-18;10:08:00 | 2004-05-18;11:28:00 |
| 2004-05-18;15:55:00 | 2004-05-18;16:35:00 |
| 2004-05-25;10:02:00 | 2004-05-25;11:31:00 |
| 2004-05-25;12:53:00 | 2004-05-25;14:42:00 |
| 2004-05-25;15:39:00 | 2004-05-25;17:16:00 |
| 2004-05-27;10:35:00 | 2004-05-27;11:30:00 |
| 2004-05-27;12:34:00 | 2004-05-27;15:12:00 |
| 2004-05-28;12:52:00 | 2004-05-28;14:11:00 |
| 2004-06-01;13:37:00 | 2004-06-01;15:25:00 |
| 2004-06-02;08:16:00 | 2004-06-02;09:30:00 |
| 2004-06-02;16:15:00 | 2004-06-02;17:10:00 |
| 2004-06-03;13:25:00 | 2004-06-03;16:30:00 |
| 2004-06-04;08:30:00 | 2004-06-04;09:11:00 |
| 2004-06-04;13:20:00 | 2004-06-04;13:37:00 |
| 2004-06-08;12:38:00 | 2004-06-08;13:26:00 |
| 2004-06-16;10:19:00 | 2004-06-16;11:21:00 |
| 2004-06-16;12:49:00 | 2004-06-16;14:00:00 |
| 2004-06-17;08:36:00 | 2004-06-17;12:00:00 |
| 2004-06-23;09:45:00 | 2004-06-23;11:30:00 |
| 2004-06-29;10:21:00 | 2004-06-29;11:30:00 |
| 2004-06-29;12:43:00 | 2004-06-29;14:24:00 |
| 2004-07-02;14:20:00 | 2004-07-02;15:20:00 |
| 2004-07-06;10:10:00 | 2004-07-06;11:30:00 |
| 2004-07-12;13:03:00 | 2004-07-11;14:45:00 |
| 2004-07-15;20:07:00 | 2004-07-15;20:22:00 |
| 2004-08-03;10:03:00 | 2004-08-03;11:11:00 |

# Appendix 2

**Displacement graphs of instrument positions with very small movements**

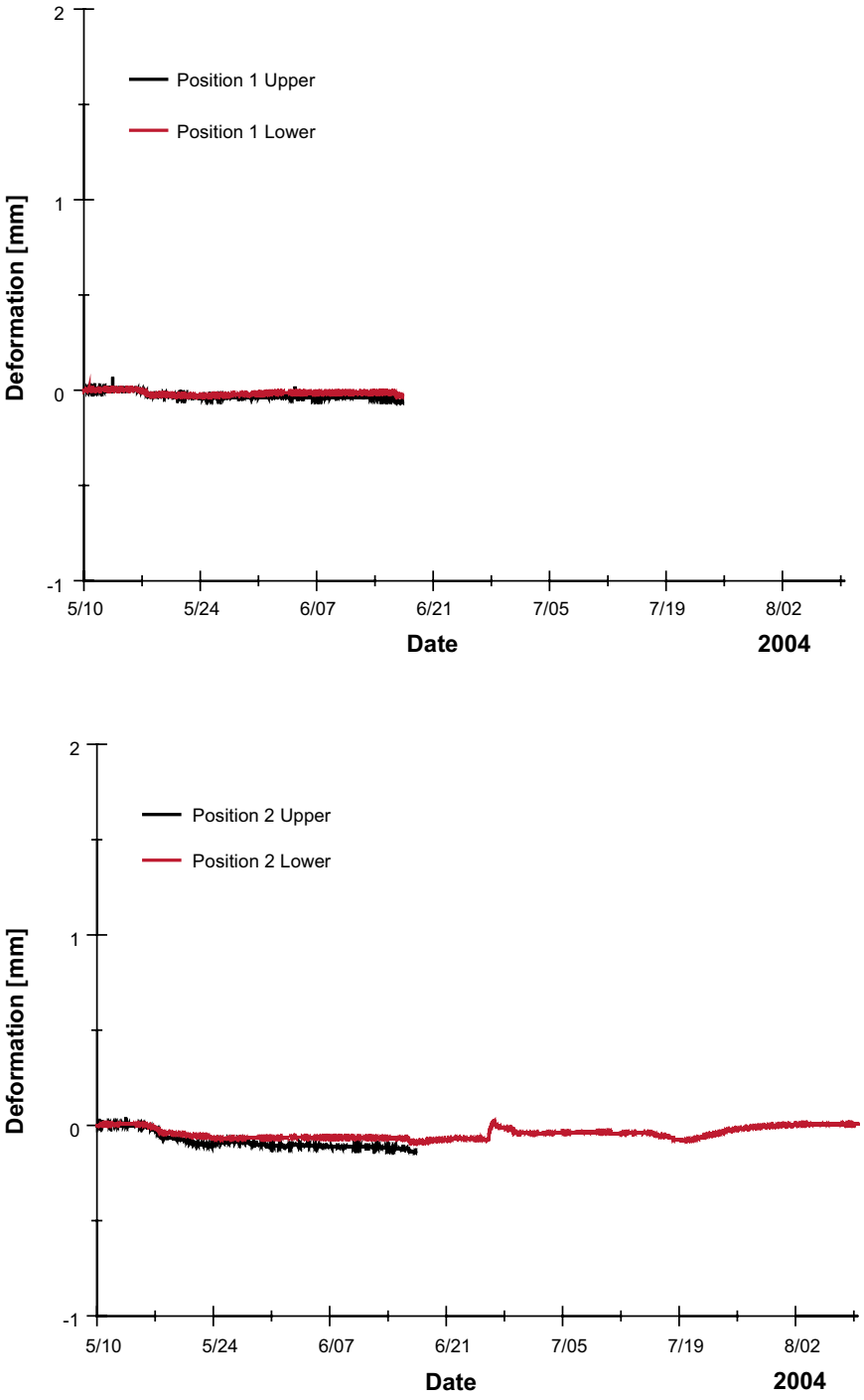

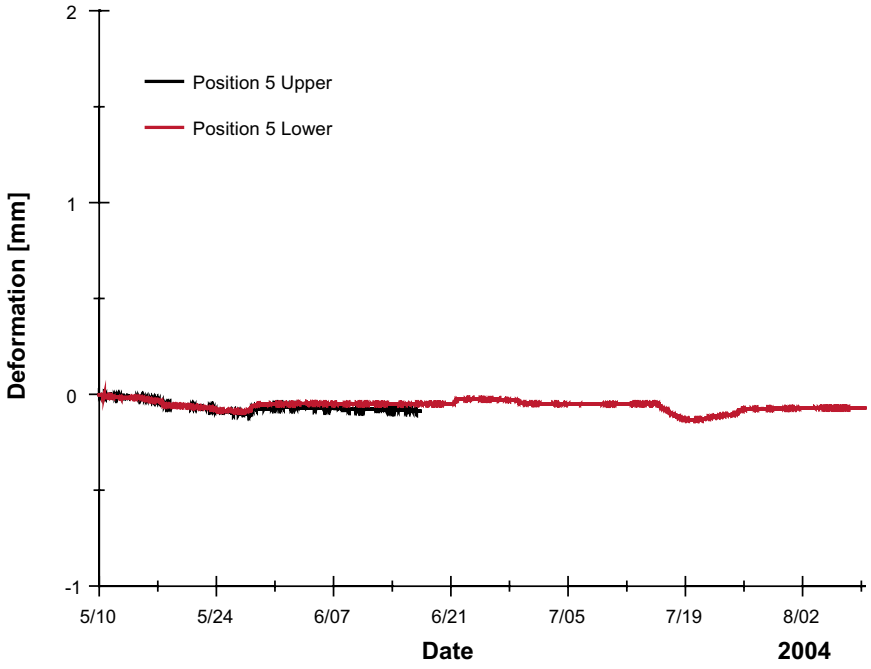
Position 5 Upper
Position 5 Lower
Deformation [mm]
2
1
0
-1
5/10
5/24
6/07
6/21
7/05
7/19
8/02
Date
2004

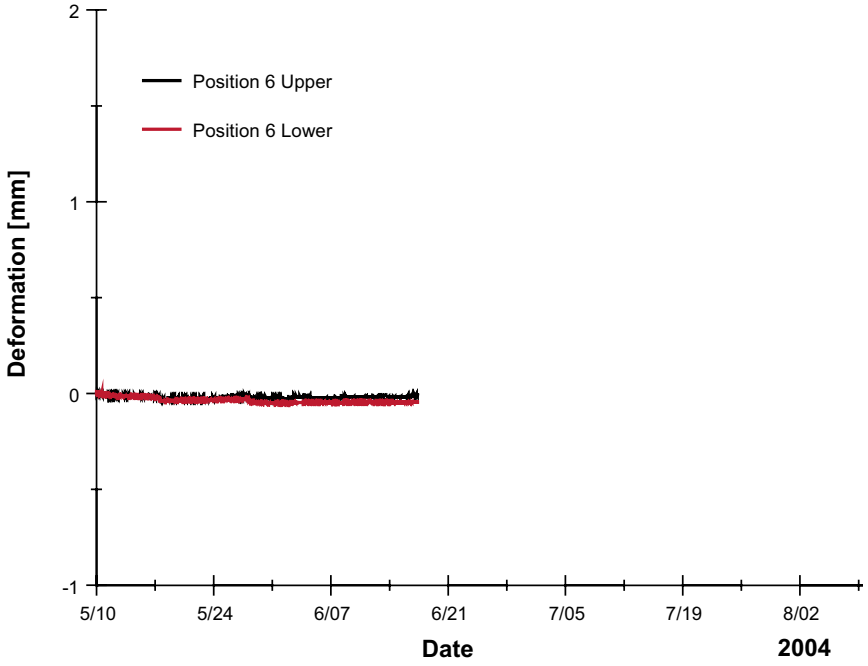
Position 6 Upper
Position 6 Lower
Deformation [mm]
2
1
0
-1
5/10
5/24
6/07
6/21
7/05
7/19
8/02
Date
2004

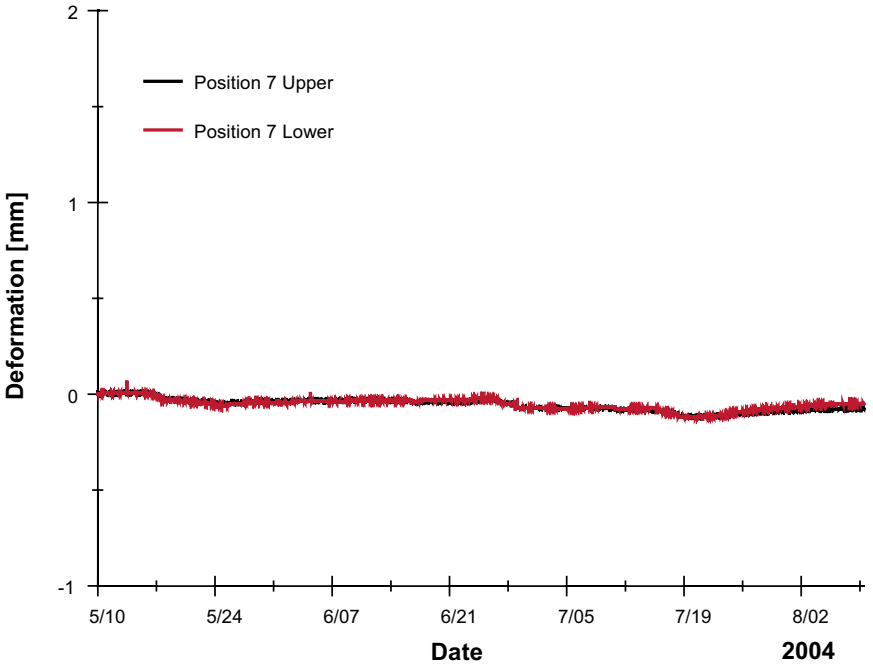
Position 7 Upper
Position 7 Lower
Deformation [mm]
2
1
0
-1
5/10
5/24
6/07
6/21
7/05
7/19
8/02
Date
2004

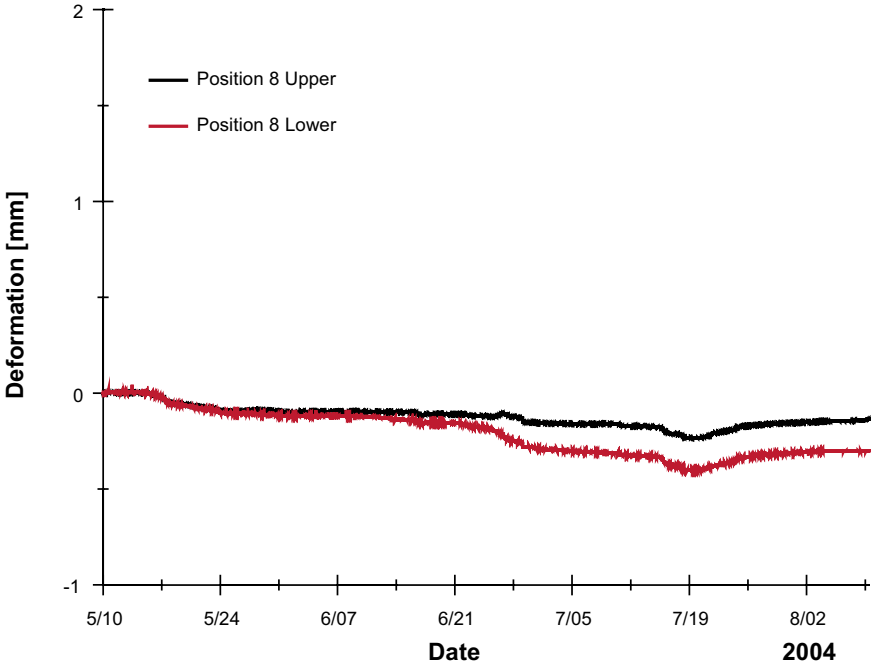
Position 8 Upper
Position 8 Lower
Deformation [mm]
2
1
0
-1
5/10
5/24
6/07
6/21
7/05
7/19
8/02
Date
2004

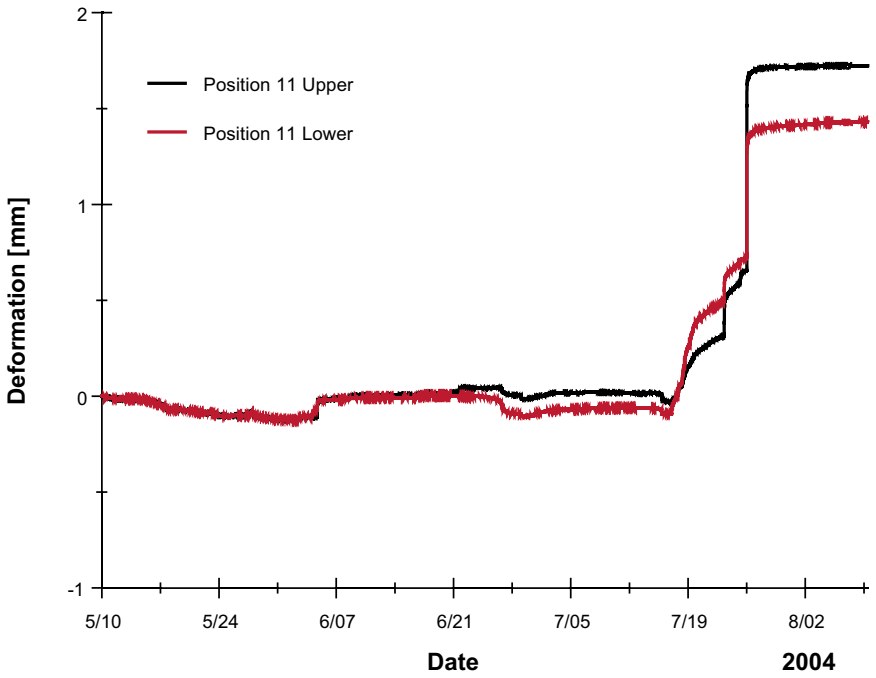
Position 11 Upper
Position 11 Lower
Deformation [mm]
2
1
0
-1
5/10
5/24
6/07
6/21
7/05
7/19
8/02
Date
2004

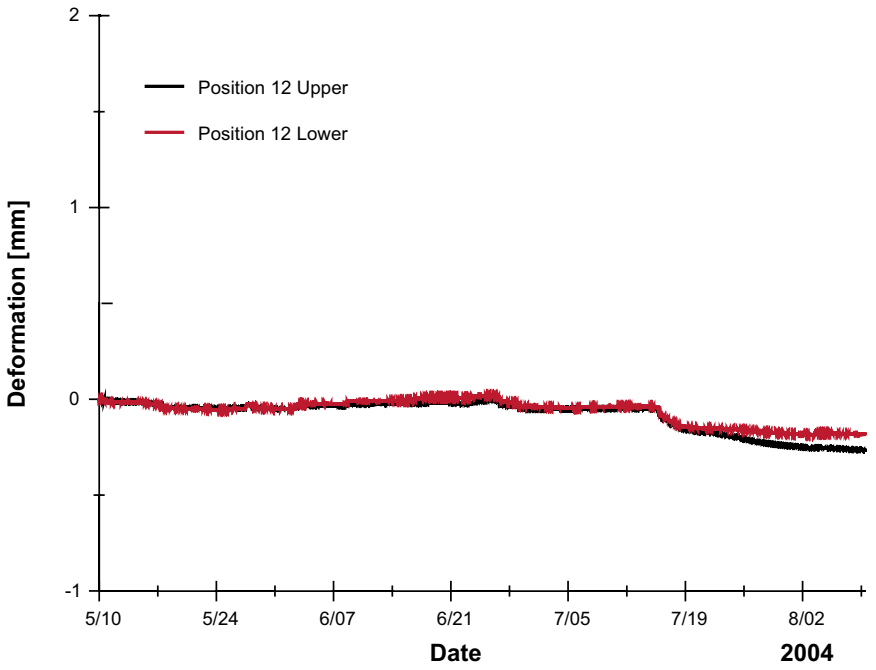
Position 12 Upper
Position 12 Lower
Deformation [mm]
2
1
0
-1
5/10
5/24
6/07
6/21
7/05
7/19
8/02
Date
2004

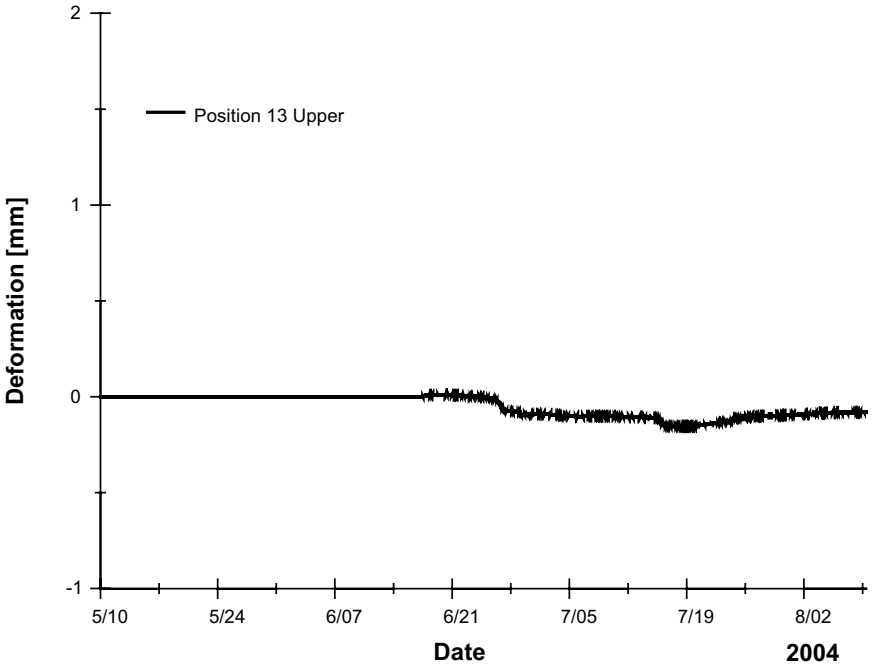
Position 13 Upper
Deformation [mm]
2
1
0
-1
5/10
5/24
6/07
6/21
7/05
7/19
8/02
Date
2004

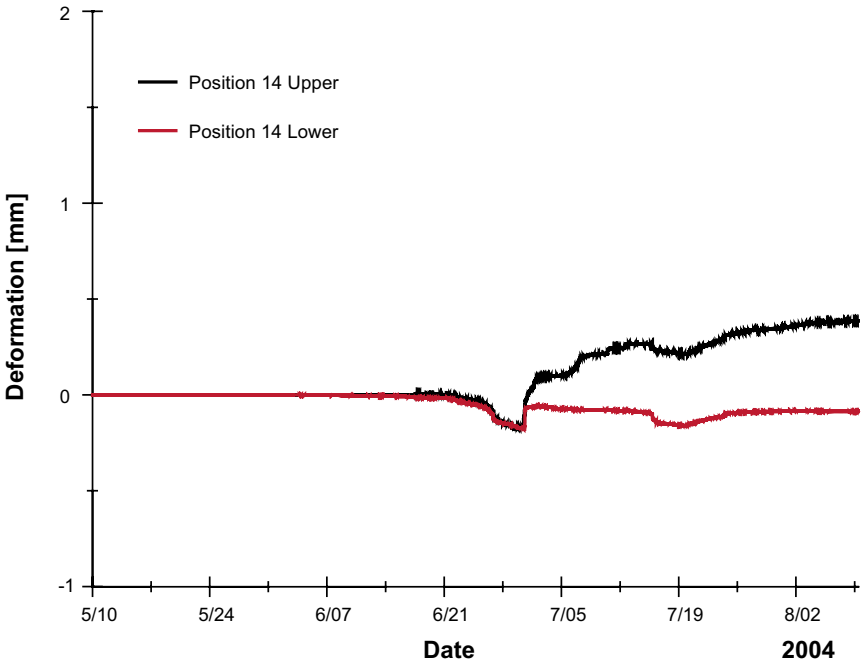
Position 14 Upper
Position 14 Lower
Deformation [mm]
2
1
0
-1
5/10
5/24
6/07
6/21
7/05
7/19
8/02
Date
2004

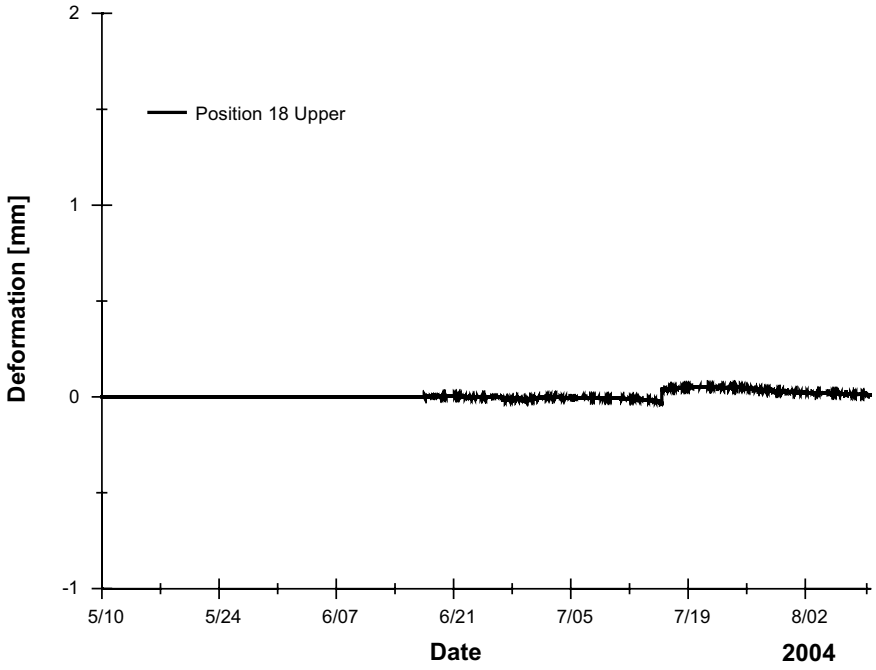
Position 18 Upper
Deformation [mm]
2
1
0
-1
5/10
5/24
6/07
6/21
7/05
7/19
8/02
Date
2004

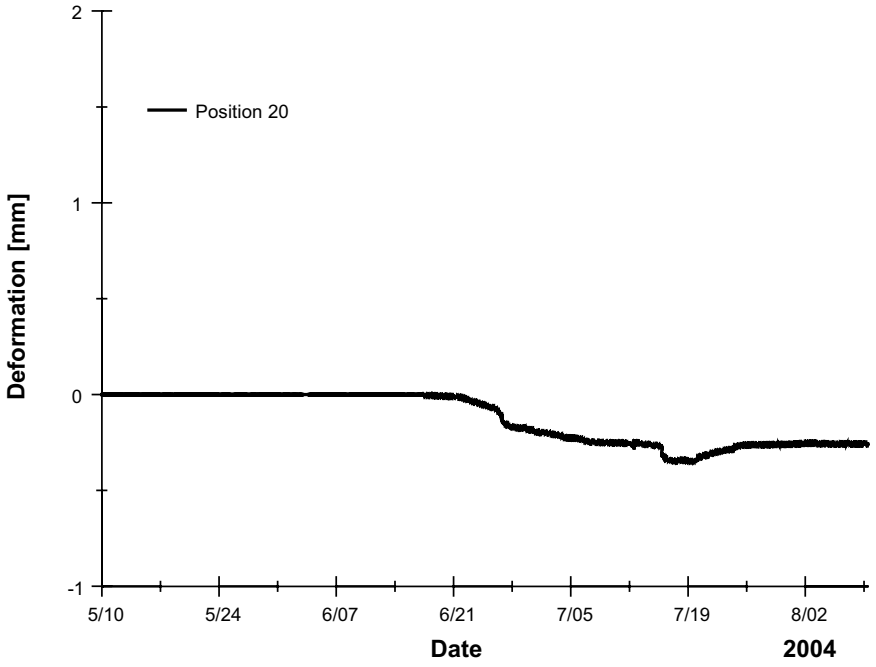
Position 20
Deformation [mm]
2
1
0
-1
5/10
5/24
6/07
6/21
7/05
7/19
8/02
Date
2004

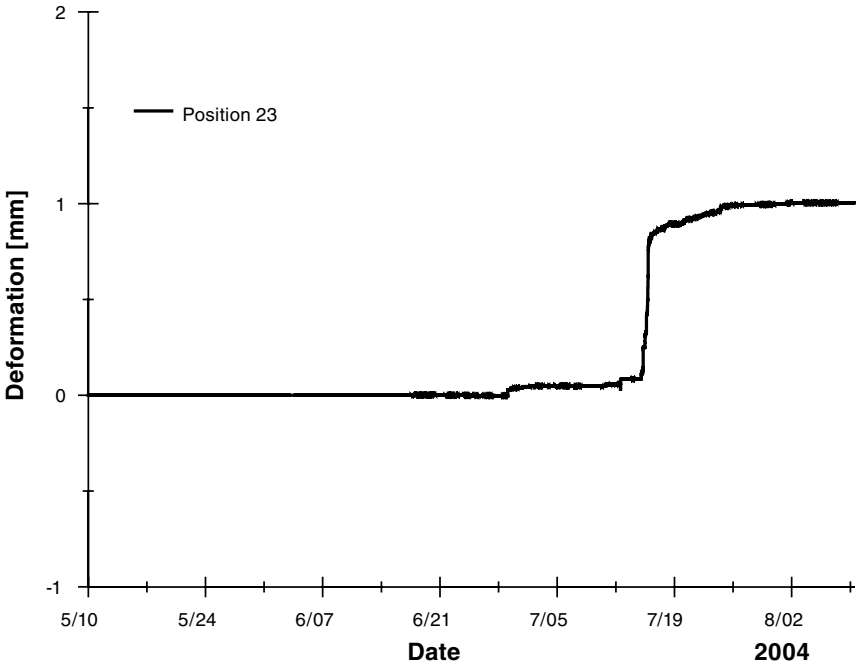
Position 23
Deformation [mm]
2
1
0
-1
5/10
5/24
6/07
6/21
7/05
7/19
8/02
Date
2004

# Appendix 3

Volumes of water tapped from the bladder during the release of confinement pressure. Except for the two first decrements, water had to be tapped several times to maintain the pressure at the planned level. In example, too keep the pressure close to 350 kPa five taps had to be made.

| Planned pressure drop [kPa] | Achieved pressure drop [kPa] | | Date | Time | Tap 1 [ml] | Tap 2 [ml] | Tap 3 [ml] | Tap 4 [ml] | Tap 5 [ml] |
|---|---|---|---|---|---|---|---|---|---|
| | From | To | | | | | | | |
| 700 – 650 | 705.5 | 649.6 | 2004-07-14 | 10:35 | 980 | | | | |
| 650 – 600 | 654 | 597 | | 11:40 | 1,150 | | | | |
| 600 – 550 | 607 | 548 | | 13:10 | 1,330 | | | | |
| | 555 | 549 | | | | 140 | | | |
| 550 – 500 | 555 | 494 | | 14:14 | 1,390 | | | | |
| | 505.5 | 499 | | 14:25 | | 150 | | | |
| 500 – 450 | 508.5 | 445 | | 15:19 | 1,750 | | | | |
| | 456 | 448.3 | | 15:30 | | 220 | | | |
| | 454 | 451.6 | | | | | 100 | | |
| 450 – 400 | 454 | 397 | | 16:18 | 1,860 | | | | |
| | 407 | 399 | | 16:29 | | 250 | | | |
| | 405 | 399 | | 16:44 | | | 170 | | |
| 400 – 350 | 406 | 340 | | 17:17 | 2,530 | | | | |
| | 350 | 344 | | 17:25 | | 210 | | | |
| | 348 | 341 | | 17:31 | | | 270 | | |
| | 346 | 340 | | 17:40 | | | | 230 | |
| | 344 | 338 | | 17:56 | | | | | 220 |
| 350 – 300 | 370 | 294 | 2004-07-15 | 08:26 | 3,120 | | | | |
| | 305 | 300 | | 08:46 | | 230 | | | |
| | 304 | 300 | | | | | 150 | | |
| 300 – 250 | 308 | 233 | | 10:29 | 4,220 | | | | |
| | 254 | 251 | | 11:08 | | 130 | | | |
| 250 – 200 | 260 | 200 | | 12:53 | 4,970 | | | | |
| | 210 | 203 | | 13:06 | | 600 | | | |
| | 209 | 200 | | 13:24 | | | 830 | | |
| 200 – 150 | 214 | 164.4 | | 16:20 | 8,000 | | | | |
| | 164.4 | 148.8 | | 16:26 | | 7,070 | | | |
| | 157 | 150 | | 17:11 | | | 2,420 | | |
| 150 – 100 | 159 | 0 | | 21:06 | | | | | |